FERNANDA ALMEIDA BÓCOLI

DIGITAL MAPPING AND SENSORS TO ASSIST SOIL GENESIS AND ESTIMATION OF ECOSYSTEM SERVICES

LAVRAS – MG
2024

FERNANDA ALMEIDA BÓCOLI

DIGITAL MAPPING AND SENSORS TO ASSIST SOIL GENESIS AND ESTIMATION OF ECOSYSTEM SERVICES

The dissertation was presented to the Postgraduate Program in Soil Sciences, concentration area in environmental resources and land use, at the Federal University of Lavras as part of the requirements for obtaining the title of Doctor.

Prof. D. Sc. Sérgio Henrique Godinho Silva
Advisor

LAVRAS – MG
2024

Ficha catalográfica elaborada pelo Sistema de Geração de Ficha Catalográfica da Biblioteca Universitária da UFLA, com dados informados pelo(a) próprio(a) autor(a).

Bócoli, Fernanda Almeida.
DIGITAL MAPPING AND SENSORS TO ASSIST SOIL GENESIS AND ESTIMATION OF ECOSYSTEM SERVICES / Fernanda Almeida Bócoli. - 2024.
156 p.

Orientador(a): Sérgio Henrique Godinho Silva.

Tese (doutorado) - Universidade Federal de Lavras, 2024.
Bibliografia.

1. Digital soil mapping. 2. Ecosystem services. 3. Sensors. I. Silva, Sérgio Henrique Godinho. II. Título.

FERNANDA ALMEIDA BÓCOLI

DIGITAL MAPPING AND SENSORS TO ASSIST SOIL GENESIS AND ESTIMATION OF ECOSYSTEM SERVICES

MAPEAMENTO DIGITAL E SENSORES PARA AUXILIAR EM ESTUDOS DA GÊNESE DO SOLO E ESTIMATIVA DE SERVIÇOS ECOSSISTÊMICOS

The dissertation was presented to the Postgraduate Program in Soil Sciences, concentration area in environmental resources and land use, at the Federal University of Lavras as part of the requirements for obtaining the title of Doctor.

Aprovada em 03 de julho de 2024.
Dr. Sérgio Henrique Godinho Silva - UFLA
Dra. Michele Duarte de Menezes - UFLA
Dr. Junior Cesar Avanzi - UFLA
Dra. Taciara Zborowski Horst Heinen - UTFPR
Dr. Alexandre Uezu - ESCAS

Prof. D. Sc. Sérgio Henrique Godinho Silva
Advisor

LAVRAS – MG
2024

AGRADECIMENTOS

Primeiramente a Deus que me possibilitou estudar onde eu sonhava, além de estar fazendo o que eu gosto. Agradeço também à minha mãe, Ivana Maria de Almeida, que me ensinou a sonhar e a batalhar por minhas próprias conquistas, sempre me apoiando em cada passo em todas as áreas de minha vida. Aos meus amigos queridos que sempre ficam na torcida para tudo correr bem, eu alcançar meus objetivos e ser feliz.

A cada professor que teve contribuição em minha formação desde os primeiros anos do fundamental até aqui no mestrado, pois tiveram um papel muito importante em minha vida graças aos seus ensinamentos. Em especial ao meu orientador, professor doutor Sérgio Henrique Godinho Silva, que sempre foi muito prestativo, me auxiliando em cada dúvida, sempre propondo avanços no nosso campo de pesquisa, nos fazendo crescer como pessoas e pesquisadores e com quem aprendo muito a cada dia. Um agradecimento especial também ao professor doutor Walbert Junior Reis dos Santos que teve uma participação efetiva na minha formação e incentivo para que eu ingressasse na carreira de pesquisa e docência em solos. Sou grata igualmente ao professor Nilton Curi que sempre engrandece nossos trabalhos com dicas valiosas baseadas em suas experiências tornando os trabalhos mais aplicados e robustos.

Também ao grupo de pesquisas em pedologia em que tenho tido a oportunidade de aprender e compartilhar conhecimentos sendo útil no desenvolvimento de pesquisas de nossa área, tendo oportunidades únicas pelas quais sou muito grata. Ademais, a todos colaboradores e técnicos do programa de Ciência do Solo e também das instituições anteriores que estudei que de alguma forma contribuíram com a minha formação, meu muito obrigada.

Agradeço também ao Coordenação de Aperfeiçoamento de Pessoal de Nível Superior (CAPES) que forneceu a bolsa de estudos para realização destes trabalhos aqui desenvolvidos, o Conselho Nacional de Desenvolvimento Científico e Tecnológico (CNPq) bem como a e a Fundação de Amparo à Pesquisa do Estado de Minas Gerais (FAPEMIG), também ao Instituto de Pesquisas Ecológicas (IPE) e a China Three Gorges Corporation (CTG) Brazil e pela Universidade Federal de Lavras (UFLA) pelos auxílios que contribuíram para a realização do doutorado.

“Ninguém é tão grande que não possa aprender nem tão pequeno que não possa ensinar.”

(Esopo)

GENERAL ABSTRACT

Guaranteeing food security and more efficient agricultural production is an ongoing endeavor. Therefore, studies related to the agricultural production basis, which is the soil, are fundamental, starting with pedogenetic and morphological analyses, as well as studies on larger areas such as watersheds and more detailed scales on agricultural properties, both for soil classes and key attributes like carbon and carbon stock. Thus, this work begins in Chapter I, studying a Paleosol profile with contrasting redoximorphic features. A Paleosol is a soil that retains attributes from when it was formed and has not evolved alongside the current environment, making it a potential tracer of climate changes. With the advancement of knowledge, different techniques have been used in soil studies, and proximal sensors have proven to be powerful tools that, combined with traditional analyses, can assist in pedogenic studies by providing robust data. Hence, this study used data from proximal sensors applied to the digital soil morphometrics technique, which aims at the detailed characterization of soil profiles in a quantitative and spatialized way, with the potential to provide insights into aspects related to mineralogy, hydrology, paleo, and current-soil forming processes involved. This study demonstrated that the digital morphometrics applied to the Paleosol have the potential to aid in the conservation of spring areas due to the position of this soil profile in the landscape. In Chapter II, we used fuzzy logic to conduct digital soil mapping on four watersheds of Pontal do Paranapanema-SP. The goal was to create more refined maps of these watersheds and evaluate the impact of a detailed scale on ecosystem services related to sediment dynamics and aquifer recharge. This analysis allowed us to assess how agricultural management and environmental planning could be improved to minimize erosive processes and siltation of water resources and to help preserve aquifer recharge areas. Additionally, we explored how increasing the level of detail in soil maps and ecosystem services can contribute to improving public policies applied to environmental conservation. In Chapter III, we conducted a study to predict and map carbon and carbon stock at a detailed scale at the property level. Proximal and remote sensor data, along with variables related to soil formation factors and the variability of its attributes, were tested for this purpose. The Random Forest algorithm was used for modeling. The study found that carbon stock is challenging to predict as it varies even within the same soil class, use, and parent material, which suggests that more attributes influence its distribution in the area. These findings encourage further studies to evaluate the prediction and mapping of carbon stock using other variables for different types of environments.

Keywords: Digital morphometrics; Paleosols; digital soil mapping; ecosystem services; sustainable management; carbon and carbon stocks prediction.

RESUMO GERAL

Garantir a segurança alimentar e uma produção agrícola mais eficiente é um esforço contínuo. Portanto, estudos relacionados à base da produção agrícola, que é o solo, são fundamentais, começando com análises pedogenéticas e morfológicas, bem como estudos em áreas maiores, como bacias hidrográficas, e em escalas mais detalhadas em propriedades agrícolas, tanto para classes de solo quanto para atributos chave como carbono e estoque de carbono. Assim, este trabalho inicia no Capítulo I, estudando um perfil de Paleossolo com características redoximórficas contrastantes. Um Paleossolo é um solo que retém atributos de quando foi formado e não evoluiu juntamente com o ambiente atual, sendo um potencial traçador de mudanças climáticas. Com o avanço do conhecimento, diferentes técnicas têm sido utilizadas nos estudos de solos, e os sensores próximos têm se mostrado ferramentas poderosas que, combinados com análises tradicionais, podem auxiliar nos estudos pedogênicos fornecendo dados robustos. Portanto, este estudo utilizou dados de sensores próximos aplicados à técnica de morfometria digital de solos, que visa a caracterização detalhada de perfis de solos de forma quantitativa e espacializada, com potencial para fornecer insights sobre aspectos relacionados à mineralogia, hidrologia e processos pedogenéticos passados e atuais. Este estudo demonstrou que a morfometria digital aplicada ao Paleossolo tem potencial para auxiliar na conservação de áreas de nascentes devido à posição deste perfil de solo na paisagem. No Capítulo II, utilizamos lógica fuzzy para realizar o mapeamento digital de solos em quatro bacias hidrográficas do Pontal do Paranapanema-SP. O objetivo foi criar mapas de solo mais refinados dessas bacias e avaliar o impacto de uma escala detalhada nos serviços ecossistêmicos relacionados à dinâmica de sedimentos e recarga de aquíferos. Esta análise permitiu avaliar como o manejo agrícola e o planejamento ambiental podem ser aprimorados para minimizar processos erosivos e o assoreamento dos recursos hídricos, além de ajudar na preservação de áreas de recarga de aquíferos. Adicionalmente, exploramos como o aumento do nível de detalhe nos mapas de solos e serviços ecossistêmicos pode contribuir para melhorar as políticas públicas aplicadas à conservação ambiental. No Capítulo III, realizamos um estudo para prever e mapear carbono e estoque de carbono em escala detalhada a nível de propriedade. Dados de sensores próximos e remotos, junto com variáveis relacionadas aos fatores de formação do solo e à variabilidade de seus atributos, foram testados para este fim. O algoritmo Random Forest foi utilizado para modelagem. O estudo descobriu que o estoque de carbono é difícil de prever, pois varia mesmo dentro da mesma classe de solo, uso e material de origem, o que sugere que mais atributos

influenciam sua distribuição na área. Esses achados incentivam a realização de mais estudos para avaliar a predição e o mapeamento de estoque de carbono utilizando outras variáveis para diferentes tipos de ambientes.

Palavras-chave: Morfometria digital; Paleossolos; mapeamento digital de solos; serviços ecossistêmicos; manejo sustentável; predição de carbono e estoque de carbono.

IMPACT INDICATORS

This dissertation contributes to aspects related to environmental preservation, detection, and mitigation of climate change, as well as addressing the mapping of ecosystem services to guide more conservation-oriented soil management practices and priority areas for reforestation and preservation. The topics studied may also impact the maintenance of food security and availability of potable water. Economic and environmentally low-impact methods, such as near and remote sensors, were employed to reduce the need for traditional sampling methods. The modeling used in the final chapter is one way to make analyses more representative and bridges traditional methods with sensor data. In Chapter I, relationships between the study of a Paleosol and climate change were explored, focusing on spring conservation using near sensors and digital morphometry for detailed spatial analysis of soil profiles. The studied environment showed a transition from a historically inundated past to more aerated and drier conditions presently, indicating water level variations over time, likely due to erosive processes. Conservation/restoration of vegetation near watercourses is recommended to prevent erosive processes elsewhere that have dissected the landscape. Chapter II discussed how ecosystem services are influenced by soil mapping at different scales. Using more detailed maps produced with fuzzy logic and additional sampling, it was possible to identify areas where agricultural management and environmental planning can be improved to reduce erosion, sedimentation, and preserve aquifer recharge areas. The analysis underscored the importance of data scale and accuracy for environmental management decisions. Chapter III conducted a detailed study to predict and map carbon ecosystem services and carbon stocks at the property level. Increasing soil carbon stocks is crucial for mitigating climate change and promoting more sustainable agriculture, reducing reliance on fertilizers and pesticides while ensuring food security. Using near and remote sensor data alongside soil formation factors, the study employed the Random Forest algorithm for modeling. Predicting carbon stocks proved complex, highlighting the need to consider a variety of attributes influencing local distribution. In summary, this research not only advances scientific understanding of the interaction between soils, climate change, and ecosystem services but also provides practical insights for conservation policies and sustainable management. Further investigations are recommended to expand prediction and mapping of carbon stocks across different environments, utilizing a broader range of variables and algorithms.

INDICADORES DE IMPACTO

Esta tese contribui em aspectos relacionados a preservação ambiental, detecção e mitigação das mudanças climáticas, além de abordar o mapeamento de serviços ecossistêmicos para orientar práticas mais conservacionistas de manejo do solo e áreas prioritárias para reflorestamento e preservação. Os temas estudados ainda podem ter impacto na manutenção da segurança alimentar e disponibilidade de água potável. Métodos econômicos e de baixo impacto ambiental, como sensores próximos e remotos, foram empregados para reduzir a necessidade de amostragens tradicionais, a modelagem utilizada no último capítulo trata-se de uma das formas de tornar as análises mais representativas e faz um link entre métodos tradicionais e dados de sensores. No Capítulo I, foram exploradas as relações entre o estudo de um Paleossolo e as mudanças climáticas, abordando a conservação de nascentes usando sensores próximos e morfometria digital para análise detalhada e espacial do perfil do solo. O ambiente estudado mostrou uma transição de um passado onde era inundado para condições mais aeradas e secas no presente, indicando variações no nível da água ao longo do tempo, provavelmente devido a processos erosivos. A conservação/restauração da vegetação próxima a cursos d'água é recomendada para evitar em outras áreas os mesmos processos erosivos que dissecaram a paisagem. O Capítulo II discutiu como os serviços ecossistêmicos são influenciados pelo mapeamento de solos em diferentes escalas. Utilizando mapas mais detalhados produzidos com lógica fuzzy e amostragens adicionais, foi possível indicar áreas onde se pode melhorar o manejo agrícola e o planejamento ambiental para reduzir erosão e assoreamento, além de preservar áreas de recarga de aquíferos. A análise destacou a importância da escala e acurácia dos dados para decisões de gestão ambiental. No Capítulo III, foi realizado um estudo detalhado para prever e mapear os serviços ecossistêmicos de carbono e estoque de carbono a nível de propriedade. Aumentar o estoque de carbono no solo é crucial para mitigar mudanças climáticas e promover uma agricultura mais sustentável, possibilitando o uso de menos fertilizantes e defensivos e garantindo a segurança alimentar. Utilizando dados de sensores próximos e remotos, juntamente com variáveis relacionadas aos fatores de formação do solo, o estudo empregou o algoritmo Random Forest para modelagem. A predição do estoque de carbono se mostrou complexa, destacando que é necessario considerar uma variedade de atributos que influenciam sua distribuição local. Em resumo, esta pesquisa não apenas avança o conhecimento científico sobre a interação entre solos, mudanças climáticas e serviços ecossistêmicos, mas também oferece insights práticos para políticas de conservação e manejo

sustentável. Recomenda-se investigações adicionais para ampliar a predição e mapeamento do estoque de carbono em diferentes ambientes, utilizando uma gama mais ampla de variáveis e algorítmos.

SUMMARY

PART I: Introduction and Theoretical Reference

1 General Introduction

Guaranteeing food security and more efficient agricultural production is an ongoing endeavor and relates directly to issues caused by climate change, which continues to preoccupy society and experts in the field (Lee *et al*., 2024; Liu *et al*., 2023; Shi *et al*., 2023; Paranavithana *et al*., 2023). Therefore, studies related to the agricultural production basis are fundamental. Then, the purpose of this dissertation is to characterized the soil from profile to landscape using proximal and remote sensors, relating soil data to climate change and ecosystem services such as erosion control, fresh water and carbon stock. Furthermore, it addresses the efficiency of machine learning algorithms for modeling in aiding more cost-effective evaluations and mapping of soils and their attributes.

Chapter I presents a study of a Paleosol profile through digital morphometrics. Paleosols are soils that have conserved features that were anciently developed during their formation. In Brazil, the records of Paleosols are rare (Stevanato *et al*., 2021). Such soils are more commonly found in places that have undergone more recent glaciation, active volcanism or tectonism, climate change, high fluctuations of the sea level, and ancient alluvial or lacustrine deposition (Ladeira, 2010; Wright, 1992), among others.

The study aims to detail the characterization of properties related to the contrasting pedogenesis processes of a Paleosol profile, containing hydromorphic features at the lower part of the profile, contrasting with overlying well-drained soil horizons, derived from sandstone with pelitic sediments intermixed, in Southeastern Brazil, through a combination of morphological, physical, chemical, mineralogical, and proximal sensors (pXRF - portable X-ray fluorescence, and MS - magnetic susceptibility) analyses.

The novelty of this study encompasses linking the findings of this Paleosol to the evolution of the landscape and to the estimation of climate change impacts. In addition this is rarely found in tropical regions, mainly considering their contrasting redoximorphic features, comprising the first Paleosol investigation via digital morphometrics under such conditions.

Chapter II highlights the importance of larger scales of soil maps for correctly addressing the ecosystem services and policy formulations because the soil is a critical component for maintaining the many ecosystem services, including services concerning fresh water, regulating erosion control, and water purification (Rodrigues *et al*., 2021). The main constrain for countries under development consists of the generalized scarcity of soil information at a local or detailed scale, a reality for the Brazilian territory (Coelho *et al*., 2021)

that likely contributes to sustaining the existent knowledge gap concerning soil ecosystem services under tropical conditions (Rodrigues *et al*., 2021).

One promising alternative consists of digital soil mapping (McBratney *et al*., 2003), whose framework has benefited from the power of computers to deal with large databases to produce new soil information. Policymakers should take precautions regarding the scale or resolution of soil information that will be the basis for interpretation and decision-making.

The study hypothesizes that identifying and assessing ecosystem services will be influenced by a scale increase of the current soil map. For this propose it was used the digital soil mapping technique, what will increase the available information and provide a more accurate basis for decision-making regarding farm and environmental conservation. Extensive considerations concerning the accuracy of maps and the effectiveness of the information gained was discussed. Further, knowledge and physical-based models were applied to assess direct water recharge and sediment dynamics (soil loss and sediment retention), respectively. We addressed the propagation of soil information gain by comparing the results obtained from the current less detailed soil information.

Chapter III addressed the importance of the ecosystem services carbon stock (CS) and soil organic cabon (SOC) in agricultural and preservation areas and how different land uses, soil classes, and parent material can be responsible for their variability in these areas. Besides, proximal and remote sensors data was evaluated on SOC and CS prediction and mapping, once high costs are associated to their detailed mapping. Alternatives are needed to obtain their content accurately and cost-effectively. The increase in SOC presents several benefits to productive systems by increasing productivity, besides mitigating the emission of gases such as CO_2 and methane (CH_4) into the atmosphere (Canellas *et al*., 2000; Paranavithana *et al*., 2023). However, most of the studies conducted for their quantification and mapping though modeling as an alternative to reduce costs are from temperate regions, where soil and climatic conditions act differently from those of the tropical regions (Nuralykyzy *et al*., 2023; Shi *et al.*, 2023; Li *et al*., 2018; Taghizadeh-Mehrjardi *et al*., 2020; Poeplau *et al*., 2016). Thus, factors influencing SOC dynamics may have different importance in tropical regions. Studies of this nature in tropical soils at the property level (high detail) are scarce (Mantovani *et al*., 2024).

Then, the study evaluated different parameters for modeling (22 combinations of environmental and remote and proximal sensing variables) and mapping SOC content and CS in detail using the Random Forest algorithm and a distance-based method (multilevel-b-spline), determining which variables best explain their spatial variability and characterizing their spatial

distribution on the study area with a diversity of land uses, soil classes, and parent material, within the Atlantic Forest biome. Thus, the hypotheses are that high sample density associated with high-resolution proximal and remote sensing data, as well as data on parent materials, soil classes, and land use, can provide accurate SOC and CS prediction and that variables related to parent material soil and land use will be necessary for understanding the detailed spatial variability of SOC and CS.

2 Theoretical Reference

2.1 Digital morphometrics

To perform a quantitative characterization of the spatialized attributes along the soil profile, Hartemink and Minasny (2014) proposed digital soil morphometrics. The sensors and equipment that have been used for this propose are the portable X-ray fluorescence spectrometer (pXRF), magnetic susceptibilimeter (MS), visible and near-infrared spectrometer (Vis-NIR), the Nix-PRO^{TM} color sensor, in addition to radiometers, electrical resistivity-meter, X-ray diffractometer, among others (Grauer-Gray; Hartemink, 2018; Silva *et al*., 2018; Mancini *et al*., 2021).

This approach could quantify variations among and within horizons of textural fractions, colors, mineralogy, and elemental contents spatialized into the soil profile, which can improve pedological studies. Aiding in the visualization of the soil formation process into the soil profile and finding differentiations even in morphologically homogenous profiles (Sun *et al*., 2020; Mancini *et al*., 2021; Bócoli *et al*., 2024).

2.2 Proximal sensors and equipment

2.2.1 Spectroscopy of X-ray fluorescence (pXRF)

Technological advances are achieving all areas of knowledge, which could not be different from agriculture. In tropical regions, there is a growing necessity for more field sampling to guide agricultural operations such as fertilizing, liming, and plastering. Furthermore, the economy of resources for food production, environmental conservation, and faster analysis made room for using types of equipment such as the pXRF (Ribeiro *et al*., 2017; Silva *et al*., 2020a).

On the other hand, wet or chemical analyses carried out in laboratories, although still necessary, are time-consuming, expensive, and generate waste that needs to be treated to be

disposed of without polluting the environment, in addition to the risks of these reagents to human health (Silva *et al*., 2020a). Furthermore, the pXRF has the potential to reduce the amount of wet analysis through modeling (Teixeira *et al*., 2018; Lima *et al*., 2019; Andrade *et al*., 2020a; 2020b; 2021) and also increase the representativeness of the producer database (Duda *et al*., 2017), and also the possibility of zoning their rural property and reducing fertilization through precision agriculture.

However, the use of this proximal sensor is not limited to this end. The pXRF can delimit areas with excess salinity (Swanhart *et al*., 2014), to aid in soil mapping (Silva *et al*., 2016; Mancini *et al*., 2019) or in studies of genesis and soil classification (Stockmann *et al*., 2016; Silva et al. 2019a; b; Benedet *et al*., 2020a; Bócoli *et al*., 2021), in the digital morphometrics (Silva *et al*., 2018; Grauer-Gray, Hartemink, 2018; Sun *et al*., 2020; Mancini *et al*., 2021; Bócoli *et al*., 2024), in the prediction of physical attributes (Zhu *et al*., 2011; Silva *et al*., 2020b; Benedet *et al*., 2020b), and biological attributes (Teixeira *et al*., 2021), or substituting the sulfur attack analysis (Silva *et al*., 2020a), besides the soil classification by its vegetal covering (Chakraborty *et al*., 2019).

The pXRF, when reading the sample, emits X-rays that excite electrons. What makes electrons dislodged from the innermost orbital be ejected when at the same time that another outermost electron occupies this vacancy, which emits a fluorescence specific to each element. The number of times this process repeats permits quantifying the amount of that element on the sample (Stockmann *et al*., 2016). The sensor can quantify about 45 chemical elements from the periodic table, from Mg to U (Weindorf *et al*., 2014). However, the elements quantified by the equipment vary due to its detection limit and the sample elemental constitution.

2.2.2 Magnetic susceptibility (MS)

This technique was first used in archaeological and lithological studies. After a certain period, it began to be used in studies of the characterization and genesis of soils (Dearing, 1999). This sensor was used in precision agriculture and aided in identifying the presence of ferrimagnetic materials, such as maghemite and magnetite (Rossi *et al*., 2018). Since materials containing Fe oxides are essential to be characterized mainly in tropical regions because they are correlated to P adsorption, more weathered soils have more Fe oxides and higher clay contents, so knowing the magnetism of this soil can help in the management of fertilization, for example. In pedology, Fe oxides have correlations with soil types and weathering (Mendes *et al*., 2022).

With the MS, it is possible to quantify the magnetism of minerals in the soil. The soil magnetism emitted from soils developed from low-magnetic sediments depends on the composition, concentration, and size of granules of neoformed minerals (Mathé *et al*., 2006). Soils derived from mafic rocks have a more intense magnetization than those derived from felsic ones or those with high silicate contents (Miranda, 2019). The Fe oxides, such as hematite and goethite, are widely distributed in highly weathered soils. They are classified as antiferromagnetic due to magnetic moments with low values of quantified magnetism (Butler, 1992; Dearing, 1999).

The MS can be used to verify the soil support capacity of vinasse application (Peluco *et al.*, 2013), detailed soil mapping (Siqueira *et al*., 2015), soil magnetic susceptibility mapping (Zhou *et al*., 2022), environmental tracer identifying erosion, causes of soil desertification (Lima *et al*., 2020; Liu *et al*., 2019; Cao *et al*., 2021) and pollutants (Grison *et al*., 2021). In addition, the characterization of soil drainage (Shirzaditabar; Heck, 2021), estimation of clay content (Filla *et al*., 2021), and characterization of the soil profile regarding the relationships between depth and its magnetism (Zawadzki *et al*., 2015). This sensor can also deliver inferences about mineralogy, geomorphology, chemistry, pedon morphology (Mello *et al*., 2020), and digital morphometrics (Bócoli *et al*., 2024).

2.2.3 X-ray diffractometry (XRD)

X-ray diffractometry interacts with the crystalline structure of the minerals that compose the soil through the diffracted photons. This technique is used to obtain soil mineralogy. The crystalline structure is specific to each mineral, with a periodicity of repetition of the packing of atoms in a given space. The different angles of the crystal structure formed by the bonding of these atoms cause these photons to produce wave peaks at characteristic wavelengths (Andrade *et al*., 2009; Inda Junior *et al*., 2017). This scattering of photons in XRD follows Bragg's law, represented by the formula below.

$$\mathbf{n\,\lambda = 2\,d\,sen\Theta}$$

On which:

- **n:** diffraction order;
- **λ:** wave-length;
- **d:** distance between planes of atoms;
- **Θ:** angle measured between the incident beam and certain planes of the crystal.

XRD is used in several areas,including soil science and pedological studies of genesis. In recent years, it has been combined with other sensors, making studies more robust, as in the case of studies such as Santos *et al*. (2010), Silva *et al.* (2018, 2019b), Mancini *et al.* (2021), and Silva *et al.* (2024).

2.3 Ecosystem services

Ecosystem services can be defined as all the benefits we receive from nature, divided into provisioning services (e.g., food and water), regulating services (e.g., erosion control), cultural services (e.g., recreational benefits), and supporting services (e.g., nutrient cycling) (IPBES, 2024).

Soil is crucial in maintaining the many ecosystem services within the Critical Zone, including services concerning fresh water, regulating erosion control, and water purification (Rodrigues *et al*., 2021). Thus, the nexus of direct aquifer recharge and sediment dynamic has the soil as a fundamental basis for interpretations. Robinson *et al.* (2012), further corroborated by Jónsson and Davíðsdóttir (2016), emphasized the growing need to incorporate the role of soils into ecosystem services. Pedology has been fundamental for enabling a foundation for the processes associated with generating runoff and groundwater recharge (Mello; Curi, 2012), and a soil map is an essential tool for assessing soil spatial variability across landscapes and in-depth, whose temporal variation is negligible (very stable over human life scale). The scale of the information is very important to accurately address the environmental issues, adequate land use, and promote conservation policies, which led us to need more detailed soil mapping, which can be done through digital soil mapping techniques.

2.4 Digital soil and attributes mapping

There are many approaches to creating the digital mapping of soil and its attributes, such as the generalized linear models, regressions, fuzzy logic, decision trees, Random Forest, neural networks, geostatistical, Scorpan-SSPFe model (spatial prediction function of soils with spatially autocorrelated errors) among others (Coelho *et al*., 2021; McBratney *et al*., 2003). Nevertheless, firstly, it is necessary to have previous knowledge of the area and its relationship between soil and landscape, besides knowing the soil formation factors (Jenny, 1941), which govern the soil differentiation in the region. From this previous knowledge, we determine the best methodology to follow.

The linear models, for example, suggest direct relationships between the variables, such as the soil formation factors: mineralogy and annual rainfall (Simonett, 1960), soil organic matter (SOC), pH and N, and the terrain slope (Anderson; Furley, 1975), the clay formation in function to the time of soil formation (Hay, 1960), among others. Another example would be the prediction of soil attributes (e.g., SOC, macronutrients, and pH) with the use of environmental variables (e.g., topography, climate, vegetation) or proximal sensors (e.g., portable X-ray fluorescence, pXRF; magnetic susceptibilimeter, MS) through linear regressions (Silva *et al*., 2017; Teixeira *et al*., 2018; Gomes *et al*., 2019). Nevertheless, generally, it is not possible to find direct relationships between factors, which requires more complex modeling (Phillips, 2016).

The prediction of soil classes through terrain attributes (Menezes *et al*., 2013; Silva *et al*., 2016) can occur, for example, through fuzzy logic, a non-linear relation on which the classification is diffuse, comprehending a range of values, and not just discrete values. Zadeh (1965) describes fuzzy logic as adequate to evaluate an object characterized by continuous values between 0 and 1, as an extension of the already known functions of union, intersection, and convexity, among other metrics for determining the relation between objects. Thus, this approach represents an adequate tool to delimit soil classes once they are continuous into the landscape. In this study, we will use fuzzy logic.

When more complex modeling is required, the decision trees, for example, can separate the data by groups of similarity, starting from a node that is the information that guides all the others, that branches in branches, and leaves that are the final groupings (Breiman *et al*., 2017). Schuler *et al*. (2010) used a hybrid model to realize digital soil mapping by combining the SOTER (FAO, 1995), the SoLIM (Soil Land Inference Model) (Zhu *et al*., 2001), and the algorithm of Classification and Regression Trees (CART), noting that it is a promising tool for the reduction of time and cost with the soil mapping. Pelegrino *et al.* (2016) used the algorithm CART for mapping, and after expanding the digital soil mapping of a watershed for surrounding areas with similar characteristics, obtaining good results since the algorithm aided in the choice of the best methodology for the soil delimitation.

Random forest, in turn, is a supervised training algorithm that builds and chooses randomly multiple decision trees to control the variance of the data. This algorithm can both perform regressions and classify the data. (Ho, 1995). This algorithm has presented more robust results for the digital mapping of soil and attributes than the decision trees and other algorithms

(Siewert, 2018; Silva *et al*., 2019; 2021; Mendes *et al*., 2022). Nevertheless, it has limitations with categorical variables.

Conversely, the neural network verifies all the possible relationships among the variables. It is an algorithm that uses artificial intelligence to simulate what occurs in the brain and its connections within and among neurons. Some examples of neural networks are Artificial Neural Networks (ANN), Convolutional Neural Networks (CNN), and Deep Learning Neural Networks (DNN). Padarian *et al.* (2019), utilizing the model CNN, managed to reduce the error of C maps by 30%, compared to conventional techniques that considered only punctual information of the digital elevation model (DEM). The CNN uses hyper and multispectral images to classify the variables (Lecun *et al*., 1990; Krizhevsky *et al*., 2012) as the type of soil cover or a spatialized distribution of some soil attribute. The performance of these algorithms is variable, but in many studies, the ANN had lower performance than algorithms such as RF or DNN (Siewert, 2018; Taghizadeh-Mehrjardi *et al*., 2020). Meantime, studies such as Eitelwein *et al*. (2022) verified the superiority of ANN compared with the Partial Least Squares Regression (PLS). Taghizadeh-Mehrjardi *et al*. (2020) observed that the algorithm DNN was more robust than all other tests, including the RF, to improve the spatial prediction of the SOC in contrasting climates of Iran. Deep learning can interpret the data provided by recognizing the patterns in the processing steps and then realizing the training for the analysis and classification of the data, reaching high accuracy in predictions as in the previous example.

However, the use only of machine learning (ML), which encompasses the use of artificial intelligence (AI) in these algorithms mentioned above and others, generally is not enough for an accurate prediction of the soils and their attributes, which turns the pedologist's knowledge irreplaceable (Menezes *et al*., 2013). Thus, the legacy data is essential to incorporate this knowledge into the modeling and other tools used to produce or improve the digital mapping of soil and its attributes.

Table 1. Examples of models that can be using for predicting soil classes and their attributes.

Models	Characteristics	Data type	Examples
Linear models	Direct relationships between the variables	Categorical and discrete variables	Clay formation in function to the time of soil formation (Hay, 1960)
Fuzzy logic	Diffuse classification, i.e., comprehending a range of values	Continuous values	Delimit soil classes once they are continuous into the landscape (Silva *et al*., 2016)
Decision trees	Separates the data by groups of similarity	Categorical and discrete variables	Soil mapping, and expanding the digital soil mapping for

			surrounding areas with similar characteristics (Pelegrino et al., 2016)
Random Forest	A supervised training algorithm that builds and randomly chooses multiple decision trees to control data variance needs a robust dataset	Discrete variables, limitations with categorical	Robust results for digital mapping of soil and attributes (Siewert, 2018; Silva *et al*., 2019; Silva *et al*., 2021; Mendes *et al*., 2022; Silva et al., 2024)
Neural Networks (e.g., Artificial Neural Networks (ANN), Convolutional Neural Networks (CNN), Deep Learning Neural Networks (DNN))	Verifies all the possible relationships among the variables simulate what occurs in the brain and its connections within and among neurons, automatized model	Categorical and discrete variables	Spatial prediction of the SOC using the DNN (Taghizadeh-Mehrjardi *et al*., 2020)

In Brazil, like many countries in development, due to the scarcity of economic and human resources and the long time necessary to produce soil mapping using the traditional approach, the soil maps are low detailed, except in some restricted areas (SCHULER et al., 2010; MENEZES et al., 2013; PELEGRINO et al., 2016). Thence, legacy data, i.e., preexistent data of the area, has been utilized to improve the soil maps at a low cost (PELEGRINO et al., 2016). These data are fundamental to science, and once they consider the knowledge of experienced pedologists, the quality of the generated soil maps will increase.

REFERENCES

ANDERSON, K.E., FURLEY, P.A., 1975. An assessment of the relationship between surface properties of chalk soils and slope form using principal component analysis. **Journal of Soil Science**, 1975, v. 26, p. 130– 143.

ANDRADE, J.C.; AZEVEDO, A.C.; BIGHAM, J.M.; CASTILHOS, R.M.V.; COSTA, A.C. S.; CURI, N.; FABRIS, J.D.; KÄMPF, N.; MARQUES JÚNIOR, J.; MARQUES, J.J.; MELLO, J.W.V.; MELO, V.F.; PEREZ, D.V.; PINTO, L.F.S.; SCHAEFER, C.E.G.R.; STUCKI, J.W. VIANA, J.H.M.; VIDAL-TORRADO, P.; WYPYCH, F.; ZANARDO, A.; **Química e Mineralogia do Solo:** Parte 1 - Conceitos Básicos. Viçosa: Sociedade Brasileira de Ciência do Solo, 2009. 695 p.

ANDRADE, R.; SILVA, S.H.G.; WEINDORF, D.C.; CHAKRABORTY, S.; FARIA, W.M.; GUILHERME, L.R.G.; CURI, N. Micronutrients prediction via pXRF spectrometry in Brazil: Influence of weathering degree. **Geoderma Regional**, v. 27, p. e00431, 2021.

ANDRADE, R.; FARIA, W.M.; SILVA, S.H.G.; CHAKRABORTY, S.; WEINDORF, D.C.; MESQUITA, L.F.; GUILHERME, L.R.G.; CURI, N. Prediction of soil fertility via portable X-ray fluorescence (pXRF) spectrometry and soil texture in the Brazilian Coastal Plains. **Geoderma**, v. 357, p. 113960, 2020a.

ANDRADE, R.; SILVA, S.H.G.; WEINDORF, D.C.; CHAKRABORTY, S.; FARIA, W.M.; MESQUITA, L.F.; GUILHERME, L.R.G.; CURI, N. Assessing models for prediction of some soil chemical properties from portable X-ray fluorescence (pXRF) spectrometry data in Brazilian Coastal Plains. **Geoderma**, v. 357, p. 113957, 2020b.

BENEDET, L.; FARIA, W.M.; SILVA, S.H.G; MANCINI, M. GUILHERME, L.R.G.; DEMATTÊ, J.A.M.; CURI, N. Soil subgroup prediction via portable X-ray fluorescence and a visible near-infrared spectroscopy. **Geoderma**, v. 365, p. 1-10, abr. 2020a. Elsevier BV. https://doi.org/10.1016/j.geoderma.2020.114212.

BENEDET, L.; FARIA, W.M.; SILVA, S.H.G.; MANCINI, M.; DEMATTÊ, J.A.M.; GUILHERME, L.R.G.; CURI, N. Soil texture prediction using portable X-ray fluorescence spectrometry and visible near-infrared diffuse reflectance spectroscopy. **Geoderma**, v. 376, p. 114553, out. 2020b. Elsevier BV. http://dx.doi.org/10.1016/j.geoderma.2020.114553.

BÓCOLI, F.A.; SANTOS, W.J.R. dos; SILVA, S.H.G.; TEIXEIRA, A.F. dos S.; MANCINI, M.; CURI, N. Study of an abnormal occurrence of Oxisols in strongly undulated relief in the south of Minas Gerais, Brazil, with support of pXRF and geomorphology. **Ciência e Agrotecnologia**, v. 45, p. e018121, 2021. FapUNIFESP (SciELO). http://dx.doi.org/10.1590/1413-7054202145018121.

BÓCOLI, F.A.; SILVA, S.H.G.; AVANZI, J.C.; SILVA, B.M.; FARIA, V.L. de; TOTTI, M.C.V.; INDA, A.V.; FROSI, G.; LIMA, S. de S.F.; UEZU, A. Paleosol marked by contrasting formation processes: a pilot study using digital morphometrics in southeastern brazil. **Catena**, v. 234, p. 107550, jan. 2024. Elsevier BV. http://dx.doi.org/10.1016/j.catena.2023.107550.

BREIMAN, L.; FRIEDMAN, J.H.; OLSHEN, R.A.; STONE, C.J. **Classification and Regression Trees**. Taylor & Francis Group: an informa business, 368 p., 25 oct. 2017. Routledge. http://dx.doi.org/10.1201/9781315139470. 1st Edition in 1984.

BUTLER, R.F. Paleomagnetism: magnetic domains to geologic terranes. Portland: Blackwell Science Inc., 1992. 249 p.

CANELLAS, L.P.; BERNER, P.G.; SILVA, S.G. da; BARROS e SILVA, M.; SANTOS, G. de A. Frações da matéria orgânica em seis solos de uma toposseqüência no Estado do Rio de Janeiro. **Pesquisa Agropecuária Brasileira**, v. 35, n. 1, p. 133-143, jan. 2000. FapUNIFESP (SciELO). http://dx.doi.org/10.1590/s0100-204x2000000100016.

CAO, Z.; ZHANG, K.; HE, J.; YANG, Z.; ZHOU, Z. Linking rocky desertification to soil erosion by investigating changes in soil magnetic susceptibility profiles on karst slopes. **Geoderma**, v. 389, p. 114949, maio 2021. Elsevier BV. http://dx.doi.org/10.1016/j.geoderma.2021.114949.

CHAKRABORTY, S.; LI, B.; WEINDORF, D.C.; DEB, S.; ACREE, A.; DE, P.; PANDA, P. Use of portable X-ray fluorescence spectrometry for classifying soils from different land use land cover systems in India. **Geoderma**, v. 338, p. 5-13, mar. 2019. Elsevier BV. http://dx.doi.org/10.1016/j.geoderma.2018.11.043.

COELHO, F.F.; GIASSON, E.; CAMPOS, A.R.; TIECHER, T.; COSTA, J.J.F.; COBLINSKI, J.A. Digital soil class mapping in Brazil: a systematic review. **Scientia Agricola**, v. 78, n. 5, p. 20190227-20190227, jan. 2021. FapUNIFESP (SciELO). http://dx.doi.org/10.1590/1678-992x-2019-0227.

DEARING, J. Environmental Magnetic Susceptibility. **Using the Bartington MS2 system**, 43 p., 1999.

EITELWEIN, M.T.; TAVARES, T.R.; MOLIN, J.P.; TREVISAN, R.G.; SOUSA, R.V. de; DEMATTÊ, J.A.M. Predictive Performance of Mobile Vis–NIR Spectroscopy for Mapping Key Fertility Attributes in Tropical Soils through Local Models Using PLS and ANN. **Automation**, v. 3, n. 1, p. 116-131, 3 fev. 2022. MDPI AG. http://dx.doi.org/10.3390/automation3010006.

FAO. **Global and national soils and terrain digital databases** (SOTER). World Soil Resources, Reports 74. (FAO: Rome). 1995.

FILLA, V.A.; COELHO, A.P.; FERRONI, A.D.; BAHIA, A.S.R. de S.; MARQUES JÚNIOR, J. Estimation of clay content by magnetic susceptibility in tropical soils using linear and nonlinear models. **Geoderma**, v. 403, p. 115371, dez. 2021. Elsevier BV. http://dx.doi.org/10.1016/j.geoderma.2021.115371.

GOMES, L. C.; FARIA, R. M.; SOUZA, E. de; VELOSO, G. V.; SCHAEFER, C. E. G.R.; FERNANDES FILHO, E. I. Modelling and mapping soil organic carbon stocks in Brazil. **Geoderma**, v. 340, p. 337-350, abr. 2019. Elsevier BV. http://dx.doi.org/10.1016/j.geoderma.2019.01.007.

GRAUER-GRAY, J., HARTEMINK, A.E. Raster sampling of soil profiles. **Geoderma**, v. 318, p. 99–108, 2018. http://dx.doi.org/10.1016/j.geoderma.2017.12.029.

GRISON, H.; PETROVSKY, E.; HANZLIKOVA, H. Assessing anthropogenic contribution in highly magnetic forest soils developed on basalts using magnetic susceptibility and concentration of elements. **Catena**, v. 206, p. 105480, nov. 2021. Elsevier BV. http://dx.doi.org/10.1016/j.catena.2021.105480.

HARTEMINK, A. E.; MINASNY, B. Towards digital soil morphometrics. **Geoderma**, v. 230-231, p. 305-317, out. 2014. Elsevier BV. http://dx.doi.org/10.1016/j.geoderma.2014.03.008.

HAY, R.L. Rate of clay formation and mineral alteration in a 4000-years-old volcanic ash soil on St. Vincent, B.W.I. **American Journal of Science**, 1960, v. 258, p. 354– 368.

HO, T.K. Random Decision Forests**. Proceedings of the 3rd International Conference on Document Analysis and Recognition**, Montreal, QC, 14–16 August 1995. p. 278–282, 1995.

INDA JUNIOR, A.V.; BISSANI, C.A.; CERETTA, C.A.; COSTA, C. das N.; LIMA, C.V.S.; RHEINHEIMER, D.; MEURER, E.J.; KLAMT, E.; GIASSON, E.; CARMONA, F.C.; CAMARGO, F.A. de O.; ANGHINONI, I.; SILVA, L.S. da; VAHL, L.C.; NASCIMENTO,

P.C. DO; SELBACH, P.A.; SOUSA, R.O. DE. S., ROSELE C. dos. **Fundamentos de Química do Solo**, 6ª ed. 2017. 270 p.

IPBES - Intergovernmental Science-Policy Platform on Biodiversity and Ecosystem Services. Ecosystem Service: Definition. 2024. Disponível em: https://www.ipbes.net/glossary-tag/ecosystem-service. Acesso em: 20 jun. 2024.

JENNY, H., 1941. **Factors of soil formation**: A system of quantitative Pedology. McGraw-Hill Book Co., Inc., New York.

JÓNSSON, J.Ö.G., DAVÍÐSDÓTTIR, B. Classification and valuation of soil ecosystem services. **Agricultural Systems**, v. 145, p. 24-38, 2016. Elsevier BV. http://dx.doi.org/10.1016/j.agsy.2016.02.010.

KRIZHEVSKY, A.; SUTSKEVER, I.; HINTON, G. E.: Imagen et classification with deep convolutional neural networks, **in:** Advances in neural information processing systems, MIT Press, 1097–1105, 2012.

LADEIRA, F.S.B. Solos do passado: origem e identificação. **Revista Brasileira de Ciência do Solo**, v. 34, n. 6, p. 1773-1786, dez. 2010. FapUNIFESP (SciELO). http://dx.doi.org/10.1590/s0100-06832010000600001.

LECUN, Y.; BOSER, B. E.; DENKER, J. S.; HENDERSON, D.; HOWARD, R. E.; HUBBARD, W. E.; JACKEL, L. D. Handwritten digit recognition with a back-propagation network, **in:** Advances in neural information processing systems, MIT Press, 396–404, 1990.

LEE, C.C.; ZENG, M.; LUO, K. How does climate change affect food security? Evidence from China. **Environmental Impact Assessment Review**, v. 104, p. 107324, jan. 2024. Elsevier BV. http://dx.doi.org/10.1016/j.eiar.2023.107324.

LIMA, P.L.T.; SILVA, M.L.N.; QUINTON, J.; ARMSTRONG, A.; INDA, A.V.; BATISTA, P.V.G.; POGGERE, G.C.; CURI, N. Tracing the origin of reservoir sediments using magnetic properties in Southeastern Brazil. SEMINA. CIÊNCIAS AGRÁRIAS (ONLINE), v. 41, p. 847, 2020.

LIMA, T.M. de; WEINDORF, D.C.; CURI, N.; GUILHERME, L.R.G.; LANA, R.M.Q.; RIBEIRO, B.T. Elemental analysis of Cerrado agricultural soils via portable X-ray fluorescence spectrometry: Inferences for soil fertility assessment. **Geoderma**, v. 353, p. 264-272, nov. 2019. Elsevier BV. http://dx.doi.org/10.1016/j.geoderma.2019.06.045.

LI, X.; MCCARTY, G.W.; KARLEN, D.L.; CAMBARDELLA, C.A. Topographic metric predictions of soil redistribution and organic carbon in Iowa cropland fields. **Catena**, v. 160, p. 222-232, jan. 2018. Elsevier BV. http://dx.doi.org/10.1016/j.catena.2017.09.026.

LIU, J.; ZHANG, P.; GAO, Y. Effects of vegetation rehabilitation on soil inorganic carbon in deserts: a meta-analysis. **Catena**, v. 231, p. 107290, out. 2023. Elsevier BV. http://dx.doi.org/10.1016/j.catena.2023.107290.

LIU, L.; ZHANG, K.; FU, S.; LIU, B.; HUANG, M.; ZHANG, Z.; ZHANG, F.; YU, Y. Rapid magnetic susceptibility measurement for obtaining superficial soil layer thickness and its erosion monitoring implications. **Geoderma**, v. 351, p. 163-173, out. 2019. Elsevier BV. http://dx.doi.org/10.1016/j.geoderma.2019.05.030.

MANCINI, M.; WEINDORF, D.C.; SILVA, S.H.G.; CHAKRABORTY, S.; TEIXEIRA, A.F. dos S.; GUILHERME, L.R.G.; CURI, N. Parent material distribution mapping from tropical soils data via machine learning and portable X-ray fluorescence (pXRF) spectrometry in Brazil. **Geoderma**, v. 354, p. 113885, nov. 2019. Elsevier BV. http://dx.doi.org/10.1016/j.geoderma.2019.113885.

MANCINI, M.; SILVA, S.H.G.; HARTEMINK, A.E.; ZHANG, Y.; FARIA, Á.J.G. de; SILVA, F.M.; INDA, A.V.; DEMATTÊ, J.A.M.; CURI, N. Formation and variation of a 4.5 m deep Oxisol in southeastern Brazil. **Catena**, v. 206, p. 105492, nov. 2021. Elsevier BV. http://dx.doi.org/10.1016/j.catena.2021.105492.

MANTOVANI, V.A.; TERRA, M. de C.N.S.; RODRIGUES, A.F.; SILVA, C.A.; GUO, L.; MELLO, J.M. de; MELLO, C.R. de. Unprecedentedly high soil carbon stocks and their spatial variability in a seasonally dry Atlantic Forest in Brazil. **Catena**, v. 235, p. 107696, fev. 2024. Elsevier BV. http://dx.doi.org/10.1016/j.catena.2023.107696.

MATHÉ, V.; LÉVÊQUE, F.; MATHÉ, P.E.; CHEVALLIER, C.; PONS, Y. Soil anomaly mapping using a caesium magnetometer: limits in the low magnetic amplitude case. **Journal of Applied Geophysics**, v.58, p.202-217, 2006. DOI: 10.1016/j.jappgeo.2005.06.004.

MCBRATNEY, A., MENDONÇA SANTOS, M., MINASNY, B. On digital soil mapping. **Geoderma**, v. 117, p. 3–52, 2003. https://doi.org/10.1016/S0016-7061(03)00223-4.

MELLO, C.R.D., CURI, N. Hydropedology. Hydropedology. **Ciência e Agrotecnologia**, v. 36, n. 2, p. 137–146, 2012.

MELLO, D.C. de; DEMATTÊ, J.A.M.; SILVERO, N.E.Q.; RAIMO, L.A.D.L. di; POPPIEL, R.R.; MELLO, F.A.O.; SOUZA, A.B.; SAFANELLI, J.L.; RESENDE, M.E.B.; RIZZO, R. Soil magnetic susceptibility and its relationship with naturally occurring processes and soil attributes in pedosphere, in a tropical environment. **Geoderma**, v. 372, p. 114364, ago. 2020. Elsevier BV. http://dx.doi.org/10.1016/j.geoderma.2020.114364

MENDES, W. de S.; DEMATTÊ, J.A.M.; MINASNY, B.; SILVERO, N.E.Q.; BONFATTI, B.R.; SAFANELLI, J.L.; RIZZO, R.; COSTA, A.C.S. da. Free iron oxide content in tropical soils predicted by integrative digital mapping**. Soil and Tillage Research**, v. 219, p. 105346, maio 2022. Elsevier BV. http://dx.doi.org/10.1016/j.still.2022.105346.

MENEZES, M.D. de; SILVA, S.H.G.; OWENS, P.R.; CURI, N. Digital soil mapping approach based on fuzzy logic and field expert knowledge. **Ciência e Agrotecnologia**, Lavras, v. 37, n. 1, p. 287-298, ago. 2013.

MIRANDA, M.N.R. **Estudo magnético e gamaespectrométrico da magnesita e formações ferríferas da Serra das Éguas, Brumado - BA**. 2019. 86 f. TCC (Graduação) - Curso de Geofísica, Instituto de Geociências, Universidade Federal da Bahia, Salvador, 2019.

NURALYKYZY, B.; NURZHAN, A.; LI, N.; HUANG, Q.; ZHU, Z.; AN, S. Influence of land use types on soil carbon fractions in the Qaidam Basin of the Qinghai-Tibet Plateau. **Catena**, v. 231, p. 107273, out. 2023. Elsevier BV. http://dx.doi.org/10.1016/j.catena.2023.107273.

PADARIAN, J.; MINASNY, B.; MCBRATNEY, A. B. Using deep learning for digital soil mapping. **Soil**, v. 5, n. 1, p. 79-89, 26 Feb. 2019. Copernicus GmbH. http://dx.doi.org/10.5194/soil-5-79-2019.

PARANAVITHANA, T.M.; ANAS, M.U.M.; KARUNARATNE, S.B.; MACDONALD, B.; WIMALATHUNGE, N.; BISHOP, T.F.A.; RATNAYAKE, R.R. Environmental factors and spatial dependence explain half of the inherent variation in carbon pools of tropical paddy soils. **Catena**, v. 231, p. 107278, out. 2023. Elsevier BV. http://dx.doi.org/10.1016/j.catena.2023.107278.

PELEGRINO, M.H.P.; SILVA, S.H.G.; MENEZES, M.D. de; SILVA, E. da; OWENS, P.R.; CURI, N. Mapping soils in two watersheds using legacy data and extrapolation for similar surrounding areas. **Ciência e Agrotecnologia**, v. 40, n. 5, p. 534-546, out. 2016. FapUNIFESP (SciELO). http://dx.doi.org/10.1590/1413-70542016405011416.

PELUCO, R.G.; MARQUES JÚNIOR, J.; SIQUEIRA, D.S.; PEREIRA, G.T.; BARBOSA, R.S.; TEIXEIRA, D. de B.; ADAME, C.R.; CORTEZ, L.A. Suscetibilidade magnética do solo e estimação da capacidade de suporte à aplicação de vinhaça. **Pesquisa Agropecuária Brasileira**, v. 48, n. 6, p. 661-672, jun. 2013. FapUNIFESP (SciELO). http://dx.doi.org/10.1590/s0100-204x2013000600012.

PHILLIPS, J.D. Identifying sources of soil landscape complexity with spatial adjacency graphs. **Geoderma**, v. 267, p. 58-64, abr. 2016. Elsevier BV. http://dx.doi.org/10.1016/j.geoderma.2015.12.019.

POEPLAU, C.; BOLINDER, M.A.; KÄTTERER, T. Towards an unbiased method for quantifying treatment effects on soil carbon in long-term experiments considering initial within-field variation. **Geoderma**, v. 267, p. 41-47, abr. 2016. Elsevier BV. http://dx.doi.org/10.1016/j.geoderma.2015.12.026.

RIBEIRO, B.T.; SILVA, S.H.G.; SILVA, E.A.; GUILHERME, L.R.G. Portable X-ray fluorescence (pXRF) applications in tropical Soil Science. **Ciência e Agrotecnologia**, Lavras, v. 41, n. 3, p. 245-254, jun. 2017. FapUNIFESP (SciELO). http://dx.doi.org/10.1590/1413-70542017413000117.

ROBINSON, D.A., HOCKLEY, N., DOMINATI, E., LEBRON, I., SCOW, K.M., REYNOLDS, B., EMMETT, B.A., KEITH, A.M., JONGE, L.W., SCHJØNNING, P., MOLDRUP, P., JONES, S.B., TULLER, M. Natural capital, ecosystem services, and soil change: why soil science must embrace an ecosystems approach. **Vadose Zone Journal**, v. 11, n. 1, 2012. http://dx.doi.org/10.2136/vzj2011.0051.

RODRIGUES, A.F.; LATAWIEC, A.E.; REID, B.J.; SOLÓRZANO, A.; SCHULER, A.E.; LACERDA, C.; FIDALGO, E.C.C.; SCARANO, F.R.; TUBENCHLAK, F.; PENA, I.

Systematic review of soil ecosystem services in tropical regions. **Royal Society Open Science**, v. 8, n. 3, mar. 2021. The Royal Society. http://dx.doi.org/10.1098/rsos.201584.

ROSSI, N. das G.; CANTON, L. C.; CAVALCANTE, R. M.; GOMES, F.H.; S. JUNIOR, I.G. de; COSTA, A.C.S. da. Susceptibilidade Magnética e Teores de Ferro Total de Solos do Estado de Rondônia. In: XII REUNIÃO SUL BRASILEIRA DE CIÊNCIA DO SOLO, 12., 2018, Xanxerê. **Anais [...].** Xanxerê: SBCS, 2018. p. 1-4.

SCHULER, U.; ERBE, P.; STAHR, K.; HERRMANN, L. A hybrid soil mapping approach using SOTER, SoLIM and Classification trees. In: World Congress of Soil Science: Soil Solutions for a Changing World, 19., 2010, Brisbane, Australia. **19th World Congress of Soil Science: Soil Solutions for a Changing World**. Brisbane, Australia: Published On Cdrom, 2010. p. 1-6.

SHI, J.; SONG, M.; YANG, L.; ZHAO, F.; WU, J.; LI, J.; YU, Z.; LI, A.; SHANGGUAN, Z.; DENG, L. Recalcitrant organic carbon plays a key role in soil carbon sequestration along a long-term vegetation succession on the Loess Plateau. **Catena**, v. 233, p. 107528, dez. 2023. Elsevier BV. http://dx.doi.org/10.1016/j.catena.2023.107528.

SHIRZADITABAR, F.; HECK, R.J. Characterization of soil drainage using electromagnetic induction measurement of soil magnetic susceptibility. **Catena**, v. 207, p. 105671, dez. 2021. Elsevier BV. http://dx.doi.org/10.1016/j.catena.2021.105671.

SIQUEIRA, D.S.; MARQUES, J.; PEREIRA, G.T.; TEIXEIRA, D.B.; VASCONCELOS, V.; CARVALHO JÚNIOR, O.A.; MARTINS, E.S. Detailed mapping unit design based on soil–landscape relation and spatial variability of magnetic susceptibility and soil color. **Catena**, v. 135, p. 149-162, dez. 2015. Elsevier BV. http://dx.doi.org/10.1016/ j.catena.2015.07.010.

SILVA, E.A.; WEINDORF, D.C.; SILVA, S.H.G.; RIBEIRO, B.T.; POGGERE, G.C.; CARVALHO, T.S.; GONÇALVES, M.G.M.; GUILHERME, L.R.G.; CURI, N. Advances in Tropical Soil Characterization via Portable X-Ray Fluorescence Spectrometry. **Pedosphere**, v. 29, n. 4, p. 468-482, ago. 2019a. http://dx.doi.org/10.1016/s1002-0160(19)60815-5.

SILVA, F.M.; SILVA, S.H.G.; ANDRADE, R.; COBLINSKI, J.A.; INDA, A.V.; FROSI, G.; LIMA, S. de S.F.; MENEZES, M.D. de; TAVARES, T.R.; GUILHERME, L.R.G. Proximal sensors for modeling clay mineralogy and characterization of soil textural fractions developed from contrasting parent materials. **Catena**, v. 241, p. 108053, jun. 2024. Elsevier BV. http://dx.doi.org/10.1016/j.catena.2024.108053.

SILVA, F.M.; WEINDORF, D.C.; SILVA, S.H.G.; SILVA, E.A.; RIBEIRO, B.T.; GUILHERME, L.R.G.; CURI, N. Tropical Soil Toposequence Characterization via pXRF Spectrometry. **Soil Science Society of America Journal**, v. 83, n. 4, p. 1153-1166, Jul. 2019b. Wiley. http://dx.doi.org/10.2136/sssaj2018.12.0498.

SILVA, S.H.G.; SILVA, E.A.; POGGERE, G.C.; PÁDUA JUNIOR, A.L.; GONÇALVES, M.G.M.; GUILHERME, L.R.G.; CURI, N. Modeling and prediction of sulfuric acid digestion

analyses data from PXRF spectrometry in tropical soils. **Scientia Agricola**, v. 77, n. 4, p. 1-12, jan. 2020a. FapUNIFESP (SciELO). http://dx.doi.org/10.1590/1678-992x-2018-0132.

SILVA, S.H.G.; TEIXEIRA, A.F. dos S.; MENEZES, M.D. de; GUILHERME, L.R.G.; MOREIRA, F.M. de S.; CURI, N. Multiple linear regression and random forest to predict and map soil properties using data from portable X-ray fluorescence spectrometer (pXRF). **Ciência e Agrotecnologia**, v. 41, n. 6, p. 648-664, dez. 2017. FapUNIFESP (SciELO). http://dx.doi.org/10.1590/1413-70542017416010317.

SILVA S.H.G.; WEINDORF D.C.; FARIA W.M.; PINTO L.C.; MENEZES M.D.; GULHERME, L.R.G.; CURI, N. Proximal sensor-enhanced soil mapping in complex soil-landscape areas of Brazil. **Pedosphere**, v. 31 n. 4, p. 615–626, 2021.

SILVA, S.H.G.; WEINDORF, D.C.; PINTO, L.C.; FARIA, W.M.; ACERBI JUNIOR, F.W.; GOMIDE, L.R; MELLO, J.M. de; PÁDUA JUNIOR, A.L. de; SOUZA, I.A. de; TEIXEIRA, A.F. dos S.; GUILHERME, L.R.G.; CURI, N. Soil texture prediction in tropical soils: a portable x-ray fluorescence spectrometry approach. **Geoderma**, v. 362, p. 114136, mar. 2020b. Elsevier BV. http://dx.doi.org/10.1016/j.geoderma.2019.114136.

SILVA, S.H.G.; HARTEMINK, A.E.; TEIXEIRA, A.F. dos S.; INDA, A.V.; GUILHERME, L.R.G.; CURI, N. Soil weathering analysis using a portable X-ray fluorescence (PXRF) spectrometer in an Inceptisol from the Brazilian Cerrado. **Applied Clay Science**, v. 162, p. 27-37, set. 2018. Elsevier BV. http://dx.doi.org/10.1016/j.clay. 2018.05.028.

SILVA, S.H.G.; POGGERE, G.C.; MENEZES, M.D.; CARVALHO, G.S.; GUILHERME, L.R.G.; CURI, N. Proximal sensing and digital terrain models applied to digital soil mapping and modeling of Brazilian Latosols (Oxisols). **Remote Sens**., v. 8, p. 614–635, 2016. http://dx.doi.org/10.3390/rs8080614.

SIMONETT, D.S. **Soil genesis in basalt in North Queensland.** Transactions of the 7th International Congress of Soil Science, Madison, Wisconsin. 1960, p. 238– 243.

STEVANATO, M.; PAROLIN, M.; CAMARGO FILHO, M.; PAROLIN, E.S. de P. Paleossolos brasileiros – o estado da arte. **Revista da Anpege**, v. 17, n. 33, p. 128-145, 2 dez. 2021. ANPEGE - Revista. http://dx.doi.org/10.5418/ra2021.v17i33.11897.

STOCKMANN, U.; CATTLE, S.R.; MINASNY, B.; MCBRATNEY, A.B. Utilizing portable X-ray fluorescence spectrometry for in-field investigation of pedogenesis. **Catena**, v. 139, p. 220-231, abr. 2016. Elsevier BV. http://dx.doi.org/10.1016/j.catena.2016.01.007.

SUN, F.; BAKR, N.; DANG, T.; PHAM, V.; WEINDORF, D. C.; JIANG, Z.; LI, H.; WANG, Q. Enhanced soil profile visualization using portable X-ray fluorescence (pXRF) spectrometry. **Geoderma**, v. 358, p. 1-11, jan. 2020. Elsevier BV. http://dx.doi.org/10.1016/j.geoderma.2019.113997.

SWANHART, S.; WEINDORF, D.C.; CHAKRABORTY, S.; BAKR, N.; ZHU, Y.; NELSON, C.; SHOOK, K.; ACREE, A. Soil Salinity Measurement Via Portable X-ray Fluorescence Spectrometry. **Soil Science**, v. 179, n. 9, p. 417-423, set. 2014. Ovid Technologies (Wolters Kluwer Health). http://dx.doi.org/10.1097/ss.0000000000000088.

TAGHIZADEH-MEHRJARDI, R.; SCHMIDT, K.; AMIRIAN-CHAKAN, A.; RENTSCHLER, T.; ZERAATPISHEH, M.; SARMADIAN, F.; VALAVI, R.; DAVATGAR, N.; BEHRENS, T.; SCHOLTEN, T. Improving the Spatial Prediction of Soil Organic Carbon Content in Two Contrasting Climatic Regions by Stacking Machine Learning Models and Rescanning Covariate Space. **Remote Sensing**, v. 12, n. 7, p. 1095, 29 mar. 2020. MDPI AG. http://dx.doi.org/10.3390/rs12071095.

TEIXEIRA, A.F. dos S.; WEINDORF, D.C.; SILVA, S.H.G.; GUILHERME, L.R.G.; CURI, N. Portable X-ray fluorescence (pXRF) spectrometry applied to the prediction of chemical attributes in Inceptisols under different land uses. **Ciência e Agrotecnologia**, v. 42, n. 5, p. 501-512, set. 2018. FapUNIFESP (SciELO). http://dx.doi.org/10.1590/1413-70542018425017518.

TEIXEIRA, A.F. dos S.; SILVA, S.H.G.; WEINDORF, D.C.; CHAKRABORTY, S.; CARVALHO, T.S. de; SILVA, A.O.; GUIMARÃES, A.A.; MOREIRA, F.M. de S. Microbiological indicators of soil quality predicted via proximal and remote sensing. **European Journal of Soil Biology**, v. 104, p. 103315, abr. 2021.

WEINDORF, D.C., BAKR, N., ZHU, Y. Advances in portable X-ray fluorescence (PXRF) for environmental, pedological, and agronomic applications. **Adv. Agron**., v. 128, p. 1–45, 2014. http://dx.doi.org/10.1016/B978-0-12-802139-2.00001-9.

WRIGHT, V.P. Chapter 12 Paleosol Recognition: a guide to early diagenesis in terrestrial settings. **Developments in Sedimentology**, p. 591-619, 1992. Elsevier. http://dx.doi.org/10.1016/s0070-4571(08)70574-0.

ZADEH, L.A. Fuzzy sets. **Information and Control**, v. 8, p. 338-353, jan. 1965.

ZAWADZKI, J.; FABIJAńCZYK, P.; MAGIERA, T.; RACHWAł, M. Micro-scale spatial correlation of magnetic susceptibility in soil profile in forest located in an industrial area. **Geoderma**, v. 249-250, p. 61-68, jul. 2015. Elsevier BV. http://dx.doi.org/10.1016 /j.geoderma.2015.02.008.

ZHOU, Y.; ZHANG, Z.; RAO, J.; CHEN, B. Predicting and mapping soil magnetic susceptibility in an agro-pastoral transitional zone: influencing factors and implications. **Soil and Tillage Research**, v. 219, p. 105352, maio 2022. Elsevier BV. http://dx.doi.org/10.1016/j.still.2022.105352.

ZHU, A.X.; HUDSON, B.; BURT, J.; LUBICH, K.; SIMONSON, D. Soil mapping using GIS, expert knowledge, and fuzzy logic. Science Society of America Journal v. 65, p. 1463-1472, 2001.

ZHU, Y.; WEINDORF, D.C.; ZHANG, W. Characterizing soils using a portable X-ray fluorescence spectrometer: 1. soil texture. **Geoderma**, v. 167-168, p. 167-177, nov. 2011. Elsevier BV. http://dx.doi.org/10.1016/j.geoderma.2011.08.010.

PART II: Articles

CHAPTER I:

Paleosol marked by contrasting formation processes: A pilot study using digital morphometrics in Southeastern Brazil

*Article published at **Catena** in January 2024.

https://doi.org/10.1016/j.catena.2023.107550

Fernanda Almeida Bócoli[a], Sérgio Henrique Godinho Silva[a], Junior Cesar Avanzi[a], Bruno Montoani Silva[a], Vanêssa Lopes de Faria[a], Maria Cecília Vieira Totti[a], Alberto Vasconcellos Inda[b], Gustavo Frosi[b], Suane de Souza Franco Lima[b], Alexandre Uezu[c], Marco Aurélio Carbone Carneiro[a], Marta Vasconcelos Ottoni[d], Nilton Curi[a]*

[a]Department of Soil Science, Federal University of Lavras, Lavras, Minas Gerais 37.200-900, Brazil

[b]Department of Soils, Agronomy Faculty, Federal University of Rio Grande do Sul, Porto Alegre, Rio Grande do Sul 90.001-970, Brazil

[c]Faculty for Environmental Conservation and Sustainability (ESCAS), IPˆE—Institute for Ecological Research, 47 km of Dom Pedro I highway, Nazaré Paulista, São Paulo 12960-000, Brazil

[d]Department of Hydrology, Geological Survey of Brazil (SGB), Rio de Janeiro, RJ, Brazil

*Corresponding author: niltcuri@ufla.br (N. Curi).

ABSTRACT

Although soil formation results from the interactions of five classical factors and various pedogenic processes, such interactions can drastically change over time, which may be recorded in the so-called Paleosols. These soils may be formed under contrasting environmental conditions. Given the study of Paleosols be rare in Brazil, this pilot study aimed to detail the morphological, physical, chemical (including elemental content and magnetic susceptibility (MS)), and mineralogical properties of a Paleosol with contrasting paleo- and current-drainage conditions, derived from sandstone having pellitic (fine) sediments intermixed, with support via digital morphometrics. Samples were collected in a regular grid of 15x15 cm along the soil profile down to 1.8 m depth. The soil samples were analyzed via portable X-ray fluorescence (pXRF) spectrometry and for assessment of magnetic susceptibility (MS), texture, fertility, and organic matter content. The mineralogy of the clay, silt, and sand fractions were determined via X-ray diffraction analyses. The pXRF and MS results were spatialized to the Paleosol profile. The first 108 cm of the soil profile are well-drained having reddish colors, contrasting with the underlying poorly- drained unity having greyish colors. The MS values were higher in the first 108 cm of the soil profile, reaching the lowest values in the 2Cg horizon at 142–180 cm depth. Quartz was the main mineral in sand and silt fractions, while kaolinite largely dominates the clay fraction in association with hematite. In the 2Cg horizon, the absence of hematite is related with the paleoredoximorphic conditions there. The Ti/Zr ratio indicated differences in parent materials of the reddish and greyish units of the Paleosol. The midslope position of the Paleosol makes colluvial deposition unlikely. The combined use of pXRF, MS, morphological, physical, chemical, and mineralogical analyses provided valuable details on the variation of the contrasting formation processes of the Paleosol studied.

Keywords: Ancient soils; Proximal sensors; Oxidation; Reduction; Spatial variability.

1 Introduction

Soil systems are complex, resulting from the interactions among the soil forming factors (Jenny, 1941) coupled with specific pedogenic processes (Phillips, 2016; Schaetzl and Anderson, 2005). Although changes caused by these interactions occur continually in time, some soils have conserved features anciently developed during their formation; they are the so-called Paleosols. The concept adopted in this paper considers a Paleosol as a soil that formed on a landscape in the past, with distinctive morphological properties resulting from a soil-forming environment that no longer exists at the site (Soil Science Society of America, 2008). Paleosols can help in describing paleoenvironments, paleoclimates, evidences of old geomorphological surfaces, paleopedogenic processes, and inferences about the paleoarchaeology (Ladeira, 2010).

In Brazil, the records of Paleosols are rare (Stevanato et al., 2021). Previous studies have been conducted in south and southeastern regions (Nascimento et al., 2017; Silva et al., 2017). Such soils are more commonly found in places that have undergone more recent glaciation, active volcanism or tectonism, climate change, high fluctuations of the sea level, and ancient alluvial or lacustrine deposition (Ladeira, 2010; Wright, 1992), among others.

Given the increasing variety of new tools to characterize soils, new approaches have emerged to investigate a soil profile in more detail, such as the digital soil morphometrics. This approach has provided different perspectives on the detailed study of soil profiles (Hartemink and Minasny, 2014). Thus, proximal sensors have allowed additional insights on soil genesis besides the spatial variation of soil properties within a

soil profile (Grauer-Gray and Hartemink, 2018; Mancini et al., 2021; Silva et al., 2018; Sun et al., 2020).

Among the proximal sensors, portable X-ray fluorescence (pXRF) spectrometry and magnetic susceptibility (MS) measurements have been capable of refining the variability of morphological properties within and in between soil horizons (Bócoli et al., 2023; Grauer-Gray and Hartemink, 2018; Mancini et al., 2021; Silva et al., 2018; Sun et al., 2020). While the former delivers elemental contents present in the samples, the latter measures the magnetic susceptibility, which is related to soil mineralogy, especially ferrimagnetic minerals, such as magnetite and maghemite (Curi et al., 1984). These properties may be related to several other features of soils besides factors and processes of formation (Mello et al., 2020).

Due to intense erosion, mainly associated to humid conditions, the Brazilian landscape has substantially changed over time, including interruptions in the geological column in some states (Resende et al., 2019). So, some soils are located on current landscapes, which are in disagreement with their morphology. In this study, the redoximorphic features below the reddish A and B horizons (0–108 cm) are anomalous with the midslope position of the soil studied, raising the possibility of this unity (portion of the soil profile) may be formed under a more gentle paleorelief, in which the water table was high in the soil profile. Subsequent landscape dissection and drainage improvement may explain the current overlying reddish unity. The ancient redoximorphic processes in the soil profile supports the interpretation of a Paleosol (Soil Science Society of America, 2008).

This pilot study aims to detail the characterization of properties related to the contrasting pedogenesis processes of a Paleosol profile, containing hydromorphic features at the lower part of the profile, contrasting with overlying well-drained soil

horizons, derived from sandstone with pellitic sediments intermixed, in Southeastern Brazil, through a combination of morphological, physical, chemical, mineralogical, and proximal sensors (pXRF and MS) analyses. The main hypothesis is that the combination of such techniques, via digital soil morphometrics, may provide additional details to field morphology, highlighting the understanding of the paleo- and current-soil forming processes involved. The novelty of this study encompasses the linking of the findings of this Paleosol to the evolution of the landscape and to the estimation of climate change impacts, besides this soil being rarely found in tropical regions, mainly considering their contrasting redoximorphic features, comprising the first Paleosol investigation via digital morphometrics under such conditions.

2 Material and methods

2.1 Soil location and sampling

The selected Paleosol, which was very difficult to access and sample, consists of a rare finding in Brazil that deserves this detailed characterization, constituting a pilot study. This Paleosol profile is located at the Pontal do Paranapanema region (Fig. 1), western São Paulo state, Brazil. It was classified as typic Dystrophic Tb Haplic Cambisol, following the Brazilian Soil Classification System (SiBCS) (Santos et al., 2015a; 2018), corresponding to Oxic Dystrustept per the US Soil Taxonomy (Soil Survey Staff, 2014), Dystric Rhodic Cambisol (Loamic, Ochric) per the World Reference Base (FAO, 2022), and Cambosol Ustic per Chinese Soil Taxonomy (CRG-CST, 2001), intermediary to a typic eutrophic Tb Haplic Gleysol (per SiBCS), Aeric Endoaquent (per US Soil Taxonomy), Eutric Gleysol (Loamic, Ochric) (per WRB), and Gleysol Orthic (per Chinese Soil Taxonomy).

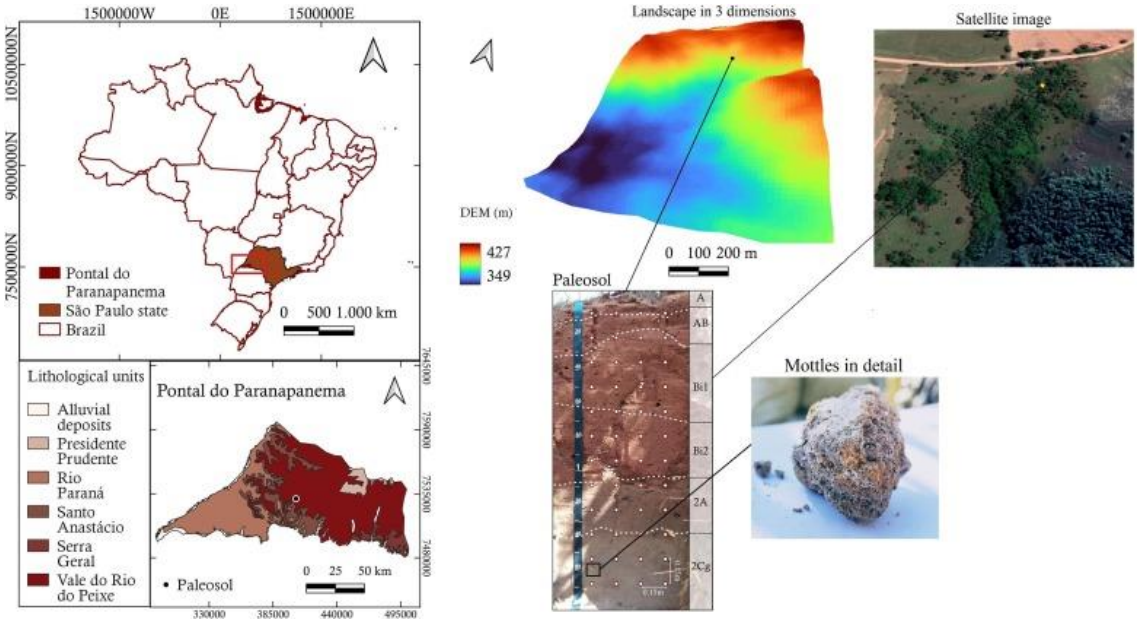

Fig. 1. Location of the Paleosol studied, sampling points within the profile, and regional lithological units from Pontal do Paranapanema region, São Paulo state, Brazil. Dashed lines represent the boundaries of the soil horizons delineated in the field.

The Paleosol is situated at the latitude 7,530,747 S and longitude 404,737 W, UTM, zone 22 K, *datum* SIRGAS 2000. It occupies the midslope position on a landscape with a gently undulated relief (7% slope). The climate of the region is Aw, framed as a tropical, in which the summer is rainy with average temperatures above 22 ◦C, and the winter is dry (Alvares et al., 2013). The soil profile was developed primarily from sandstone of the Bauru Group, Adamantina Formation, included in the Vale do Rio do Peixe lithological unit (Fig. 1). In such sandstones, mixture of pellitic sediments are common. These fine layers have much lower permeability than the sandstone. According to Stradioto and Chang (2020), this sandstone is mainly composed of quartz and feldspars and have micas and augite as the main accessory minerals. The native vegetation is represented by the semi-perennial tropical forest (Oliveira-Filho and Fontes, 2000).

2.2 Soil sampling and laboratory analyses

Soil samples were collected to 1.8 m of depth, on a regular grid design of 15x15 cm, comprising a total of 48 samples. This grid interval was adopted after evaluating the morphological features during the field work and based on the range of grid intervals found in the literature (Zhang and Hartemink, 2017; Sun et al., 2020, Mancini et al., 2023). Soil horizons were identified and morphologically described according to the Manual for Description and Sampling of Soil in the Field (Santos et al., 2015b).

Composite samples, obtained after careful mixing of four simple samples collected at each depth, were air-dried and gently sieved (2 mm) to obtain the air-dried fine earth (ADFE) fraction, and then submitted to the following chemical and physical analyses: pH in water, using a Digimed® (São Paulo, Brazil) pH-meter model DM-23-DC (Donagema et al., 2011), exchangeable contents of Ca^{2+}, Mg^{2+}, and Al^{3+}using a 1 mol/L KCl extraction solution (Mclean et al., 1958), available contents of K^{+} and P using the Mehlich-1 extraction solution (Mehlich, 1953), H +Al using the SMP extractor (Shoemaker et al., 1961); soil organic matter (SOM) following Nelson and Sommers (1996), and using the van Bemmelen factor (1.724); remaining P (P- Rem) content, which refers to P content not adsorbed by soil organic and mineral particles (Alvarez et al., 2000) (all quantifications were performed via inductively coupled plasma optical emission spectroscopy, model Spectro Blue, Spectro Analytical Instruments, Germany); and particle size analysis by the pipette method (Gee and Bauder, 1986). The sand fraction was later separated into: very coarse (2–1 mm), coarse (1–0.5 mm), medium (0.5–0.25 mm), fine (0.25–0.105 mm), and very fine (<0.105 mm) sand, using dry sieving. Effective cation exchange capacity, cation exchange capacity at pH 7, sum of bases, base saturation, and Al^{3+} saturation were calculated based on the previous analyses.

2.2.1 Analyses via portable X-ray fluorescence (pXRF) spectrometry and magnetic susceptibility (MS) measurements

Twenty grams of ADFE of each collected sample (48 samples in total) were irradiated using a portable X-ray fluorescence (pXRF) spectrometer, Bruker® model Tracer 5g, connected to power line, containing a 50 keV and a 100 μA Rh X-ray tube using the "Soil" mode. The analyses were performed in triplicate, during 60 s each (Silva et al., 2021; Weindorf and Chakraborty, 2016). Then, the mean elemental contents of the triplicates per sample were calculated and used in further analyses. The calibration of the equipment was performed using a check sample (CS) provided by the manufacturer and two samples certified by the National Institute of Standards and Technology (NIST) (2710a and 2711a). The recovery values (Koch et al., 2017) (content reported by the pXRF/certified content ×100) were (2710a/2711a/CS): Al – 84/73/92; Ca – 39/45/–; Cr - –/107/–; Cu – 81/69/91; Fe – 71/65/88; K – 60/46/ 83 (41 mg/kg); Mg (–/65/–); Mn – 68/60/82; P (214/234/–); Si – 57/ 48/87; Ti – 77/65/–; V – 51/27/–; Zn – 87/82/– (3 mg/kg); Zr (85/–/–). The dashed lines indicate either no result by pXRF or no certified content in the material.

For magnetic susceptibility (MS) measurements, 10 g of ADFE of each collected sample were analyzed in triplicate with a Bartington MS2B susceptibilimeter at low (LF) and high (HF) frequencies, according to Dearing (1999). The results are expressed on a mass-normalized basis, applying the following equation:

$$MS(\chi) = \chi LF \text{ or } \chi HF \text{ result/sample weight} \quad (1)$$

where: MS =magnetic susceptibility (x 10^{-7} m^3 kg^{-1}); χLF and χHF result = result obtained for low and high frequency, respectively; and sample weight (g).

The difference of the results obtained at high and low frequencies (FD) was calculated per soil particle size fraction as follows:

$$FD\% = [(\chi LF \text{ or } \chi HF)\ \chi LF] \times 100 \qquad (2)$$

These calculations contribute to the identification of ferrimagnetic minerals, since the reflection of the maghemite peaks in X-ray diffraction (XRD) analysis may coincide with the hematite peaks (Poggere et al., 2018).

2.2.2 X-ray diffraction (XRD) analysis

Samples of coarse sand, fine sand, silt, and clay fractions were gently macerated in an agate mortar to obtain homogeneous non-oriented powder 600 mg samples (Brindley and Brown, 1980), passed through a 0, 25 mm sieve. After that, they were analyzed with a Bruker D2 PHASER diffractometer, in which the irradiation varied from 4 to 52º 2θ at 0.02º 2θ s^{-1}. This diffractometer is equipped with the LYNXEYETM, a practically instantaneous linear model, which uses the DIFFRAC. SUITE™ software to obtain the XRD patterns. The results were interpreted with the help of tables prepared by Brindley and Brown (1980).

2.3 Spatial evaluation of the soil profile

The elemental contents determined via pXRF and the MS values were spatialized to the soil profile utilizing the multilevel B-spline method (Lee et al., 1997), within the software QGIS 3.22 (QGIS Development Team, 2022). This procedure contributes to better visualize the variation of such measurements along the soil profile, within and in between soil horizons (Hartemink et al., 2020).

3 Results and discussions

3.1 Soil morphology, fertility, texture and magnetic susceptibility analyses

By analyzing the soil profile in the field, it is noteworthy that two opposing processes occurred under different time periods. The first 108 cm of the profile is marked by oxidation conditions (favoring the formation of hematite that caused the red color of soil matrix), while redoximorphic conditions occurred in the 108–180 cm of the profile, producing greyish colors in the 2Cg horizon (Table 1). For the formation of hematite, oxidation conditions are required in combination with higher availability of Fe(III), favored by free drainage (Kämpf et al., 2012).

The soil underneath presents a 2A horizon (108–142 cm) (Table 1), followed by gleyzation features in the deeper portions of the profile. This part of the soil profile was probably formed on an ancient, gentler landscape, which was, later on, dissected by water erosion (Resende et al., 2021).

Given the greyish color of the lowest part of the soil profile (142–180 cm) (Table 1), below the 2A horizon, probably this soil occupied an area more gentle and prone to accumulation of water, favored by the pellitic sediments intermixed with the sandstone, causing the gleization process (Barbosa et al., 2019). The small red and red-yellow mottles observed in this soil horizon support the possibility of perched water table oscillation (Kämpf and Curi, 2000). Interestingly, its actual location on the landscape (midslope position with 7% slope) does not favor water accumulation, indicating a probable change on the landscape from the time this unity was formed to the present day. Resende et al. (2019) stated that the landscape in Brazil has changed a lot as a function of intense water erosion. This erosion has been so effective that some strata of the

geologic column, which are quite common in another parts of world, are absent in a substantial portion of Brazil.

Table 1. Synthetic morphological description of the studied soil profile from Pontal do Paranapanema, São Paulo state, Brazil.

Horizon	Depth (cm)	Soil Color* (moist)		Structure
A	0-12	2.5YR 3/2	Dusky red	Granular
AB	12-23	2.5YR 3/3	Dark reddish brown	Granular
Bi1	23-65	2.5YR 3/4	Dark reddish brown	Granular
Bi2	65-108	2.5YR 3/6	Dark red	Granular
2Ab	108-142	7.5YR 3/4	Dark brown	Subangular blocky
2Cg	142-180 cm+	10YR 5/2	Grayish brown	Massive

*Soil color by the Munsell Soil Color Chart.

Soil pH varied from 4.8 to 6.0, and the lower values were mainly found in the upper part of the soil profile (Table 2). This part has been submitted to weathering-leaching causing acidification, a common feature of most Brazilian soils (Resende et al., 2021). Conversely, the unity below presented greater contents of nutrients, highlighting the almost twice greater contents of exchangeable Ca^{2+} and Mg^{2+}, greater cation exchange capacity at pH 7, sum of bases, and pH values. Available P content was null in all depths evaluated, except for the first one, probably related to nutrient recycling by vegetation, although it was very low (0.02 mg dm^{-3}). Low or null contents of exchangeable Al^{3+}were found in all soil samples, probably related to its consumption during the formation of kaolinite, feldspars, and mica (see Fig. 5). The SOM content decreased from the A to Bi2 horizon and then sharply increased in the 2A horizon (from 0.35 to 0.89 dag kg^{-1}), corroborating the latter designation during the morphological description and sampling. This variation of SOM content serves as a registration of the alteration from a paleo-more gentle landscape, favoring water and, hence, SOM accumulation (confirmed by greater

SOM contents), to a current more undulated landscape that prevents water accumulation, decreasing the SOM contents found in the current surface of the profile.

Table 2. Results of soil fertility analyses of the studied soil profile, from Pontal do Paranapanema, São Paulo state, Brazil.

Depth	pH	K^+	P	Ca^{2+}	Mg^{2+}	Al^{3+}	H+Al	SB	t	T	BS	Al sat	SOM	P-Rem
cm		--mg dm^{-3}--		---------- $cmol_c\,dm^{-3}$ ----------							----- % -----		dag kg^{-1}	mg L^{-1}
0-10	5.2	70.03	0.02	0.76	0.35	0.0	1.8	1.29	1.29	3.09	41.73	0.00	0.73	50.8
10-25	4.8	63.77	0.00	0.65	0.27	0.1	3.6	1.08	1.18	4.68	23.15	8.47	0.43	44.8
25-40	5.2	61.92	0.00	0.67	0.36	0.1	1.7	1.19	1.29	2.89	41.13	7.75	0.39	42.3
40-55	5.3	57.04	0.00	0.97	0.28	0.0	1.6	1.40	1.40	3.00	46.54	0.00	0.42	43.1
55-70	5.5	59.9	0.00	0.79	0.19	0.1	1.6	1.13	1.23	2.73	41.52	8.13	0.53	50.3
70-85	5.4	57.25	0.00	0.84	0.21	0.0	2.8	1.20	1.20	4.00	29.92	0.00	0.40	49.0
85-100	5.4	56.59	0.00	0.99	0.23	0.0	1.4	1.37	1.37	2.77	49.28	0.00	0.35	52.4
100-115	5.2	64.99	0.00	1.84	0.5	0.0	1.9	2.51	2.51	4.41	56.84	0.00	0.89	46.9
115-130	5.5	63.80	0.00	1.82	0.64	0.0	2.4	2.62	2.62	5.02	52.26	0.00	0.85	50.9
130-145	5.9	61.28	0.00	1.33	0.52	0.0	1.3	2.01	2.01	3.31	60.64	0.00	0.33	59.9
145-160	6.0	78.92	0.00	1.32	0.53	0.0	1.3	2.05	2.05	3.35	61.26	0.00	0.32	63.3
160-175	5.1	60.96	0.00	1.30	0.46	0.0	2.2	1.92	1.92	4.12	46.51	0.00	0.27	44.8

SB: sum of bases; t: effective cation exchange capacity; T: cation exchange capacity at pH 7; BS: base saturation; Al sat: saturation by Al^{3+}; SOM: soil organic matter; and P-Rem: remaining P.

The particle size distribution of the soil profile (Table 3) showed the highest sand contents in the deepest sample collected, where the fine sand fraction is predominant (~60 %). Also, the fine sand and silt contents are very different in various portions of the profile, indicating a possible variation of the soil parent material (Resende et al., 2014). While medium sand contents were homogenous in depth, the total sand fraction varied between the upper portion (from 61 to 79 %) and the lower portion of the soil profile (from 78 to 90 %). The clay contents ranged from 8.0 to 20 %; the highest contents occurred in the upper portion of the soil profile. More importantly, the clay content in the lower portion is considerably lower, reaching half of the lowest content (8 %) found in the upper portion of the soil profile (16 %). Silt contents were also divergent in the soil profile, varying from 1 % in the lower portion to 21 % in the upper portion. This fraction content is highest at the depth of 70 cm (21 %) and the lowest values are found in the

lower portion of the soil profile. The silt/clay ratio being equal or higher than 0.7 in the Bi1 and Bi2 horizons excludes the classification of this soil as Latosol (Santos et al., 2015a; Santos et al., 2018), indicating this soil did not suffer a high degree of weathering.

Table 3. Texture analyses of the studied soil profile, from Pontal do Paranapanema, São Paulo state, Brazil.

Depth	Clay	Silt	Very coarse sand	Coarse sand	Medium sand	Fine sand	Very fine sand	Total sand	Silt/clay ratio
cm	----------	----------	----------	----------	%----------	----------	----------	----------	
0-10	17	9	0	0	6	51	17	74	0.55
10-25	19	2	0	1	6	55	17	79	0.12
25-40	19	17	0	1	6	37	20	65	0.89
40-55	20	14	0	2	6	37	21	66	0.73
55-70	18	21	0	0	6	35	20	61	1.20
70-85	16	13	0	0	6	41	24	71	0.78
85-100	15	15	0	0	6	40	24	71	1.01
100-115	16	7	0	0	6	45	26	78	0.43
115-130	15	5	0	0	6	50	24	81	0.32
130-145	10	1	0	2	6	58	23	89	0.08
145-160	8	2	0	1	6	60	23	90	0.21
160-175	9	1	0	2	6	60	22	90	0.08

The magnetic susceptibility (MS) analysis of A and Bi1 soil horizons indicated magnetic minerals in all the particle size fractions, with the greatest contents in the clay fraction (Table 4). In the clay fraction, the MS values doubled from the A to the Bi1 horizon, which may indicate some lateral loss of clay from the A horizon (Table 3) (Gonçalves et al., 2019), with possible removal of some maghemite.

In the coarse sand fraction of the A horizon, the same values for low and high frequencies of MS, with consequent null value of FD % (Table 4), indicate the presence of only macro-sized multidomain (MD) ferrimagnetic minerals of lithogenic origin in this soil fraction (Preetz et al., 2017). In the Bi1 horizon, the FD value of 12.2 % suggests the predominance of ultrafine-grained ferrimagnetic minerals formed during pedogenesis (super-paramagnetic – SP – minerals) (Preetz et al., 2017).

Table 4. Magnetic susceptibility (χ) in low frequency (χ_{LF}), high frequency (χ_{HF}) and the frequency difference (FD) per granulometric fraction and per the air-dried fine earth (ADFE) of the studied profile, from Pontal do Paranapanema, São Paulo state, Brazil.

χ	Horizon	Coarse sand	Fine sand	Silt	Clay	ADFE
	A	8.6	5.2	3.9	52.4	10.1
χ_{LF}	Bi1	5.6	1.9	15.3	104.7	20.5
	2Ab	0.0	0.7	16.9	35.0	6.2
($x10^{-7}$ m^3 kg^{-1})	2Cg	0.0	0.7	3.9	4.8	1.3
	A	8.6	4.7	3.6	44.4	9.0
χ_{HF}	Bi1	4.9	1.6	14.1	88.6	17.7
	2Ab	0.0	0.7	15.7	30.3	5.6
($x10^{-7}$ m^3 kg^{-1})	2Cg	0.0	0.7	3.9	4.2	1.2
	A	0.0	0.5	0.3	8.0	1.1
χ_{FD}	Bi1	0.7	0.3	1.2	16.0	2.8
(χ_{LF} - χ_{HF})	2Ab	0.0	0.0	1.2	4.7	0.6
($x10^{-7}$ m^3 kg^{-1})	2Cg	0.0	0.0	0.0	0.6	0.1
	A	0.0	9.1	8.6	15.3	10.9
FD	Bi1	12.2	17.6	8.0	15.3	13.7
	2Ab	0.0	0.0	7.1	13.5	9.7
(%)	2Cg	0.0	0.0	0.0	12.5	8.3

In the silt fraction of the A and Bi1 soil horizons, values of FD of 8.6 and 8.0 %, respectively, suggest similar proportions of MD and SP minerals, while in the clay fraction, the FD value of 15.3 % indicates substantial predominance of SP minerals. In the silt fraction of the 2A horizon, the FD value of 7.1 % suggests equilibrium between MD and SP minerals, while in the clay fraction the value of FD of 12.5 % indicates predominance of SP minerals.

In the coarse and fine sand fractions of 2A and 2Cg soil horizons, the MS values of 0 and $0.7x10^{-7}$ m^3 kg^{-1} indicate absence and only traces of magnetic minerals, respectively (Dearing, 1999). The much lower values of MS in the silt and clay fractions of the 2Cg soil horizon (Table 4) is in agreement with the paleoredoximorphic conditions prevailing there, causing destabilization and removal of magnetite from the silt fractionand maghemite from the clay fraction of the Paleosol (Kämpf and Curi, 2000; Resende et al., 2011). This process is caused by the reduction of Fe (III) to Fe(II) under

reduction conditions (waterlogging preventing appropriate amounts of oxygen in soil pores), dismantling Fe(III)- bearing minerals, such as the magnetic ones (magnetite and maghemite), besides hematite and goethite (Kämpf and Curi, 2000; Schaetzl and Anderson, 2005); thus, it provides the greyish color and the low MS values of the 2Cg horizon.

The spatialization of MS data (Fig. 2) showed variation across the soil profile (the data presented in Figs. 2, 3 and 4 to be discussed later, may assist in horizons recognition and boundaries definition). The higher MS values were found in the Bi horizon. Probably the lower MS values in the A horizon are related to the greater content of SOM, which tends to reduce MS. Dearing (1999) classified the SOM as diamagnetic, presenting a weak or even negative susceptibility, reducing the final MS value of matrices presenting higher SOM contents. Moreover, the lowest MS values were found at 115–175 cm depth, indicating that this portion of the soil profile has the lowest contents of magnetic minerals, corroborating the hypothesis that it was formed under paleoredoximorfic conditions. As such, these conditions tend to destabilize the magnetic minerals, by reducing the Fe(III) to Fe(II) forms (Kämpf and Curi, 2000), with consequent removal. Shirzaditabar and Heck (2021), studying soils with different drainage conditions, found lower MS values for hydromorphic soils and higher values for well-drained soils, similar to the findings for the Gleysol and the Cambisol unities of the soil profile studied herein. There is a small part of the 2A horizon at its right superior side with contrasting much higher FD % values (Fig. 2), which may indicate that this part is more related to the Bi1 horizon situated above. It was not observed any indication of such difference during the field morphological analysis.

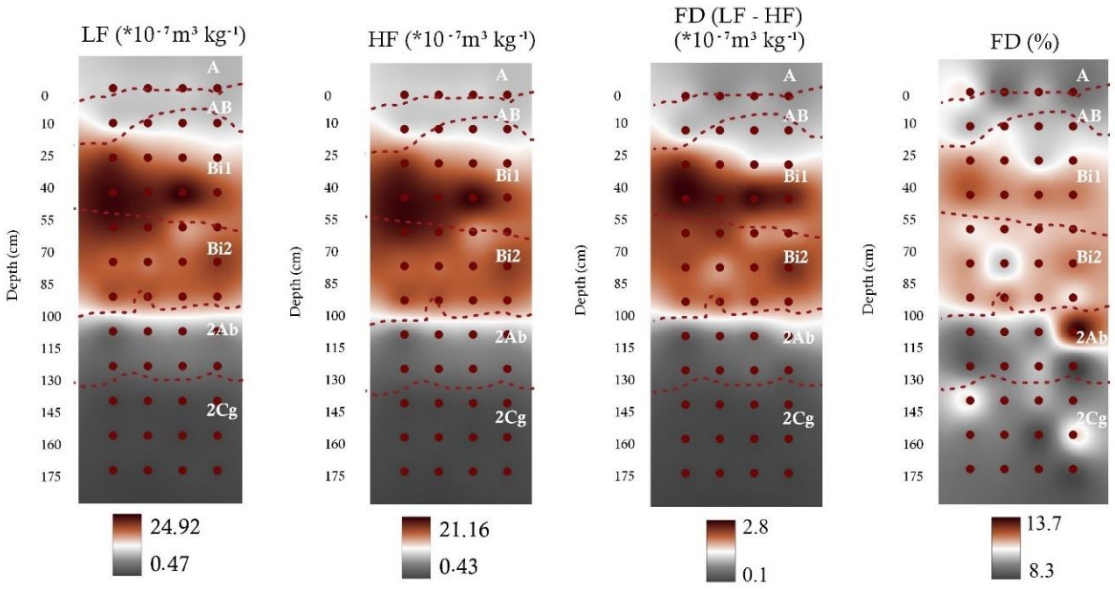

Fig. 2. Spatial representation of magnetic susceptibility data in low frequency (LF), high frequency (HF), and the frequency difference (FD) of the studied profile from Pontal do Paranapanema, São Paulo state, Brazil.

When comparing the MS values of ADFE, the lowest values were found for the 2Cg horizon, probably related to the instability of the magnetic minerals under paleoredoximorphic conditions (Kämpf and Curi, 2000; Resende et al., 2011). The increase of low and high frequency values of MS for the A to the Bi1 soil horizons reinforces the indication of lateral loss of clay from the A horizon (Gonçalves et al., 2019), with removal of some magnetite and maghemite.

3.2 Portable X-ray fluorescence (pXRF) and X-ray diffraction (XRD) analyses

The variation of the elemental contents detected by pXRF in the soil profile (Fig. 3) shows that some elements have a clear pattern of distribution. For instance, K increased downwards, starting from 115 cm of depth, coinciding with the 2A horizon of the soil. This increment is not associated with increasing available K content (Table 2), probably because K constitutes part of the crystalline structure of feldspars and mica (Fig. 5). The

P and Zn had low variations along the soil profile, presenting low contents. The Ca, Mg, and Si contents decreased until a certain depth (Ca and Mg between 85–100 cm and Si at ~ 55 cm) and then increased again. Different from K, Ca and Mg contents increased in depth in accordance to the increase of their exchangeable forms. The correlations between Ca, Mg, and K from pXRF and their exchangeable/ available contents agree with reports from other studies conducted in Brazilian soils (Benedet et al., 2021; Silva et al., 2018; Teixeira et al., 2018).

The Cr, Cu, Fe, Mn, Ti, V, and Zr have higher contents in the upper part of the soil profile (A and Bi horizons) and lower contents below that depth (Fig. 4). Gloaguen and Passe (2017) studied the natural accumulation of Cr, Cu, Pb, Ni, and Zn in different soils derived from Quaternary sediments and in sandy soils derived from Mesozoic rocks, at Recôncavo Baiano region, Brazil, and concluded that the pedogenesis and the geology explain the concentration of such elements in these soils, similar to the present study.

The sandstone parent material influences the elemental content of the soil (Moniz and Carvalho, 1973), as expected. Heavy metals tend to accumulate mainly in the clay fraction of soils (Pikuła and Stepień, 2021). In the present study, greater content of elements was found in horizons featuring higher clay content (Fig. 3 and Table 3). The Fe content, for instance, revealed a drastic reduction from 145 cm depth downwards, corresponding to the portion of the soil where paleogleization processes prevailed (2Cg horizon), promoting the solubilization of Fe(II) forms and consequent removal by leaching.

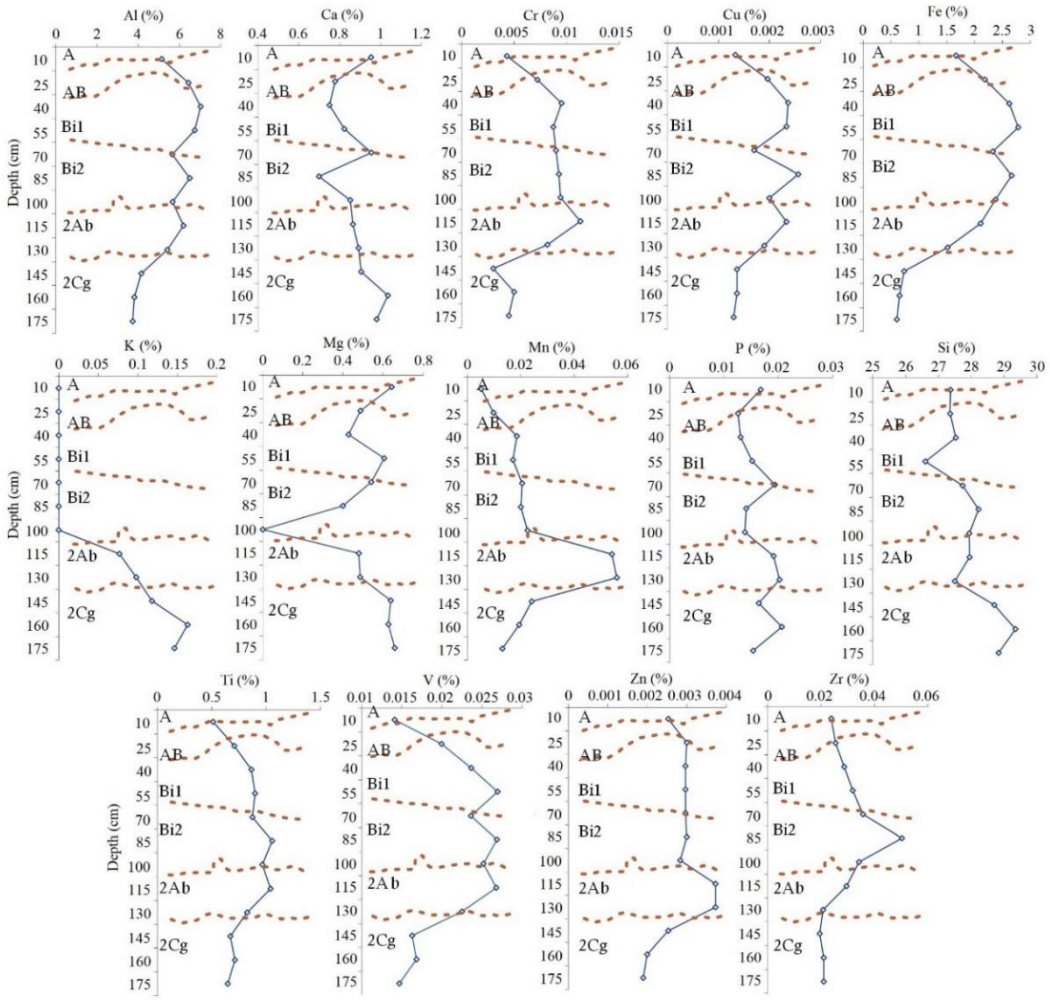

Fig. 3. Mean elemental contents of the studied soil profile, obtained with pXRF, from Pontal do Paranapanema, São Paulo state, Brazil. Dashed lines indicate horizon boundaries, established during morphological description.

The Ti/Zr ratio showed values of 21.45, 21.00, 39.74, and 34.00, respectively, for the A, Bi1, 2A, and 2Cg horizons, clearly indicating different parent materials for the Cambisol and Gleysol unities, since both elements are known as very stable and immobile in soil enviroments (Gozükara et al., 2021; McNulty et al., 2018; Schaetzl and Anderson, 2005; Stockmann et al., 2016). One possible explanation for such differences in parent materials refers to the well-known association of pellitic sediments intermixed with

sandstone (Resende et al., 2019). The current midslope position of the Paleosol studied with 7% slope make the colluvia possibility unlikely.

Regarding the spatialization of elemental contents (Fig. 4), the distribution of several elements followed the occurrence of the different unities of the Paleosol. Noticeable, Al, Cr, Cu, Fe, Ti, V, Zn, and Zr accumulated in the Bi horizon and were lower downwards. The opposite trend occurred for Si and K. However, Mn clearly accumulated in the 2A horizon, reinforcing the occurrence of different soil parent materials. The accumulation of Al, Cr, Cu, Fe, Ti, V, Zn, and Zr in the Bi horizons is associated with their greater clay content (Table 3). Mancini et al. (2021) and Sun et al. (2020) also observed that some elements accumulated in the B horizon, respectively, of a Latosol (Oxisol) and an Alfisol, coincident with relative greater accumulation of clay in such horizons of the soil profiles.

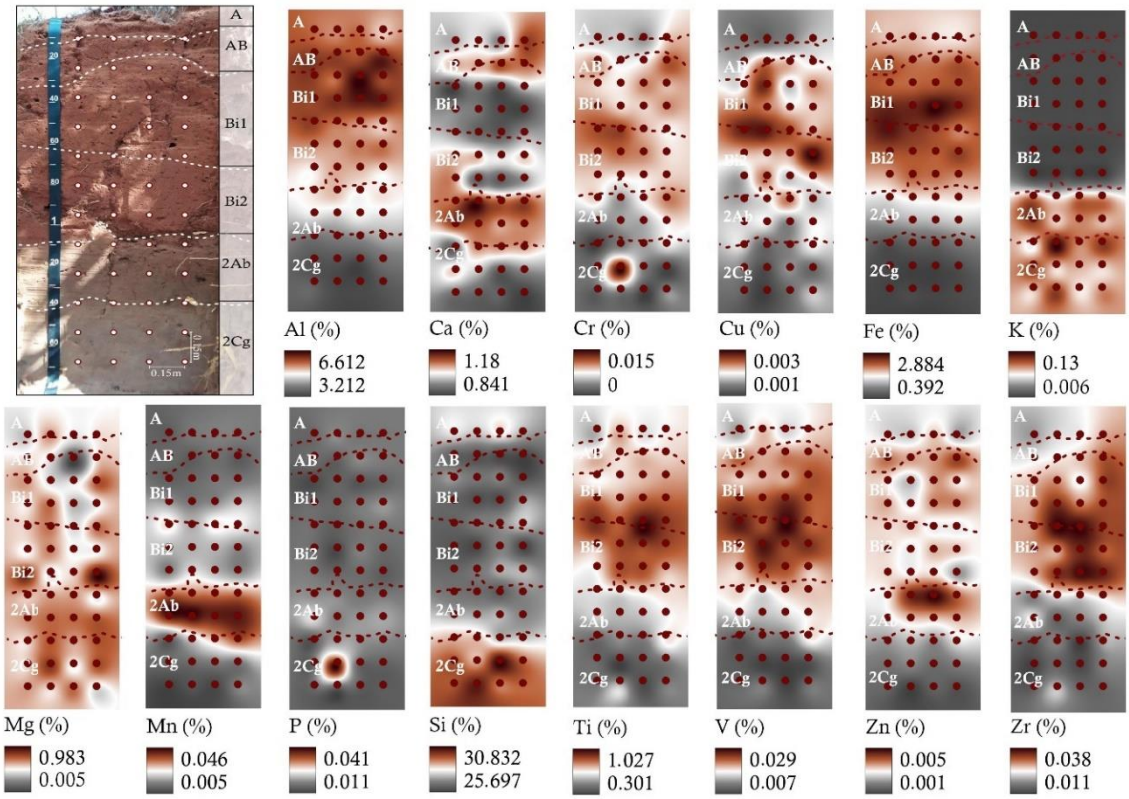

Fig. 4. Spatial representation of elemental contents of the studied profile, obtained with pXRF, from Pontal do Paranapanema, São Paulo state, Brazil.

Regarding the XRD analyses (Fig. 5), quartz predominates in the silt, coarse and fine sand fractions of all soil horizons. Small peaks of feldspars (probably K-feldspars) were identified in the coarse and fine sand fractions of 2A and 2Cg horizons (Fig. 5b; 5c; 5d). Moreover, mica was identified in the silt (probably muscovite) and clay (probably illite) fractions of the 2Cg horizon (Fig. 5d). Both findings help explain the increment of K obtained via pXRF in these soil horizons (Fig. 4), and agree with reports of Moniz and Carvalho (1973) when studying soils of the same region and derived from the same parent material.

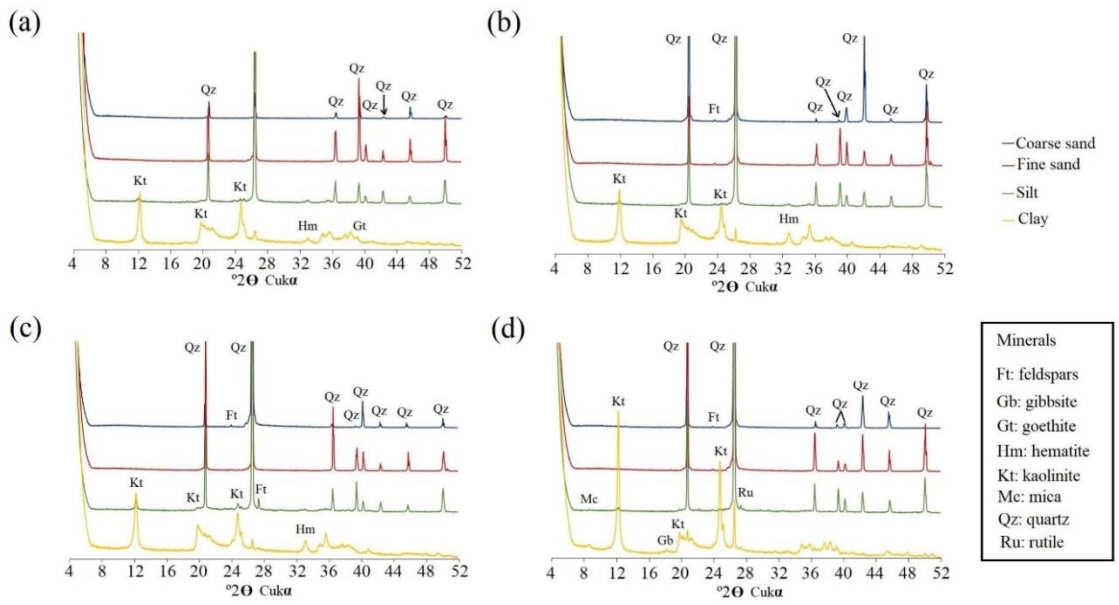

Fig. 5. X-ray diffraction analyses of particle size fractions of the soil studied, in Pontal do Paranapanema, São Paulo state, Brazil. **(a)** A horizon; **(b)** Bi1 horizon; **(c)** 2Ab horizon; and **(d)** 2Cg horizon.

In the clay fraction, kaolinite was the dominant mineral in all soil horizons, mainly in the 2Cg horizon. Hematite was not identified only in this horizon, as expected, since

the paleoredoximorphic conditions probably caused its decomposition (Barbosa et al., 2019; Kämpf and Curi, 2000; Resende et al., 2011).

A small gibbsite peak was found only in the clay fraction of the 2Cg horizon (Fig. 5d), which is in agreement with the findings of Motta and K¨ampf (1992) and Pozza et al. (2007, 2009) when studying a Haplic Gleysol profile in the Central Plateau of Brazil. Rutile was only detected in the silt and clay fractions of the 2Cg horizon. Taking into account this Ti-bearing mineral is very stable and immobile in soil systems, even under redoximorphic conditions (K¨ampf et al., 2009), this finding may also corroborate the lithological discontinuity possibility discussed earlier.

According to pXRF results per particle size fraction of the soil (Fig. 6), Al is predominant in the clay fraction of all soil horizons. The same trend occurs for P, Zn, Ti, Cu, Cr, Fe, and V (except for the 2A horizon, which contains greater V content in the silt fraction). Conversely, Zr and Mn contents are predominant in the silt fraction, except for the 2Cg horizon that has higher contents of Mn in the clay fraction. Grauer-Gray and Hartemink (2018) found higher contents of Zr for soils richer in clay or silt (Alfisol and Mollisol) and lower contents for sandy soil (Entisol). Silva et al. (2018) also observed this trend for both Zr and Mn, mainly in the Cr horizon of a Cambison (Inceptisol) in the Brazilian Cerrado biome.

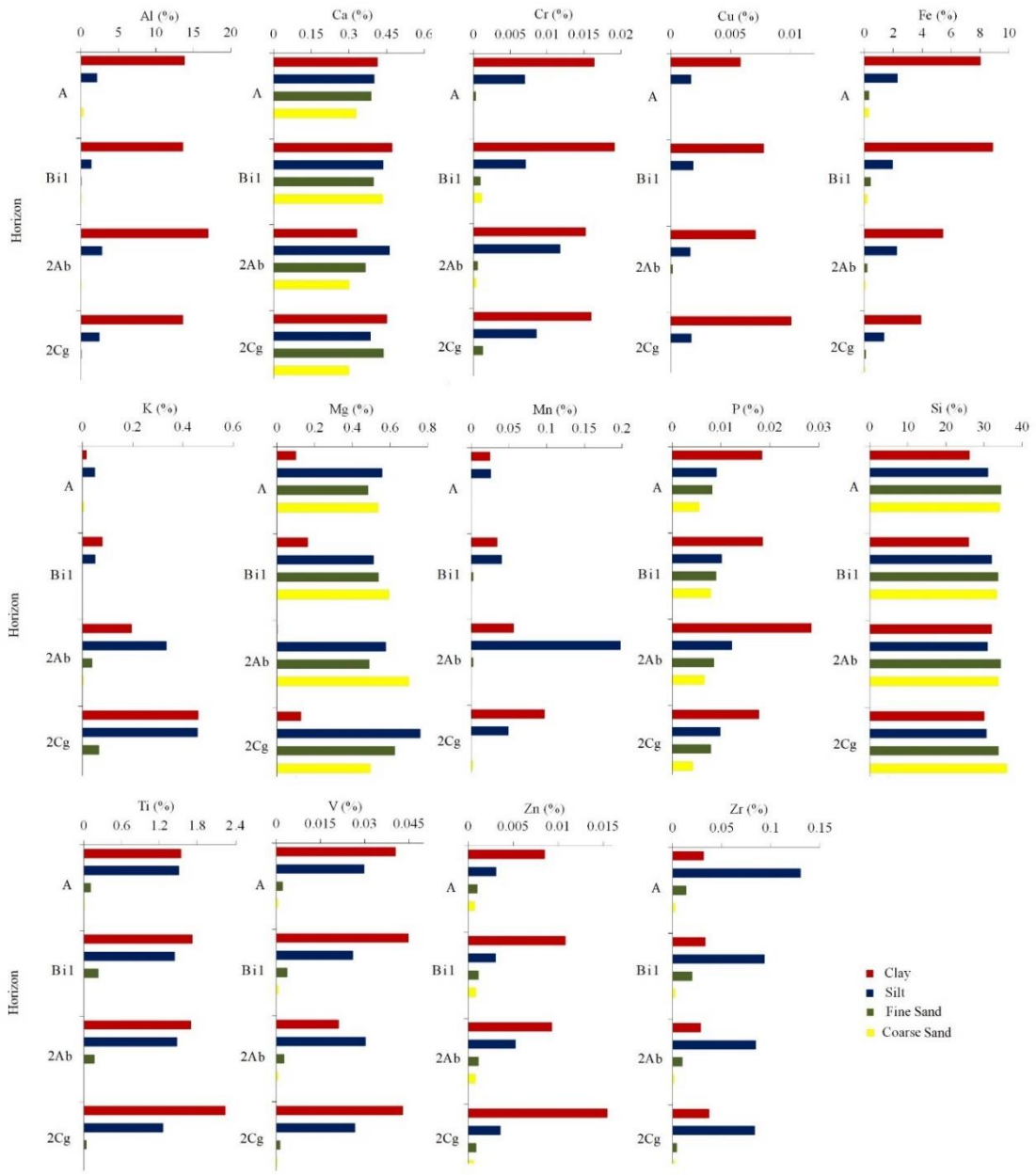

Fig. 6. Elemental contents per particle size fraction of the studied profile, obtained with pXRF, from Pontal do Paranapanema, São Paulo state, Brazil.

Nevertheless, Si, Mg, and Ca were well distributed along the soil profile in all soil fractions. The Si distribution is mainly associated to the dominance of quartz in the sand and silt fractions, and to kaolinite in the clay fraction of the soil studied.

4. Final remarks

The combination of analyses used in this pilot work was able to detail the contrasting pedogenesis processes of the Cambisol and Gleysol unities of the studied soil profile, confirming the field morphological description, in addition to revealing differences in parent materials, not- detected during the field work. The digital morphometrics approach, mainly in terms of magnetic susceptibility data spatialization, elucidated a clear variation in the boundaries between the Bi2 and 2A soil horizons, without any indication in field morphology.

The drain head where the Paleosol is situated (Fig. 1) is environmentally important mainly in relation to springs protection, because its conformation tends to expose the perched water table. So, it is important to detail the characterization of the soils there in order to plan conservation practices aiming to prevent the clogging of springs (Mello et al., 2019). As the sediments tend to remain retained on the native vegetation (semi-perennial tropical forest) of these areas, they play a role as filters, with beneficial impacts on water quality (Mello and Curi, 2012). The undulated topography of this drain head does not allow much impact on water recharge potential. Also, the seepage erosion should also be considered, in which the subsurface flow, favored in this case by the pellitic (fine) sediments intermixed with the sandstone, may transport soil particles entrained in the seepage water (Soil Science Society of America, 2008) to lower landscape positions and may potentially pollute water bodies and springs (Mello et al., 2019), mainly in terms of heavy metals, N, and P.

The detailed characterization of the Paleosol may be useful for estimation of water and sediment paleodischarge and paleodrainage area, and sediment budgets (Bhattacharya et al., 2016) and for paleodischarge reconstruction (Shen et al., 2021), then assisting with characterization of climate change impacts.

The authors understand that there are Paleosols not yet studied in Brazil, for example the Latosols (Oxisols) located on the summits (*chapadas*) of the Brazilian Central Plateau, making part of the Cerrado biome (22% of the county). These *chapadas* were formed by pediplanation, under bioclimatic conditions much drier than nowadays (Curi et al., 1993). In other words, the relief is relict from dry climate and the Oxisols were formed under humid climate (Resende et al., 2014). Then, these Latosols are polygenetic: they are Paleosols. This approach may encourage future studies in this research line.

5. Conclusions

The Paleosol studied herein presented contrasting redoximorphic features, suggesting a change on the landscape to promote such variation. Moreover, the Ti/Zr ratio, delivered by pXRF, indicated different parent materials forming the reddish and gleyic unities of the Paleosol.

The topographical evolution includes a gentler slope in the past, allowing a high perched water table, favored by the pellitic (fine) sediments intermixed with the sandstone. These fine layers, having much lower permeability, induced paleoredoximorphic processes and the resulting greyish colors in the lower part of the Paleosol profile. After that, there was an intense erosion resumption, a very common condition in Brazil, dissecting the former landscape and favoring the current oxidation processes in the upper part of the soil profile, with hematite formation and consequent reddish colors.

In this pilot study, the combined use of field morphology, physical, chemical, and mineralogical analyses, complemented by pXRF and MS data, provided details on the

variation of soil properties formed under current pedalization and elutriation versus paleogleyzation, and delivered some insights on enhancing conservation practices and on assisting the characterization of climate change impacts.

Declaration of Competing Interest

The authors declare the following financial interests/personal relationships which may be considered as potential competing interests: the authors report financial support was provided by Coordination of Higher Education Personnel Improvement, by National Council for Scientific and Technological Development, and by Minas Gerais State Foundation of Support to the Research.

Data availability

Data will be made available on request.

Acknowledgments

The authors acknowledge Conselho Nacional de Desenvolvimento Científico e Tecnológico (CNPq), Coordenação de Aperfeiçoamento Pessoal de Nível Superior (CAPES), Fundação de Amparo à Pesquisa do Estado de Minas Gerais (FAPEMIG), and Serviço Geológico Brasileiro (SGB) for financial support and scholarships. The Instituto de Pesquisas Ecológicas (IPÊ) and the China Three Gorges Corporation (CTG) provided financial support and allowed the conduction of this research in the field.

References

Alvares, C.A., Stape, J.L., Sentelhas, P.C., Gonçalves, J.L.M., Sparovek, G., 2013. Köppen's climate classification map for Brazil. Meteorologische Zeitschrift. 22, 711-728. https://doi.org/10.1127/0941-2948/2013/0507.

Alvarez, V.V.H., Novais, R.F., Dias, L.E., Oliveira, J.A., 2000. Determinação e uso do fósforo remanescente. Bol. Informativo da SBCS. 25, 27-32.

Barbosa, G.S., Maltoni, K.L., Panosso, A.R., 2019. The colors of soil as a parameter to delimitate the environment of a Palm Swampy. Bol. Goiano de Geografia, Goiânia. 39, 1-25. https://doi.org/10.5216/bgg.v39i0.52021.

Benedet, L., Acuña-Guzman, S.F., Faria, W.M., Silva, S.H.G., Mancini, M., Teixeira, A.F.S., Pierangeli, L.M.P., Acerbi Júnior, F.W., Gomide, L.R., Pádua Júnior, A.L., Souza, I.A., Menezes, M.D., Marques, J.J., Guilherme, L.R.G., Curi, N., 2021. Rapid soil fertility prediction using X-ray fluorescence data and machine learning algorithms. Catena. 197, 105003. https://doi.org/10.1016/j.catena.2020.105003.

Bócoli, F.A., Silva, S.H.G., Mancini, M., Inda, A.V., Teixeira, A.F.S., Andrade, R., Silva, F.M., Santos, W.J.R., Pádua, E.J., Curi, N., 2023. Catena of Ultisols from southeastern Brazil: assessing variation within and among pedons. Geoderma Regional. 33, e00653. http://doi.org/10.1016/j.geodrs.2023.e00653.

Brindley, G.W., Brown, G., 1980. Crystal Structures of Clay Minerals and their X-ray Identification, 1st ed. Mineralogical Soc. of Great Britain and Ireland, London.

CRG-CST (Cooperative Research Group of Chinese Soil Taxonomy). 2001. Chinese Soil Taxonomy. Beijing, Science Press.

Curi, N., Larach, J.O.I., Kämpf, N., Moniz, A.C., Fontes, L.E.F., 1993. Vocabulário de Ciência do Solo. SBCS.

Curi, N., Kämpf, N., Resende, M., 1984. Mineralogia, química, morfologia e geomorfologia de solos originados de rochas efusivas das Encostas Superior e Inferior do Nordeste, no Rio Grande do Sul. Revista Brasileira de Cienc. do Solo. 8, 269-276.

Dearing, J., 1999. Environmental Magnetic Susceptibility: Using the Bartington MS2 system 2nd ed. Kenilworth, Chi Publishing.

Donagema, G.K., Campos, D.V.B., Calderano, S.B., Teixeira, W.G., Viana, J.H.M., 2011. Manual de Métodos de Análise de Solo, 2nd ed. Embrapa Solos, Rio de Janeiro.

FAO, 2022. World reference base for soil resources/ International soil classification system for naming soils and creating legends for soil maps, 4th ed. FAO, Rome.

Gee, G.W., Bauder, J.W., 1986. Particle-size analysis. In: Klute, A. (ed.) Methods of Soil Analysis. Am. Soc. of Agronomy, Madison pp. 383-412.

Gloaguen, T.V., Passe, J.J., 2017. Importance of lithology in defining natural background concentrations of Cr, Cu, Ni, Pb and Zn in sedimentary soils, northeastern Brazil. Chemosphere. 186, 31-42. http://dx.doi.org/10.1016/j.chemosphere.2017.07.134.

Gonçalves, M.G.M., Ker, J.C., Oliveira, F.S., Ramos, L.O.S., Pacheco, A.A., Curi, N., 2019. Lateral loss of clay in the genesis of Luvisols in the Semi-Arid Depression of the Jequitinhonha Valley, Minas Gerais - Brazil. Cienc. e Agrotecnologia. 43, e018219. https://doi.org/10.1590/1413-7054201943018219.

Gozukara, G., Zhang, Y., Hartemink, A.E., 2021. Using vis-NIR and pXRF data to distinguish soil parent materials – An example using 136 pedons from Wisconsin, USA. Geoderma 396, 115091. https://doi.org/10.1016/j.geoderma.2021.115091.

Grauer-Gray, J., Hartemink, A.E., 2018. Raster sampling of soil profiles. Geoderma. 318, 99-108. http://dx.doi.org/10.1016/j.geoderma.2017.12.029.

Hartemink, A.E., Minasny, B., 2014. Towards digital soil morphometrics. Geoderma. 230-231, 305-317. https://doi.org/10.1016/j.geoderma.2014.03.008.

Hartemink, A.E., Zhang, Y., Bockheim, J.G., Curi, N., Silva, S.H.G., Grauer-Gray, J., Lowe, D.J., Krasilnikov, P., 2020. Soil horizon variation: a review. Advances in Agronomy. 160, 125-185. http://dx.doi.org/10.1016/bs.agron.2019.10.003.

Jenny, H., 1941. Factors of soil formation: A system of quantitative Pedology. McGraw-Hill, Book Co., Inc., New York.

Kämpf, N., & Curi, N. 2000. Óxidos de ferro - Indicadores de atributos e ambientes pedogênicos e geoquímicos. In: R. F. NOVAIS, V. V. H. ALVAREZ, & C. E. G. R. SCHAEFER (Eds.), Tópicos em Ciência do Solo. SBCS, Viçosa, pp. 107–138.

Kämpf, N., Curi, N., & Marques, J. J., 2009. Óxidos de alumínio, silício, manganês e titânio. In V. F. Melo & L. R. F. Alleoni (Eds.), Química e mineralogia do solo (1st ed.). SBCS.

Kämpf, N., Marques, J.J., Curi, N., 2012. Mineralogia de Solos Brasileiros: Principais Aspectos. In: Ker, J.C., Curi, N., Schaefer, C.E.G.R., Vidal-Torrado, P. (Eds.). Pedologia: fundamentos. SBCS, Viçosa, pp. 80-145.

Koch, J., Chakraborty, S., Li, B., Kucera, J.M., Van Deventer, P., Daniell, A., Faul, C., Man, T., Pearson, D., Duda, B., Weindorf, C.A., Weindorf, D.C., 2017. Proximal sensor analysis of mine tailings in South Africa: An exploratory study. J. Geochemical Explor. 181, 45–57. https://doi.org/10.1016/j.gexplo.2017.06.020.

Ladeira, F.S.B., 2010. Soils of the Past: Origin and Identity. Revista Brasileira de Cienc. do Solo. 34, 1773-1786. http://dx.doi.org/10.1590/S0100-06832010000600001.

Lee, S., Wolberg, G., Shin, S.Y., 1997. Scattered Data Interpolation with Multilevel B-Splines. IEEE Transactions on Visualization and Computer Graphics. 3, 228-244. http://dx.doi.org/10.1109/2945.620490.

Mancini, M., Silva, S.H.G., Avanzi, J.C., Hartemink, A.E., Inda, A.V., Demattê, J.A.M., de Lima, W., Curi, N., 2023. Digital morphometrics and genesis of soils with buried horizons and lithological discontinuities in southeastern Brazil. Geoderma Reg. 32, e00612.

Mancini, M., Silva, S.H.G., Hartemink, A.E., Zhang, Y., Faria, Á.J.G., Silva, F.M., Inda, A.V., Demattê, J.A.M., Curi, N., 2021. Formation and variation of a 4.5 m deep Oxisol in southeastern Brazil. Catena. 206, 105492. http://dx.doi.org/10.1016/j.catena.2021.105492.

Mclean, E.O., Heddleson, M.R., Bartlett, R.J., Holowaychuk, N., 1958. Aluminum in soils: I. Extraction methods and magnitudes in clays and Ohio soils 1. Soil Sci. Soc. of Am. Journal. 22, 382-387. https://doi.org/10.2136/sssaj1958.03615995002200050005x.

McNulty, B.A., Fox, N., Berry, R.F., Gemmell, J.B., 2018. Lithological discrimination of altered volcanic rocks based on systematic portable X-ray fluorescence analysis of drill core at the Myra Falls VHMS deposit. Canada. J. Geochemical Explor. 193, 1–21. https://doi.org/10.1016/j.gexplo.2018.06.005.

Mehlich, A., 1953. Determination of P, Ca, Mg, K, Na and NH_4. North Carolina Soil Testing Division, Raleigh, NC.

Mello, C.R.D., Curi, N., 2012. Hydropedology. Hydropedology. Ciência e Agrotecnologia 36 (2), 137–146.

Mello, D.C., Demattê, J.A.M., Silvero, N.E.Q., Raimo, L.A.D.L., Poppiel, R.R., Mello, F.A.O., Souza, A.B., Safanelli, J.L., Resende, M.E.B., Rizzo, R., 2020. Soil magnetic susceptibility and its relationship with naturally occurring processes and soil attributes in pedosphere, in a tropical environment. Geoderma. 372, 114364. http://dx.doi.org/10.1016/j.geoderma.2020.114364.

Mello, C.R., Norton, L.D., Pinto, L.C., Curi, N., 2019. Hydropedology in the tropics, 1st ed. Editora UFLA, Lavras.

Moniz, A.C., Carvalho, A., 1973. Sequência de evolução de solos derivados do arenito Bauru e de rochas básicas da região noroeste do estado de São Paulo. Bragantia. 32, 309-335. http://dx.doi.org/10.1590/s0006-87051973000100017.

Motta, P.E.F., Kämpg, N., 1992. Iron oxide properties as support to soil morphological features for prediction of moisture regimes in Oxisols of Central Brazil. Pflanzenernahr. Bodenk. 155, 385–390.

Nascimento, D.L., Ladeira, F.S.B., Batezelli, A., 2017. Pedodiagenetic Characterization of Cretaceous Paleosols in Southwest Minas Gerais, Brazil. Revista Brasileira de Cienc. do Solo. 41, e0160065. http://dx.doi.org/10.1590/18069657rbcs20160065.

Nelson, D.W., Sommers, L., 1996. Total carbon, organic carbon, and organic matter: Chemical methods. In: Black, C.A. (Ed.), Methods of Soil Analysis, Part 3. Soil Science of America and American Society of Agronomy, Madison, pp. 961–1010.

Oliveira-Filho, A., Fontes, M., 2000. Patterns of Floristic Differentiation among Atlantic Forests in Southeastern Brazil and the Influence of Climate. Biotropica. 32, 793-810. https://doi.org/10.1111/j.1744-7429.2000.tb00619.x.

Phillips, J.D., 2016. Identifying sources of soil landscape complexity with spatial adjacency graphs. Geoderma. 267, 58-64. http://dx.doi.org/10.1016/j.geoderma.2015.12.019.

Pikuła, D., Stępień, W., 2021. Effect of the Degree of Soil Contamination with Heavy Metals on Their Mobility in the Soil Profile in a Microplot Experiment. Agronomy. 11, 878. https://doi.org/10.3390/agronomy11050878.

Poggere, G.C., Inda, A.V., Barrón, V., Kämpf, N., Brito, A.D.B., Barbosa, J.Z., Curi, N., 2018. Maghemite quantification and magnetic signature of Brazilian soils with

contrasting parent materials. Appl. Clay Sci., 161, 385-394. http://dx.doi.org/10.1016/j.clay.2018.05.014.

Pozza, A.A.A., Curi, N., Costa, E.T.S., Guilherme, L.R.G., Marques, J.J.G.S.M., Motta, P.E. F., 2007. Retenção e dessorção competitivas de ânions inorgânicos em gibbsita natural de solo. Pesq. Agropec. Bras. 42, 1627–1633.

Pozza, A.A.A., Curi, N., Guilherme, L.R.G., Marques, J.J.G.S.M., Costa, E.T.S., Zuliani, D. Q., Motta, P.E.F., Martins, R.S., Oliveira, L.C.A., 2009. Adsorção e dessorção aniônicas individuais por gibbsita pedogenética. Quim Nova 32, 99–105.

Preetz, H., Igel, J., Hannam, J.A., Stadler, S., 2017. Relationship between magnetic properties and reddening of tropical soils as indicators of weathering. Geoderma 303, 143–149. https://doi.org/10.1016/j.geoderma.2017.05.007.

QGIS Development Team, 2022. QGIS Geographic Information System. Open-Source Geospatial Foundation. https://qgis.org/en/site/.

Resende, M., Curi, N., Ker, J.C., Rezende, S.B., 2011. Mineralogia de solos brasileiros - Interpretações e aplicações, (2nd ed.). Editora UFLA.

Resende, M., Curi, N., Rezende, S.B., Corrêa, G.F., Ker, J.C., 2014. Pedologia: Base para distinção de ambientes, 6th ed. Editora UFLA, Lavras.

Resende, M., Curi, N., Rezende, S.B., Silva, S.H.G., 2019. Da rocha ao solo: Enfoque ambiental, 1st ed. Editora UFLA, Lavras.

Resende, M., Curi, N., Poggere, G.C., Barbosa, J.Z., Pozza, A.A.A., Teixeira, A.F.S., 2021. Pedologia, fertilidade, água e planta: Inter-relações e aplicações, 2nd ed. Editora UFLA, Lavras.

Santos, R.D., Curi, N., Shimizu, S.H., 2015a. Guia prático para classificação de solos brasileiros. Editora UFLA, Lavras.

Santos, R.D., Santos, H.G., Ker, J.C., Anjos, L.H.C., Shimizu, S.H., 2015b. Manual de descrição e coleta de solo no campo, 7th ed. SBCS, Viçosa.

Santos, H.G., Jacomine, P.K.T., Anjos, L.H.C., Oliveira, V.A., Lumbreras, J.F., Coelho, M.R., Almeida, J.A., Araújo Filho, J.C., Oliveira, J.B., Cunha, T.J.F., 2018. Sistema Brasileiro de Classificação de Solos, 5th ed. Embrapa Solos, Brasília.

Schaetzl, R., Anderson, S., 2005. Soils: Genesis and geomorphology, (1st ed.). Cambridge University Press.

Shirzaditabar, F., Heck, R.J., 2021. Characterization of soil drainage using electromagnetic induction measurement of soil magnetic susceptibility. Catena. 207, 105671. http://dx.doi.org/10.1016/j.catena.2021.105671.

Shoemaker, H.E., Mclean, E.O., Pratt, P.F., 1961. Buffer methods for determining lime requirement of soils with appreciable amounts of extractable aluminum. Soil Sci. Soc. of Am. Journal. 25, 274-277. https://doi.org/10.2136/sssaj1961.03615995002500040014x.

Silva, M.L., Batezelli, A., Ladeira, F.S.B., 2017. The mineralogy of paleosols in the Marília Formation and their importance in the environmental evolution of the Maastrichtian of the Bauru Basin in southeastern Brazil. Brazilian Journal of Geology. 47, 403-426. http://dx.doi.org/10.1590/2317-4889201720170101.

Silva, S.H.G., Hartemink, A.E., Teixeira, A.F.S., Inda, A.V., Guilherme, L.R.G., Curi, N., 2018. Soil weathering analysis using a portable X-ray fluorescence (pXRF) spectrometer in an Inceptisol from the Brazilian Cerrado. Appl. Clay Sci. 162, 27-37. http://dx.doi.org/10.1016/j.clay. 2018.05.028.

Silva, S.H.G., Ribeiro, B.T., Guerra, M.B.B., Carvalho, H.W.P., Lopes, G., Carvalho, G.S., Guilherme, L.R.G., Resende, M., Mancini, M., Curi, N., Rafael, R.B.A., Cardelli, V., Cocco, S., Corti, G., Chakraborty, S., Li, B., Weindorf, D.C., 2021.

PXRF in Tropical Soils: Methodology, Applications, Achievements and Challenges. Advances in Agronomy. 167, 1-62. https://doi.org/10.1016/bs.agron.2020.12.001.

Soil Science Society of America, 2008. Glossary of Soil Science Terms 2008. Am. Soc. of Agronomy and Soil Sci. Soc. of Am.

Soil Survey Staff, 2014. Keys to soil taxonomy, 12th ed. United States Department of Agriculture Natural Resources Conservation Service.

Stevanato, M., Parolin, M., Camargo Filho, M., Parolin, E.S.P., 2021. Brazilian Paleosols: state of the art. Revista da ANPEGE. 17, 128-145. http://dx.doi.org/10.5418/ra2021.v17i33.11897.

Stockmann, U., Cattle, S.R., Minasny, B., McBratney, A.B., 2016. Utilizing portable X-ray fluorescence spectrometry for in-field investigation of pedogenesis. Catena 139, 220–231. https://doi.org/10.1016/j.catena.2016.01.007.

Stradioto, M.R., Chang, H.K., 2020. Diagênese de Arenitos do Grupo Bauru no Estado de São Paulo. Cienc. e Nat. 42, e88. http://dx.doi.org/10.5902/2179460x42694.

Sun, F., Bakr, N., Dang, T., Pham, V., Weindorf, D.C., Jiang, Z., Li, H., Wang, Q., 2020. Enhanced soil profile visualization using portable X-ray fluorescence (PXRF) spectrometry. Geoderma. 358, 1-11. http://dx.doi.org/10.1016/j.geoderma.2019.113997.

Teixeira, A.F.S., Weindorf, D.C., Silva, S.H.G., Guilherme, L.R.G., Curi, N., 2018. Portable X-ray fluorescence (pXRF) spectrometry applied to the prediction of chemical attributes in Inceptisols under different land use. Cienc. e Agrotecnologia. 42, 501-512. https://doi.org/10.1590/1413-70542018425017518.

Weindorf, D.C., Chakraborty, S., 2016. Portable X-ray Fluorescence Spectrometry Analysis of Soils. Methods of Soil Anal. 84, 1384-1392. https://doi.org/10.1002/saj2.20151.

Wright, V.P., 1992. Paleosol Recognition: a guide to early diagenesis in terrestrial settings. In: Wolf, K.H., Chilingarian, G.V. Diagenesis, III: Developments in Sedimentology. 12, 591-619. https://doi.org/10.1016/S0070-4571(08)70574-0.

Zhang, Y., Hartemink, A.E., 2017. Sampling designs for soil organic carbon stock assessment of soil profiles. Geoderma 307, 220–230. https://doi.org/10.1016/j.geoderma.2017.08.013.

CHAPTER II:

On the importance of digital soil mapping scale for ecosystem service assessment and policy - a study involving soil sediments dynamic and direct aquifer recharge

* Article prepared according to the rules of the **Ecosystem Services** journal

Fernanda Almeida Bócoli[a], Junior Cesar Avanzi[a], Bruno Montoani Silva[a], Vanêssa Lopes de Faria[a], Maria Cecília Vieira Totti[a], Michele Duarte de Menezes[a], Alexandre Uezu[b], Dione Pereira Cardoso[a], Nilton Curi[a], Sérgio Henrique Godinho Silva[a]*

[a] Department of Soil Science, Federal University of Lavras (UFLA), Lavras, Minas Gerais, 37,200-900, Brazil

[b] Faculty for Environmental Conservation and Sustainability (ESCAS), IPÊ - Institute for Ecological Research, 47 km of Dom Pedro I highway, Nazaré Paulista, São Paulo, 12,960-000, Brazil

* Corresponding author: sergio.silva@ufla.br

Abstract

Soil is crucial in maintaining many ecosystem services, including services concerning fresh water, regulating erosion control, and water purification. Thus, the nexus of direct aquifer recharge and sediment dynamic has the soil as a fundamental basis for interpretations to improve territorial and environmental planning. Thus, fuzzy logics were applied in four watersheds from the Pontal do Paranapanema region, Brazil, to quantitatively formalize soil-landscape knowledge and increase the scale of current soil information available. Further, knowledge and physical-based models were applied to assess direct water recharge and sediment dynamics (soil loss and sediment retention). An increase in detail is evident when comparing the soil maps produced by fuzzy logic with the existing maps. Notably, Latossolos and Argissolos persist as the dominant soil classes, with only a few differences in their spatial distribution. The most remarkable increase in digital soil map detail involved the floodplain portions. Aquifer discharge is the ecosystem supply that is more affected by the soil mapping scale. Also, trade-offs or synergies among ecosystem services were spatially detected since soil-landscape units that foster water infiltration, storage, and direct aquifer recharge are those that prevent soil loss with avoided erosion. Incorporating terrain attributes and legacy data effectively predicted soil spatial distribuition in the studied watersheds. For all studied watersheds, the overall accuracy surpassed 60%, and the Kappa index was higher in Pelanca and Morro do Diabo watersheds, with values exceeding 0.50, indicating a high agreement level in the predictions. Detailed soil mapping has provided the precise locations within each watershed where ecosystem services occur more intensely and their distribution across the landscape.

Keywords: Provisioning services; aquifer recharge; soil loss; avoided sediment.

1 Introduction

Water flows overland as runoff directly to streams or infiltrates into the subsurface to become groundwater. The downward flow of water toward the water table, adding to the groundwater reservoir, is defined as direct recharge (Vries and Simmers, 2002). Groundwater is significant in maintaining the water regime, especially during dry periods (Mello et al., 2019). Whether water access to the ground surface is higher than the soil infiltration capacity, surface runoff occurs, whose rate depends on the rainfall, soil-landscape, land cover, and land use characteristics (Ramke, 2018). Changes in runoff can alter water availability. Once runoff increases, water erosion is impacted, reflected by increasing sediment load of water bodies via rainfall detachment of soil particles and direct surface runoff (Oliveira et al., 2019). In turn, the increase in sediment yield affects water quality and reservoir management (Magalhães et al., 2022). Direct aquifer recharge and sediment dynamics (soil loss or sediment retention) through natural landscapes are essential for hydrological control. Thus, their assessment is critical for policymakers and policies toward valuation.

Soil is crucial in maintaining the many ecosystem services within the Critical Zone, including services concerning fresh water, regulating erosion control, and water purification (Rodrigues et al., 2021). Thus, the nexus of direct aquifer recharge and sediment dynamic has the soil as a fundamental basis for interpretations. Robinson et al. (2012), further corroborated by Jónsson and Davíðsdóttir (2016), emphasized the growing need to incorporate the role of soils into ecosystem services. Pedology has been fundamental for enabling a foundation for the processes associated with generating runoff and groundwater recharge (Mello and Curi, 2012), and a soil map is an essential tool for assessing soil spatial variability across landscapes and in-depth, whose temporal variation is negligible (very stable over human life scale).

Jónsson and Davíðsdóttir (2016) pre-defined key steps to valuing soil with respect to ecosystem services that could be summarized as follows: i) to describe the area (e.g., dominant land use, climate conditions, land management practice, land cover, soil type, soil health and others.); ii) to identify the beneficiaries of the services rendered from the area; iii) to define the scale of the beneficiaries of ecosystem services (local, regional or global) (Kumar, 2010); iv) to use the best information and tools available concerning ecosystem service. In studies focused on local scales, climate and sometimes soil bedrock

variation could be neglected due to low variability, and thus, the primary drivers of water-related ecosystem services consist of land cover and soil-landscape features. Land use, land cover, and digital terrain maps have been easily obtained from remote sensing products and freely released on different platforms worldwide. The main constrain for countries under development consists of the generalized scarcity of soil information at a local or detailed scale, a reality for the Brazilian territory (Coelho et al., 2021) that likely contributes to sustaining the existent knowledge gap concerning soil ecosystem services under tropical conditions (Rodrigues et al., 2021). Technically, policymakers should take precautions regarding the scale or resolution of soil information that will be the basis for interpretation and decision-making. Consequently, effects propagated to further ecosystem services interpretative maps should also be addressed.

Roughly, a map illustrates the space and environment, coded and simplified to allow communication (Haynes et al., 2007). Thus, maps may contribute to improving awareness and understanding of the provision of ecosystem services from the perspective of different stakeholders. For those phenomena that present a solid spatial-temporal component, maps can play a decisive role in communicating information (Dransch et al., 2010). Although very informative, small-scale soil maps are not suitable for watershed land-use planning, requiring maps on a scale of 1:50,000 or larger (Costa et al., 2009). One promising alternative consists of digital soil mapping (McBratney et al., 2003), whose framework has benefited from the power of computers to deal with large databases to produce new soil information. This database includes environmental covariates proxies of soil-forming factors (Jenny, 1941), which have become widely available at various spatial resolutions due to the development of remote sensing products. As such, terrain attributes have helped refine maps and provided an accurate prediction of soils (Pelegrino et al., 2016; Silva et al., 2016a; Silva et al., 2021; Amorim et al., 2023) since they show different aspects of the terrain that can help with the so-called soil-landscape relationship. Since more quantitative information has been generated, the framework of the spatial predictive model brings the accuracy assessment to attest spatial information reliability (McBratney et al., 2003), necessary for further interpretations.

Although it is necessary to improve territorial and environmental planning (Braido and Tommazelli, 2012), more detailed soil-landscape information is needed for further ecosystem service assessment. From a pure pedometric approach, machine learning algorithms have been intensively explored (Wadoux et al., 2020), and a large sampling

size has been related to the accuracy of soil predictive models (Somarathna et al., 2017). Alternatively, using soil knowledge can be more economical and has been proven to be accurate when quantitatively formalized by rule-based reasoning through fuzzy logic approach (Akumu et al., 2016; Machado et al., 2019; Moonjun et al., 2020). In addition, different from the traditional soil mapping approach, soil types or information derived from that are assigned pixel by pixel, portraying soil as a spatial continuum instead of a homogeneous polygon (Zhu et al., 1996). Such a level of detail is in tune with the more realistic concept of hydrologic connectivity and might better represent water or sediment transfer across landscapes (Bracken et al., 2015; Hanel et al., 2015).

Thus, fuzzy logics were applied in four pilot watersheds to quantitatively formalize soil-landscape knowledge and increase the scale of current soil information available. Extensive considerations concerning the accuracy of maps were provided, and the effectiveness of the information gained was discussed. Further, knowledge and physical-based models were applied to assess direct water recharge and sediment dynamics (soil loss and sediment retention), respectively. We addressed the propagation of soil information gain by comparing the results obtained from the current less detailed soil information.

2 Material and Methods

2.1 Study area

This study involves four representative watersheds from the Pontal do Paranapanema region, state of São Paulo, in Brazil. The total region covers 18,844.60 km² presenting some deforested areas with land use inadequacy, which makes these soils more prone to degradation (Arana et al., 2018; Carpi Junior et al., 2012; Silva et al., 2016b; Zanatta et al., 2012).

The four studied watersheds are Nelore (954.48 ha), Morro do Diabo (4,338.33 ha), Pelanca (833.19 ha), and Santa Beatriz (1,178.73 ha) (Fig. 1) encompassing mostly rural landscapes. The watersheds are spatially widespread throughout the study region to properly represent different environments concerning soil-landscape, land use, and lithological units.

The primary geology of the Pontal do Paranapanema is sandstone, a sedimentary rock that descends from materials brought by wind and water erosion through the

landscape (Moniz and Carvalho, 1973), which creates a variable composition of this rock. Nevertheless, it mainly comprises quartz, a mineral resistant to physical and chemical weathering (Amadeu et al., 2021). The Santo Anastácio and Rio Paraná lithological units share similar characteristics as both belong to the Caiuá Group. They diverge mainly in their stratification and their formation processes. Santo Anastácio originated from eolian dunes, whereas Rio Paraná formed from the edge plain of the sand sea. Both formations developed in continental desert environments during the Cretaceous period (Perrota et al., 2005). Their mineralogical composition consists of quartz, feldspar, and chalcedony, with occasional carbonate or siliceous cement, predominantly exhibiting a psammitic nature (Fernandes, 1998). Within the Pelanca watershed, two distinct lithological units exist – Santo Anastácio to the north and Rio Paraná to the south. While Nelore and Morro do Diabo watersheds are located within the Rio Paraná lithological unit. The Santa Beatriz watershed is situated in the Vale do Rio do Peixe lithological unit within the Bauru Group, also formed during the Cretaceous period under the influence of sand sheets and dunes with loess deposits, primarily composed of aeolian sediments (Fernandes, 1998; Perrota et al., 2005). Its mineralogical composition is predominantly quartz, feldspar, and even arkose, which are sandstones relatively rich in feldspar. Additionally, it presents layers with carbonate cementation, with a common silty or clayey matrix (Fernandes, 1998).

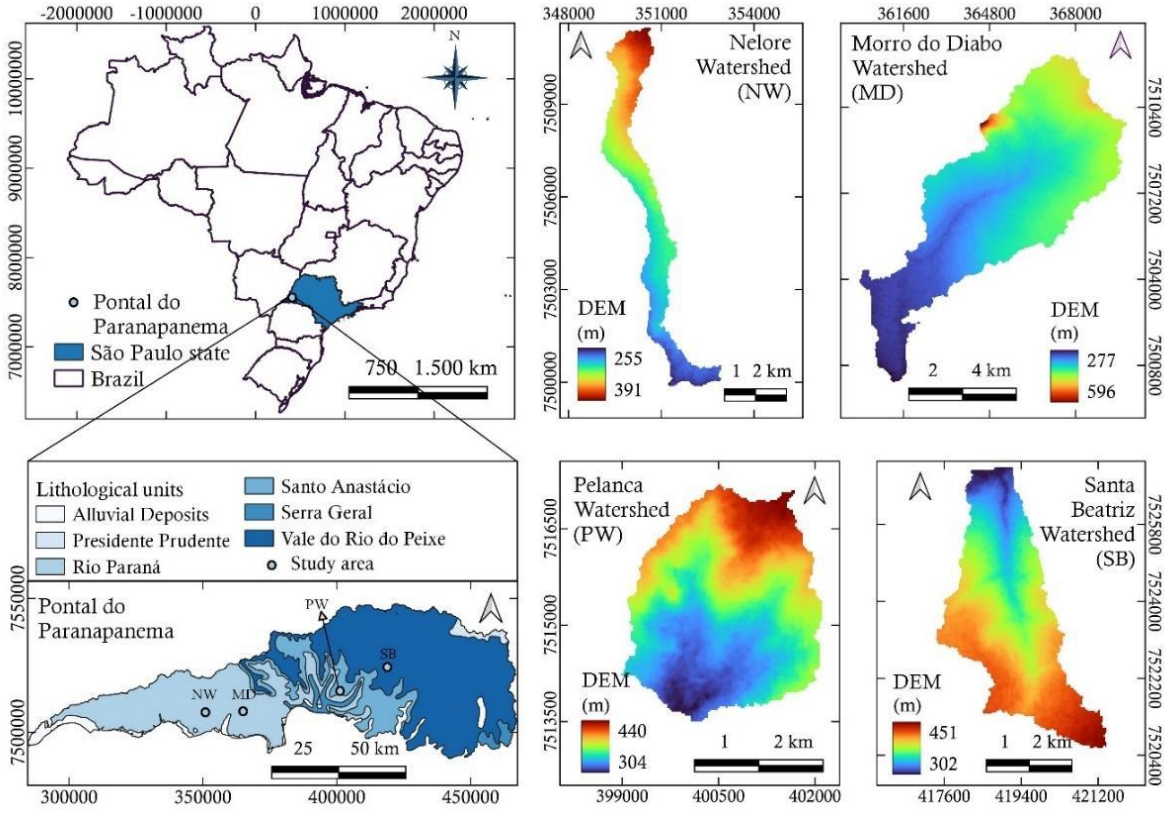

Fig. 1. Location, lithological deposits, and the digital elevation model (DEM), in meters, of the watersheds Nelore (NW), Morro do Diabo (MD), Pelanca (PW), and Santa Beatriz (SB), from Pontal do Paranapanema, state of São Paulo, Brazil. UTM coordinate system, datum SIRGAS 2000, 22S.

The climate in the Pontal do Paranapanema is classified as Cfa, characterized as subtropical, with hot summer and mean temperatures higher than 22 ºC, and dry season presenting rainfall higher than 30 mm, according to Köppen's (1948) climatic classification. Braido and Tommaselli (2010), characterizing a historical climatic series from 1971 to 2007 in the Pontal do Paranapanema region, verified that the annual rainfall is 1,295 mm, with the lowest rainfall observed in the west part of the region, precisely where the study area is located. According to their historical average the lowest recorded rainfall occurs in August, 41 mm, and the highest in January, 170 mm.

2.2 Terrain attributes maps

Once climate, native vegetation, and bedrock can be considered homogenous across watersheds, relief is the main soil-forming factor (Jenny, 1941) driver of soil variability. Digital terrain attributes are regarded as proxies of relief variation. Thus, a digital elevation model was obtained from a Shuttle Radar Topography Mission (SRTM) (NASA, 2013) at 30 m. From the DEM, 18 terrain attributes were calculated in SAGA GIS 7.8.2 software (Conrad et al., 2015). Table 1 lists the terrain attributes used and the following description. Terrain attributes are related to water and sediment movement, soil drainage, aiding information of local catena, and soil parent material, successfully applied in diverse studies involving digital soil mapping in Brazil (Menezes et al., 2014; Silva et al., 2016a; Pelegrino et al., 2016; Silva et al., 2019; Amorim et al., 2023).

Table 1. Description of the generated terrain attributes used to develop the digital soil maps.

Terrain attributes (TA)	**Description**
Channel Network Base Level (CNBL)	Interpolates the base-level elevation of the channel network and then subtracts the values obtained from the original data, resulting in the approximate depth of a watershed's base flow (Conrad, 2002).
Channel Network Distance (CND)	Values reveal how far each pixel is from the drainage network.

Convergence Index (CI)	Analyzes the terrain's ridges and valleys, returning positive values for places with a concave aspect and negative values for convex ones (Gallant and Wilson, 2000). The result is calculated in percentages from aspects of neighboring cells.
Digital Elevation Model (DEM)	Shows the altitude of each terrain surface point.
Multiresolution Index of Valley Bottom Flatness (MRVBF)	An index calculated from the slope and percentage elevation of the terrain, analyzing the DEM in a generalized way combined with increasingly less accentuated slopes, evidencing the depressions of the area (Gallant and Dowling, 2003).
Multiresolution Index of the Ridge Top Flatness (MRRTF)	Despite being similar to the MRVBF, it starts from a contrary principle, thus highlighting the peaks of the terrain (Gallant and Dowling, 2003).
Relative Slope Position (RSP)	Calculates the relational distance from a given point to the lowest areas of the landscape.
Topographic Wetness Index (TWI)	Related to trends in soil moisture content according to local relief (Beven and Kirkby, 1979).
Total Catchment Area (TCA)	Processes the DEM to find the lowest areas of the landscape and is related to the water flow of a watershed.
Valley Depth (VD)	It represents the difference between the elevation of a point and the top of the landscape when the index is lower and is closer to the deeper areas of the terrain.
Vertical Distance to Channel Network (VDCN)	Returns the altitude above the channel network in meters as the elevation data (Conrad, 2002).

2.3 Digital soil mapping

During a field campaign, paths were planned to detect physiographic contrasts following a transect sampling scheme (IBGE, 2015) to elucidate soil and landscape relationships. Thus, soil morphology analyses, sampling (Santos et al., 2015), and laboratory analysis (Donagema et al., 2011) were performed for classification purposes (Santos et al., 2018). During the exploratory expedition, 17 georeferenced points were collected from two depths (0 - 20 cm and 80 - 100 cm), totaling 34 soil samples. These

points were chosen strategically to represent the soil-landscape relationship observed in the watersheds, including Nelore (3 points), Morro do Diabo (3 points), Pelanca (6 points), and Santa Beatriz (5 points). For validation, 70 soil samples (35 georeferenced points) were collected from the same watersheds during a second expedition at the same two depths, from Nelore (5 points), Morro do Diabo (8 points), Pelanca (9 points), and Santa Beatriz (13 points). Such analysis, along with the experience of pedologists composing the workgroup and previous soil surveys (Rossi, 2017), consisted of the basis to implement the rule-based reasoning under fuzzy logic (Zhu, 1997) following the guidelines outlined by Menezes et al. (2013).

Digital terrain attributes that could potentially discriminate soil types were applied as rules through fuzzy membership curves (bell, S, and Z shapes) into Soil Land Inference Model (SoLIM) software (Zhu et al., 2001; Zhu et al., 2018). Such rules consist of thresholds established to formalize optimum or typical conditions for each soil type based on terrain attributes and the pedologists' knowledge. SoLIM operates as an inference engine that establishes pixel-by-pixel a process called soil similarity vector. Thus, the first outcome is the fuzzy membership maps consisting of the degrees of the class assignment (continuous distribution ranging from 0 to 1). These are also regarded as similarity measures between the local soil and the typical case of a given soil class. Further details about the inference process are described by Zhu and Band (1994). The final raster soil type maps were created by hardening the fuzzy membership maps by assigning the soil type with the highest membership value at each pixel in a geographical information system.

Visual analysis was performed comparing the legacy soil data developed by Rossi (2017) (traditional soil mapping at 1:250.000 scale) and the digital soil mapping (fuzzy logics), besides 17 georeferenced points collected in two depths each on the exploratory expedition to represent the soil-landscape relationship observed in the watersheds. In addition, to validate the soil maps of the four watersheds, the classification at verified locations (35 georeferenced points collected on two depths each on the second field expedition, as detailed above) was compared to the soil class outlined on digital maps. The accuracy assessment of these maps was checked by comparing the observed soil classes from Rossi (2017), and the predicted soil classes presented on the digital maps with soil classes field-verified locations. For that, the overall accuracy and the kappa index were calculated as follows (Eq. 1 and 2):

$$OA = \frac{\sum V}{\sum T} * 100 \quad (1)$$

where V represents correctly classified samples, T represents the total of available samples, and OA overall accuracy.

$$Kappa = \frac{Po - Pe}{1 - Pe} \quad (2)$$

where Po is the proportion of correctly classified samples, and Pe is the probability of random agreement. The Kappa index ranges from -1 to 1, increasing its accuracy as the values get closer to 1. These indexes have been successfully used to check the accuracy of digital soil maps in many studies (Coelho et al., 2021; Silva et al., 2021).

The user's and producer's accuracy (Ua and Pa, respectively) were also calculated (Eq. 3 and 4). The former indicates the probability of the predicted soil class matching the one verified in the field, while the latter means the likelihood of a determined soil class in the map being classified correctly (Congalton, 1991). For Ua and Pa, values close to 1 represent an adequate map.

$$Ua = \frac{Xii}{\sum_{j=1}^{r} Xij} \quad (3)$$

$$Pa = \frac{Xjj}{\sum_{j=1}^{r} Xij} \quad (4)$$

where Xii and Xjj indicate the number of correctly classified samples and Xij represents the sum of samples of a soil class in a row (Ua) or column (Pa) of a confusion matrix. These indexes were used successfully in soil mapping studies (Silva et al., 2016a; Amorim et al., 2023).

2.5 Sediment dynamic: soil loss and avoided erosion

Soil loss and sediment retention were modeled through InVEST® 3.14, a physics-based simulation program (Natural Capital Project, 2023). The sediment delivery ratio consists of a necessary basis representing the proportion of fine sediment produced in a given area towards the stream. It is computed as a function of the hydrologic connectivity of the region, following an approach first proposed by Vigiak et al. (2012).

The annual soil loss per pixel into the InVEST is estimated by the Revised Universal Soil Loss Equation (RUSLE) as Renard et al. (1997) described. This calculation considers soil loss as the product of the rainfall erosivity factor, soil erodibility factor, the slope length-gradient factor (calculated following Desmet and Govers, 1996), the cover-

management factor, and the support practice factor. Fig. 2 and Table 2 display the parameters from the RUSLE used as hyperparameters for model simulation based on an extensive literature review concerning Brazilian environments.

Sediment retention ecosystem service in InVEST is defined as avoided export, encompassing avoided pixel-based erosion estimated accounting contributions of vegetation and sediment trapping from an upslope pixel. This may also be considered the total sediment retained on the pixel. For determination of both soil loss and avoided export, the soil legacy data and digital soil maps generated by this study were taken into account.

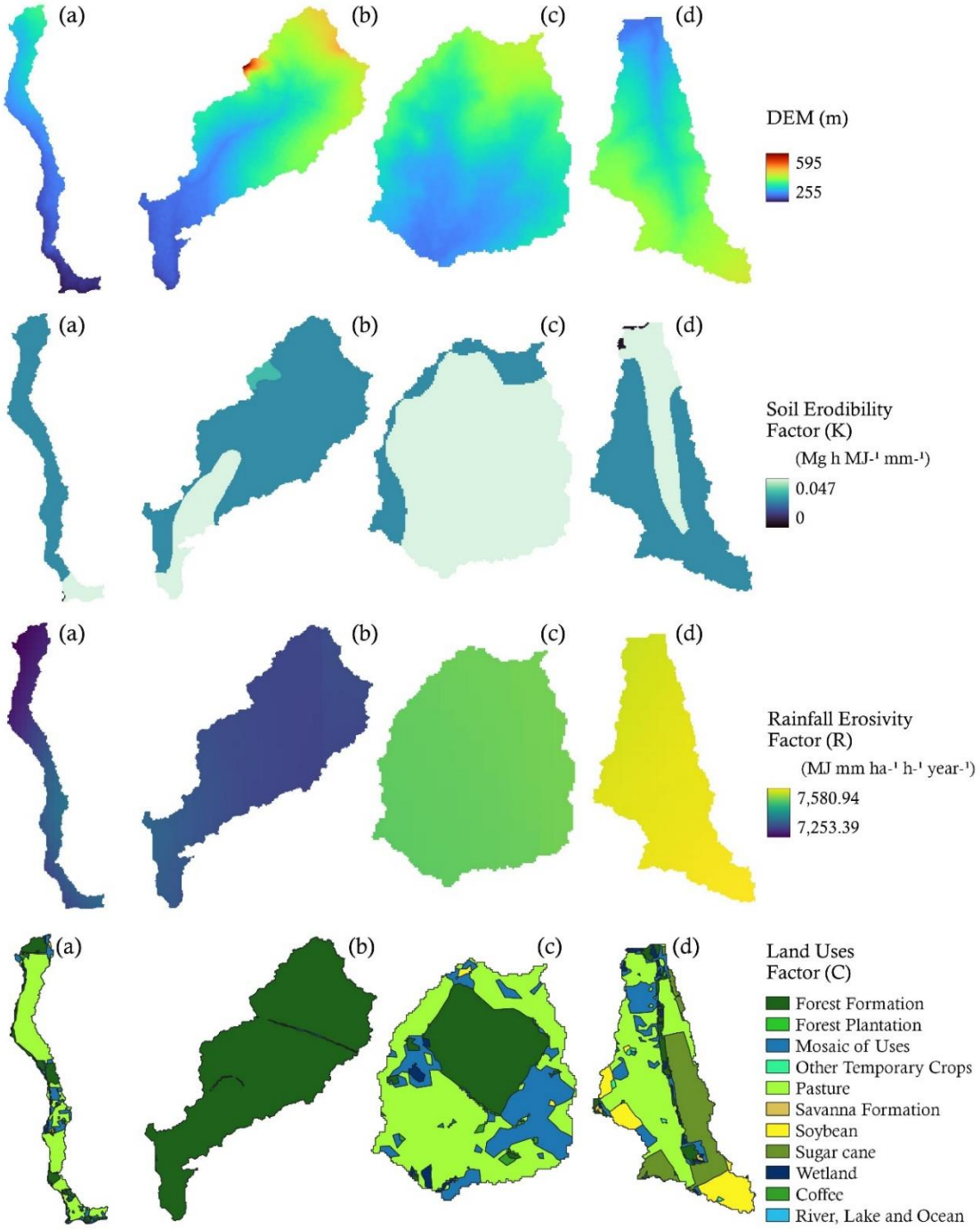

Fig. 2. Digital elevation model (DEM), soil erodibility factor (K), rainfall erosivity factor (R), and land uses of the watersheds Nelore (a), Morro do Diabo (b), Pelanca (c), and Santa Beatriz (d), from Pontal do Paranapanema, state of São Paulo, Brazil.

Table 2. Input data in the InVEST software for sediment retention modeling.

Input	Characteristics and model hyperparameters
Digital elevation model (m)	SRTM digital elevation model (30 m resolution).
Rainfall erosivity (R) (MJ mm ha^{-1} h^{-1} $year^{-1}$)	Information was derived from 27 meteorological stations located throughout the Pontal do Paranapanema region and its vicinity.
Soil erodibility factor (K) (Mg h MJ^{-1} mm^{-1})	Obtained from literature for each soil type: PA = 0.045 (Mannigel et al., 2002), PVA = 0.0466 (Mannigel et al., 2002), PV = 0.0228 (Mannigel et al., 2002), GX = 0.0044 (Mannigel et al., 2002), LA = 0.0570, LV = 0.0061 (Mannigel et al., 2002), OX = 0.0610 (Silva and Álvares, 2005), and RL = 0.0344 (Mannigel et al., 2002).
Cover management factor (C)	Obtained from literature for each C factor: coffee = 0.02 (Bertoni and Lombardi Neto, 1999), forest formation = 0.004 (Fujihara, 2002), mosaic of land uses = 0.1 (ANA, 2012), other temporary crops = 0.40 (ANA, 2012), pasture = 0.02 (Bertoni and Lombardi Neto, 1999), soybean = 0.25 (Bertoni and Lombardi Neto, 1999), forest plantation = 0.05 (ANA, 2012), and sugar cane = 0.3066 (Fujihara, 2002).

Additional details on the C factor were considered for permanent preservation areas (PPA), which consist of natural vegetation protected by the Forestry Code, where direct economic exploitation is prohibited. In addition, the Brazilian environmental legislation (Brasil, 2012) obliges private properties to retain a fixed proportion of their total area with native vegetation, the so-called Legal Reserves. In both cases, the C factor values were assumed to be the same as those for the forest formation. For the watercourse, flooded field, wetlands, and swampy area, the C factor was assigned a value of 0 (zero).

Values of the following parameters were set for simulations: Biophysical data (cover-management factor – Table 2, and support practice factor, adopted a value of 1 indicating that no erosion-reduction practices are being done); threshold flow accumulation = 100; Borselly K parameter = 2; Borselli IC_0 parameter = 0.2; maximum sediment delivery ration = 0.8; maximum value of the slope length parameter = 122.

2.6 Direct aquifer recharge

Aquifers are vital components of the water cycle. Protecting and managing these underground water sources is essential to secure a reliable water supply and maintain the integrity of the natural water cycle. They provide base flow to rivers and streams as intermediate reservoirs between inputs and outputs. Concerning water inputs, the rainfall regime is uniform among watersheds. In addition, the soils figuring in input dynamics are all derived from sandstone, whose lithological constitution consists of porous and permeable that favors the storage and transmission of groundwater, as it is predominantly coarse granulometry. Thus, soil and its related landscape of occurrence might be the primary driver of water-partition dynamics, directly impacting direct aquifer recharge. Therefore, we adapted criteria from Menezes et al. (2009) that attributed values to properties related to the potential of direct aquifer recharge based on characteristics retrieved from soil type and relief, with further discussion concerning land use and land cover. The authors proved that the dynamics of the values of soil physical-based attributes showed coherence with the dynamics of the specific yield of the springs. Then, the direct water recharge calculated on this study was supported by environmental characterization, field campaign, and digital soil mapping information, scores were attributed to different soil-landscape units based on Menezes et al. (2009) and the literature review. The higher the value obtained, the higher the potential of direct aquifer discharge occurrence. The soils related to aquifer outputs or discharge are those derived from alluvial sediments in wetlands, where water flows into the soil surface.

The SoLIM inference model was also applied to derive continuous direct aquifer recharge index maps through the watersheds (Zhu et al., 1997) from fuzzy membership maps. The following equation (5) was applied:

$$D_{ij} \frac{\sum_{k=1}^{n} S_{ij}^{k} D^{k}}{\sum_{k=1}^{n} S_{ij}^{k}} \qquad (5)$$

where *Dij* consists of the index of direct aquifer recharge at location (*i, j*), D^k is the representative or typical index value of aquifer recharge representative of soil-relief *k*, and *n* is the total number of soil-relief combinations that varies for each watershed (Zhu, 1997). The level of resemblance between the environment for soil at location (*i, j*) and the environment for soil type *k* is expressed by S_{ij}^{k}. The higher the membership value of a local soil in a given soil type, the closer the property values (index of direct aquifer recharge) will be at that location to typical property values (Zhu et al., 2010). Thus, the

outcome results consist of a knowledge-based spatial predictive model of direct aquifer recharge for each watershed.

Fig. 3 displays the complete framework developed in this study following the requirements outlined by Jónsson and Davíðsdóttir (2016). Digital soil mapping techniques were applied to increase the details of the soil legacy data. Thus, both maps were applied as a fundamental basis for assessing ecosystem services.

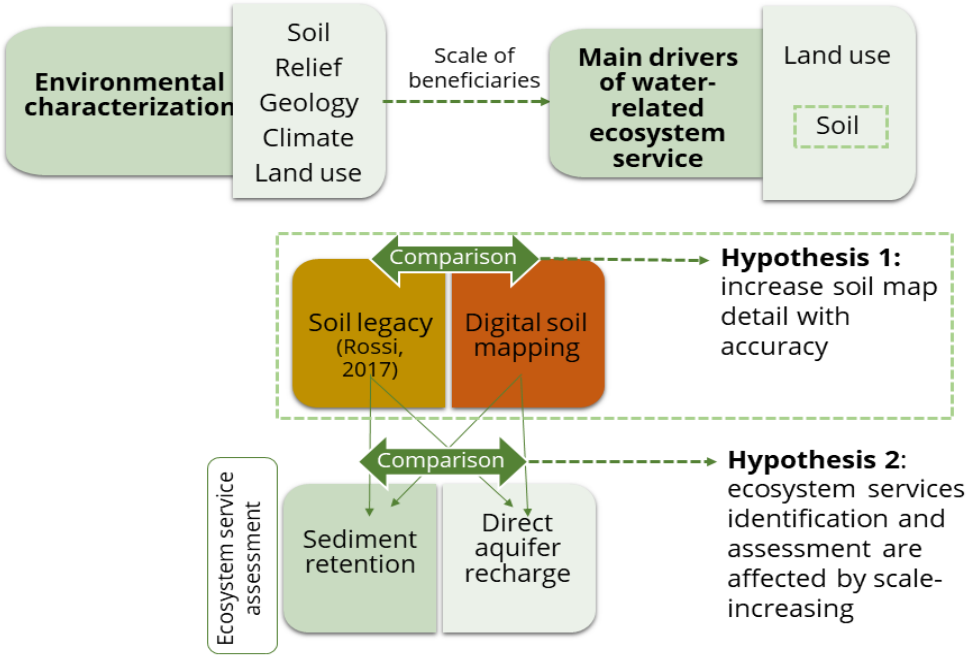

Fig. 3. The complete framework of the study case in the Pontal do Paranapanema, Brazil.

3 Results and Discussions

3.1 Digital soil mapping, accuracy assessment, and resolution considerations

With the assumption that similar environmental conditions have similar soil-landscape relationships (Jenny, 1941), typical soil-terrain conditions were established for each soil type and, further, to predict soil properties related to ecosystem services at unvisited locations. Rules were created to represent typical soil-landscape features based on terrain attributes and knowledge curves (bell, S, or Z shape) (Table 3). The higher the typical value on the curves, the more typical a terrain attribute for a given soil.

Table 3. Rules are assigned through membership curves using terrain attributes (TA) for each soil type.

Soil type	TA	Low Cross	High Cross	Low Unit	High Unit	Curve
Morro do Diabo watershed						
GX	CI	-77.86	-40.72	-59.29	-59.29	Bell shape
	RSP	-0.19	0.00	-0.09	-0.09	Bell shape
	TWI	15.56	20.11	17.83	17.83	Bell shape
LA	MRVBF	2.80	4.35	3.70	3.70	Bell shape
LV	CNBL	416.00	-	420.00	-	S-shape
	RSP	0.35	-	0.50	-	S-shape
	VD	-	40.00	-	35.00	Z-shape
OX	DEM	570.00	-	574.00	-	S-shape
PV	DEM	340.00	420.00	385.00	385.00	Bell shape
RL	DEM	500.00	570.00	530.00	530.00	Bell shape
	RSP	0.85	-	0.90	-	S-shape
	VDCN	77.00	-	90.00	-	S-shape
Nelore watershed						
GX	CI	-39.29	-20.20	-29.74	-29.74	Bell shape
	MRRTF	-	0.10	-	0.00	Z-shape
	TCA	203096.06	476694.28	339895.17	339895.17	Bell shape
	VD	36.78	51.01	43.90	43.90	Bell shape
LV	CND	0.50	-	15.00	-	S-shape
	RSP	0.01	-	0.79	-	S-shape
PA	MRVBF	3.71	4.00	3.86	3.86	Bell shape
PV	VD	17.00	37.00	27.00	27.00	Bell shape
Pelanca watershed						
GX	CND	-	0.00	-	-8.11	Z-shape
	CI	-	25.00	-	-54.39	Z-shape
	RSP	-0.10	0.03	-0.04	-0.04	Bell shape
	TCA	105,034.65	7308686.50	3706860.50	3706860.50	Bell shape
	TWI	13.24	18.29	15.76	15.76	Bell shape
LV	RSP	0.17	-	0.20	-	S-shape
PV	RSP	0.03	0.20	0.17	0.17	Bell shape
Santa Beatriz watershed						
GX	MRVBF	3.00	-	4.30	-	S-shape
	RSP	-	0.03	-	0.00	Z-shape
	TWI	13.24	19.02	16.13	16.13	Bell shape
	VDCN	-	5.00		0.00	Z-shape
LV	RSP	0.13	-	0.70	-	S-shape
	VD	-	20.00	-	0.00	Z-shape
	VDCN	1.00	-	15.00	-	S-shape
PA	RSP	0.003	0.60	0.20	0.20	Bell shape

PV	RSP	0.20	0.80	0.50	0.50	Bell shape
	VDCN	6.25	14.00	10.13	10.13	Bell shape

*Soils - GX: Gleissolo Háplico; LA: Latossolo Amarelo; LV: Latossolo Vermelho; PA: Argissolo Amarelo; PV: Argissolo Vermelho; PVA: Argissolo Vermelho-Amarelo; OX: Organossolo Háplico; RL: Neossolo Litólico. TA - CND: Channel Network Distance; CI: Convergence Index; DEM: Digital Elevation Model; MRVBF: Multiresolution Index of Valley Bottom Flatness; MRRTF: Multiresolution Index of the Ridge Top Flatness; RSP: Relative Slope Position; TWI: Topographic Wetness Index; TCA: Total Catchment Area; VD: Valley Depth; VDCN: Vertical Distance to Channel Network.

It is important to emphasize that the terrain attributes most efficient for delineating soil classes showed the most remarkable difference in values between one class and another. RSP, DEM, VDCN, and CND were consistently applied for all watersheds since the variation in their values indicates distinct soil position through a catena. Taking RSP as an example, higher values indicate elevated landscape position farther from the drainage network, intermediate values represent the middle third, and lower values are associated with areas close to the drainage network. Therefore, by utilizing this TA, it becomes possible to distinguish between well-drained (LV and PV) and very poorly-drained soils (GX) based on their landscape positions. Higher values of RSP, DEM, VDCN, and CND were assigned as higher optimality values for well-drained soils. Though hillslopes, the higher the RSP and VDCN, the higher the optimal condition of Latossolos occurrence, representing the gentle summit of landscapes. Intermediate values of such terrain attributes consisted of the typical environment of Argissolos that occurred through a backslope position.

Membership curves were built considering two contrasting instances of GX formed in floodplains. The first one consists of assigning higher optimality values for higher values of terrain attributes, as follows: i) lower TCA values were related to the contributing area of a watershed; ii) lower TWI values identified terrain locations prone to moisture accumulation; and iii) lower VD were related to lower landscape areas or floodplain. Conversely, in the second instance, those assigning higher optimality values for lower values of terrain attributes, such as RSP and MRRTF, were also used in the rules but with lower values. OX and RL occurred in elevated landscape positions, where the DEM was crucial for delineating the first soil (the higher the DEM, the higher the optimality in membership curves), along with the RSP and VDCN for the second soil.

When comparing the soil maps produced by fuzzy logic (Fig. 4b, c, f, and h) with the existing maps (Rossi, 2017) (Fig. 4a, c, e, and g), an increase in detail is evident. The

final digital soil maps are compatible with a scale of 1:100,000 according to the soil survey technical report (IBGE, 2015), while the existing map had a scale of 1:250,000. Notably, Latossolos and Argissolos persist as the dominant soil classes, with only a few differences in their spatial distribution. For instance, in the Morro do Diabo and Nelore watersheds, the legacy soil map designated Latossolos as dominant, whereas the fuzzy logic mapped Argissolos in this position. Since the mapped areas are extensive, it is common for the soil formation factors used for classification on a macro scale to exhibit localized variations. In certain regions within the same watershed, it was delineated soil classes identical to those mapped in the legacy information (Fig. 4a; b), such as in the Santa Beatriz and Pelanca watersheds. In contrast, in the Morro do Diabo watershed, soil class variations, including GX, LA, and OX, were added due to new findings during the field campaign.

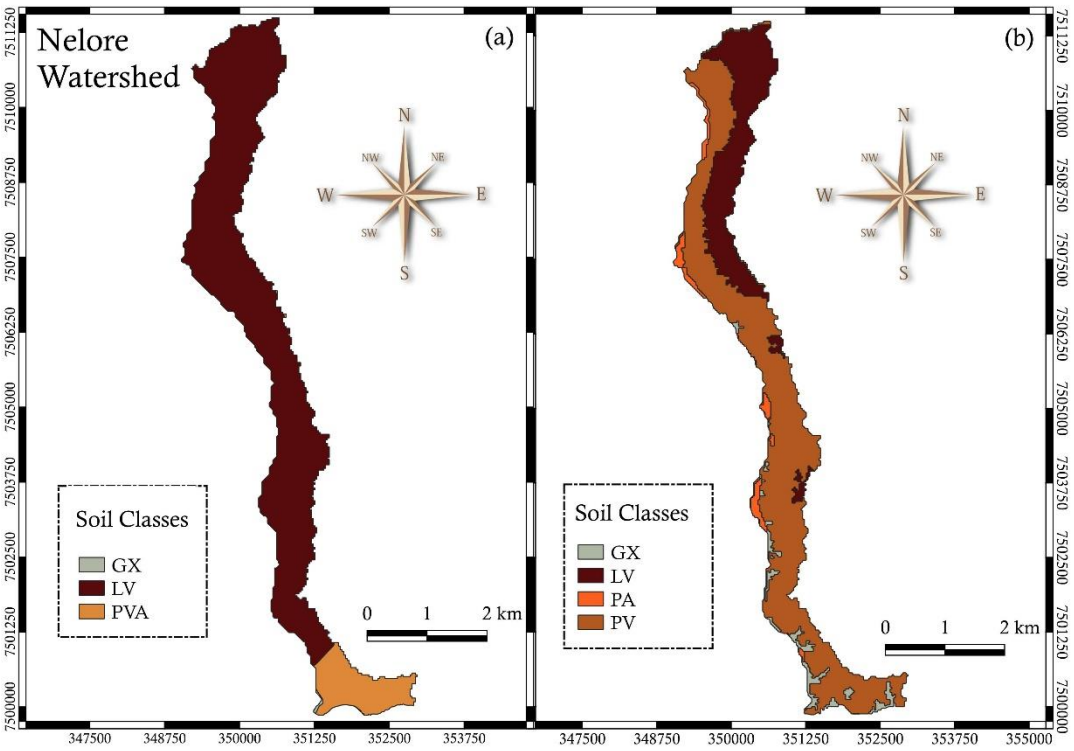

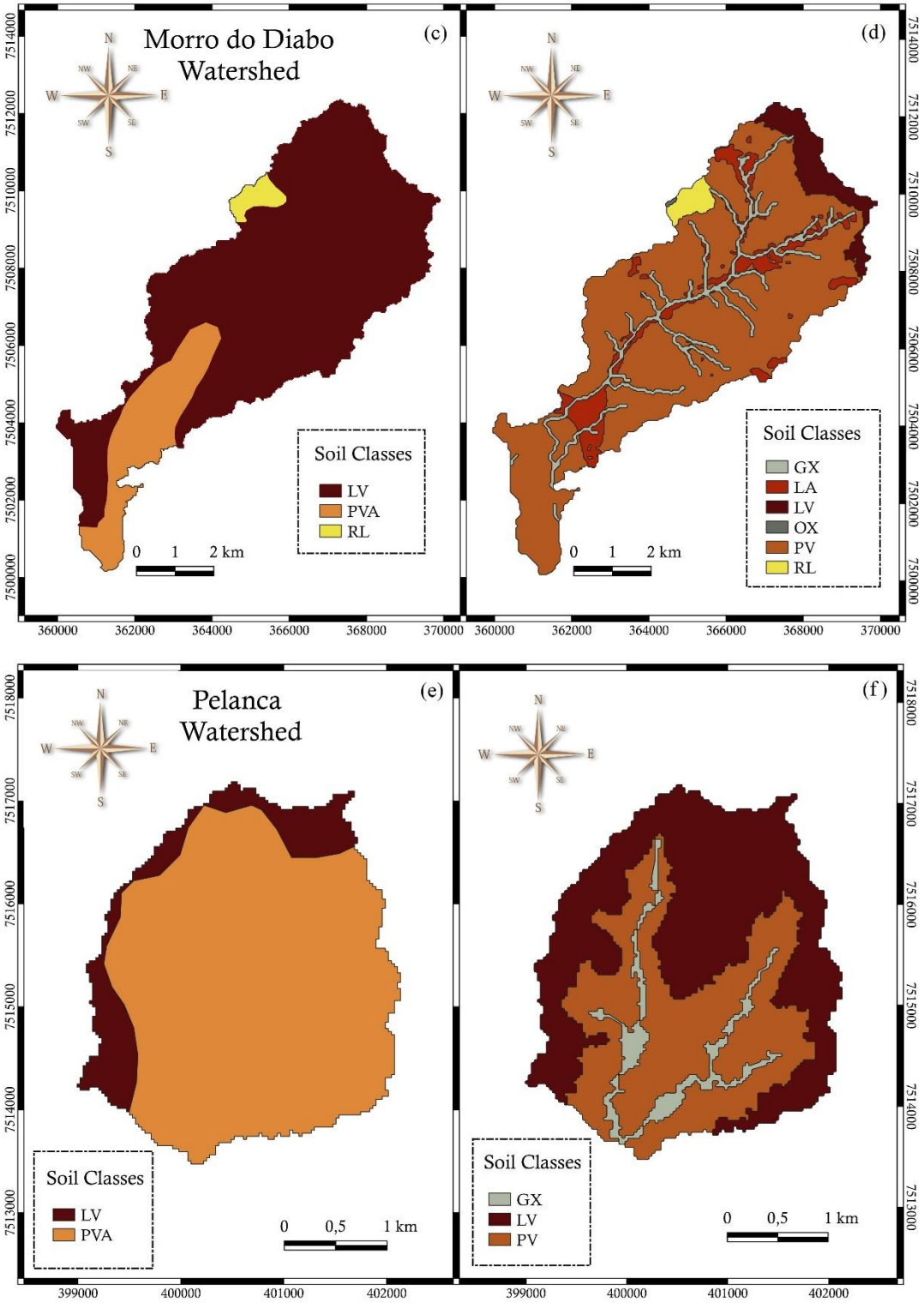
Morro do Diabo Watershed
(c)
(d)
Soil Classes
LV
PVA
RL
GX
LA
OX
PV
0 1 2 km
Pelanca Watershed
(e)
(f)
0 0,5 1 km
N
NW
NE
W
E
SW
SE
S
7514000
7512000
7510000
7508000
7506000
7504000
7502000
7500000
360000
362000
364000
366000
368000
370000
7518000
7517000
7516000
7515000
7514000
7513000
399000
400000
401000
402000

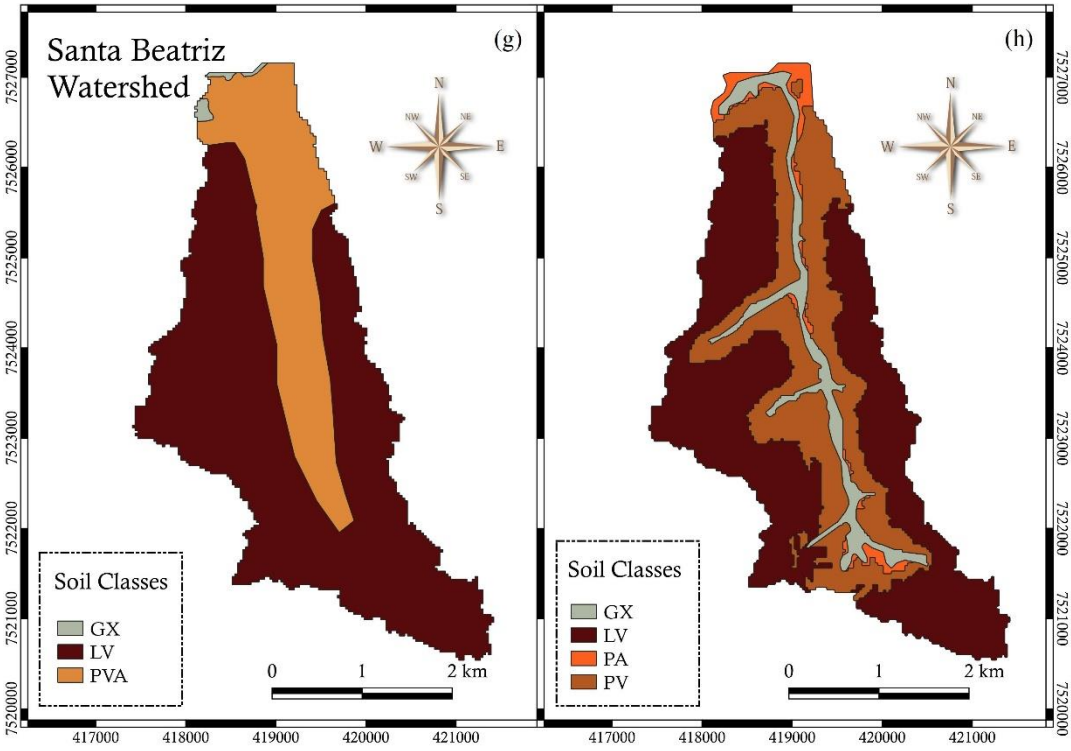

Fig. 4. Digital soil maps of the Nelore, Morro do Diabo, Pelanca, and Santa Beatriz watersheds in Pontal do Paranapanema, state of São Paulo, Brazil. Letter (a, c, e, and g) shows a soil map from Rossi (2017), and letter (b, d, f, and h) shows a soil map produced by fuzzy logic. GX: Gleissolo Háplico; LA: Latossolo Amarelo; LV: Latossolo Vermelho; PA: Argissolo Amarelo; PV: Argissolo Vermelho; PVA: Argissolo Vermelho-Amarelo; OX: Organossolo Háplico; RL: Neossolo Litólico.

The most remarkable increase in digital soil map detail involved the floodplain portions and GX. Although fragile (Arana et al., 2018), this vital landscape unit provides multiple ecosystem services, including supporting, regulating, provisioning, and cultural services (Petsch et al., 2022). Wetness indicators will generally be stronger and more prominent here than all other slope positions (Schaetz and Anderson, 2005). Floodplains and wetlands have been successfully delineated by digital terrain attributes (Machado et al., 2019; Moonjun et al., 2020) since some of them might be considered as hydrologic morphometric variables by connecting pedo-geomorphology with water dynamics (Mello et al., 2022).

Another soil-landscape relationship that imposes additional detail in the digital soil map of Nelore, Pelanca, and Santa Beatriz watersheds consisted of Latossolos and Argissolos through a catena. Latossolos were typically found across gentle summits of the landscape conducive to soil development through weathering-leaching over a stable geomorphic surface. Argissolos, in turn, occur through the transportation of material by

a rapid mass movement and/or surface water action process resulting from subsurface soil water movement (Schaetzl and Anderson, 2005).

Although visual interpretations revealed increasing information, the accuracy should be assessed to attest to the reliability of new digital soil maps. Generally, satisfactory accuracy was achieved (Table 5), especially overall accuracy. Across all watersheds, the values exceeded 60%, mainly with values equal to or higher than the average achieved digital soil map applications in Brazil (63%) reported by an extensive review by Coelho et al. (2021). The authors also found a kappa coefficient close to 50%. Comparatively, our results demonstrated higher values in the Pelanca (74%), and Morro do Diabo (53%) watersheds but lower in the Nelore (17%) and Santa Beatriz (31%) watersheds.

Table 5. Kappa index and overall accuracy obtained from digital soil mapping of each watershed.

Watershed	Kappa index	Overall accuracy
Morro do Diabo	0.53	0.63
Nelore	0.17	0.60
Pelanca	0.74	0.89
Santa Beatriz	0.31	0.67

User's and producer's accuracy indexes (Table 6) provided which soil class within each watershed was being predicted more accurately. It was observed that Argissols had higher prediction accuracies compared to Latossolos. OX and RL were also predicted with high accuracy.

Table 6. Validation of the soil maps of the watersheds: User's accuracy and Producer's accuracy indexes of each soil type.

Watershed	Soil	User's accuracy	Producer's accuracy
Morro do Diabo	Argissolo Vermelho	1.00	0.25
	Latossolo Amarelo	1.00	1.00
	Neossolo Litólico	1.00	1.00
	Organossolo Háplico	1.00	1.00
	Latossolo Vermelho	0.00	0.00
Nelore	Latossolo Vermelho	0.50	0.50
	Argissolo Vermelho	0.67	0.67
Pelanca	Latossolo Vermelho	1.00	1.00

	Argissolo Vermelho	1.00	0.86
Santa Beatriz	Argissolo Amarelo	1.00	1.00
	Latossolo Vermelho	0.75	0.75
	Argissolo Vermelho	0.33	0.33

Typical soil-landscape units observed after the field campaign and modeling applying terrain attributes are displayed in Fig. 5. Overall, soils can be divided based on different weathering degrees: young (GX, RL, and OX), mature (PV, PVA, and PA), and old (LV, LVA, and LA). GX consists of hydromorphic mineral soil, typically in floodplains (lowlands with flatter reliefs). GX presents greyish colors due to a redoximorphic environment imposed by the hydric regime influenced by flooding water, groundwater, and seepage water (Rinklebe and Langer, 2008). RL is a very shallow soil without a B horizon, which means that the bedrock is closer to the surface mainly due to geological erosion imposed by steep slopes. OX is essentially organic, formed under a high input of organic matter with decomposition constrained by environmental characteristics leading to accumulation, found mainly at higher and steeper slopes.

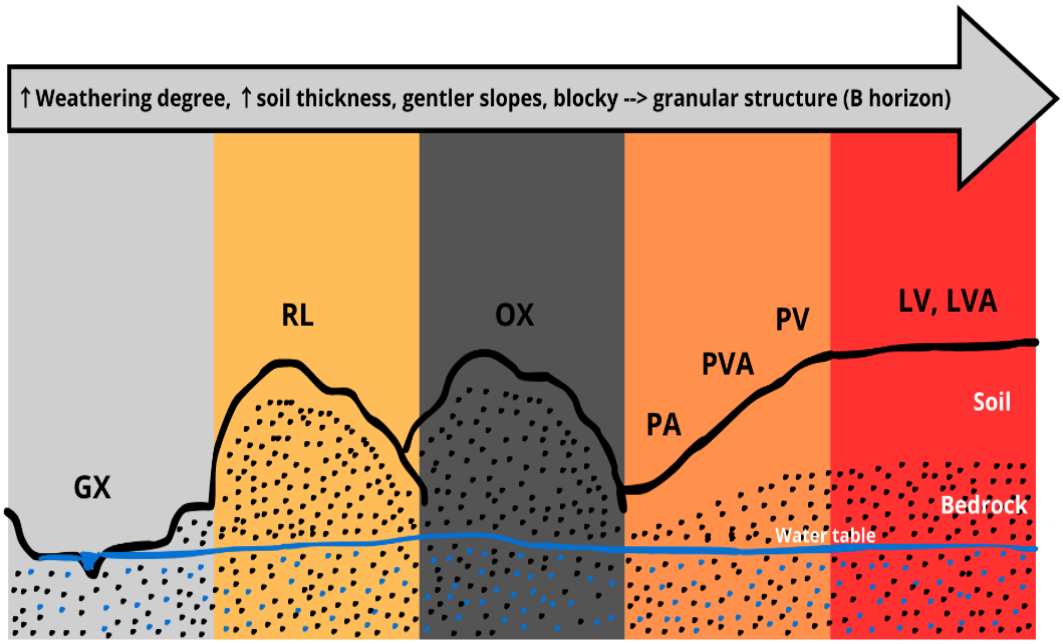

Fig. 5. Typical soil-landscape units of Pontal of Paranapanema and bedrock consist of sandstone.

The older the soil, the thicker and more stable the soil tends to be (Gonçalves et al., 2019). Although genetically connected through a catena, they contrast due to the type of soil structure in the B horizon driven by pedogenic processes. Argissolos are those formed under clay illuviation, whose pedogenic process contributes to clay skin

formation, along with the presence of kaolinite (Moniz et al., 1973), leading to a prevalence of blocky structure development. Consequently, there is a decrease in soil permeability in the B horizon compared to Latossolos. The latter consists of a very thick and porous soil due to a granular structure in the B horizon. Concerning soil granulometry (obtained in the laboratory by pipette method), Argissolos and Latossolos did not present a remarkable increase of clay in depth (on average, clay content of B horizon/clay content of A horizon 0.48 for Argissolos and 0.80 for Latossolos), whose soil texture was classified as loam for both soil and A and B horizon, reinforcing that soil structure might govern physic and hydric behavior rather than granulometry (Resende et al., 2014).

Notwithstanding, the higher content of sand (79 ± 6%) and very low silt content (4 ± 2%), a characteristic influenced by sandstone bedrock, might contribute to water movement toward water configuring in direct aquifer recharge and less soil-water retention into the soil. In addition, the mineralogy of the soils in the region is predominantly composed of quartz, a mineral extremely resistant to weathering in the sand fraction (Schaetzl and Anderson, 2015). The granulometric analysis revealed that Latossolos were formed under Bauru sandstone without any connection with preterit fluvic deposits (Moniz et al., 1973).

3.2 Soil loss and sediment retention ecosystem service and scale of information

Ecosystem services can be defined as all the benefits we receive from the nature, divided into provisioning services (e.g. food and water), regulating services (e.g. erosion control), cultural services (e.g. recreational benefits), and supporting services (e.g. nutrient cycling) (IPBES, 2024). The main drivers of soil loss in the study areas were soil types, relief, and land use. The K factor has been extensively related to soil types, as can be viewed in Table 2. Such a factor is included in RUSLE and significantly influences soil loss values. Thus, to understand the increasing detail in the soil map propagated to soil loss models, two kinds of soil information were used as model input data: the soil legacy (Fig. 4a, c, e, and g) and digital soil maps (Fig. 4b, d, f, and h). With the increasing detail from the digital soil mapping technique, it is noteworthy that the soil scale affected the final models differently.

An increase in lands with higher soil loss values at the Nelore watershed (Figure 6b) is probably attributed due to the expansion of Argissolos (Figure 4b), particularly PV, at the expense of LV, which LV consists of thick and porous soil with a higher infiltration rate and favorable downward water movement, decreasing erosion susceptibility.

Conversely, a decrease in lands with higher soil loss at the Pelanca and Santa Beatriz watersheds (Figure 4f, and 4h). In the Pelanca watershed was observed due to increased geographical expression of GX, PV, and LV over PVA (Figure 4f), whose soils present very low K values (GX = 0.0044, PV = 0.0228 and, LV = 0.0061 Mg h MJ^{-1} mm^{-1}). GX is located at flat and low lands, which are more prone to receiving sediments than lost soil. The soil color refers to iron oxides hematite and goethite (reddish and yellowish soils, respectively). Thus, PV, compared to PVA, predominates the formation of hematite due to better soil drainage and permeability, reducing surface runoff and, consequently, the erosion process. In the LV, this beneficial characteristic is even more pronounced due to the soil profile being more homogeneous. Considering the Santa Beatriz watershed, despite a reduction in the area of Latossolo Vermelho, the entire area previously mapped as PVA was reclassified as PV (Figures 4g, and 4h). Consequently, the overall susceptibility of the watershed to erosion decreased (Figures 6g, and 6h).

In the Morro do Diabo watershed, was observed that both maps depicted similar levels of soil loss (Figures 6c and 6d), even though there was a large change from LV to PV (Figure 4c, and 4d). Despite PV being more vulnerable to sheet erosion than LV, it was found that increasing the details of this soil map did not cause noteworthy changes in terms of potential soil losses. This reflects the importance of native forests in this watershed, preventing the adverse effects of more intense land uses if implemented (situated within the Morro do Diabo National Park, which Atlantic Forest predominantly covers). Moreover, examining avoided sediment exports (Figure 7c, and 7d), a distinct trend emerges when utilizing a digital soil map. The data indicates a more substantial increase in avoided export-sediment retention, potentially attributed to the Morro do Diabo watershed's inherent susceptibility to erosion, where PV was predominant. This highlights the significant role played by the vegetation in this watershed in minimizing erosion as it avoids soil displacement and traps sediment from elevated regions in the landscape.

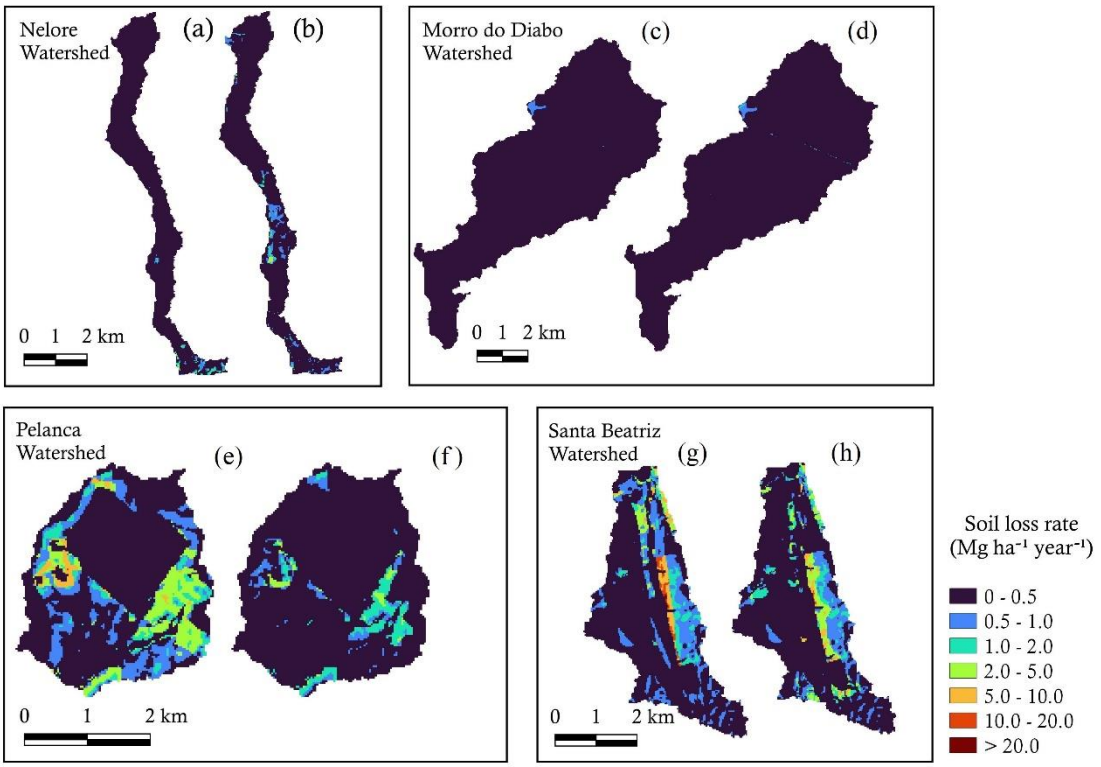

Fig. 6. Soil loss rate in the watersheds Nelore, Morro do Diabo, Pelanca, and Santa Beatriz in the Pontal do Paranapanema. Letter (a, c, e, and g) represents the sediment retention based on the legacy soil map (Rossi, 2017), and letter (b, d, f, and h) represents the sediment retention based on the maps produced herein via the digital soil mapping technique.

The potential of ecosystem service for erosion control was modeled as avoided export, which represents the contribution of vegetation to avoided erosion within a given area, as well as its ability to trap sediment originating from upslope areas (Fig. 7). Two contrasting scenarios were observed at the increase of soil information from the digital soil map: 1) an increase of areas with higher values of avoided export, as is the case of Nelore, and Morro do Diabo, and 2) a decrease of areas with higher values of erosion avoided in Pelanca, and Santa Beatriz watersheds. *Avoided export* indicates the ecosystem service from the perspective of a downstream water user: the sediment kept from the stream benefits water drinking, hydropower, and other uses.

It is important to highlight that when calculating avoided export, we must consider the entire watershed area. When there is a change in soil class at a certain point, it does not affect just that specific point. The soil downstream will or will not receive sediments

from upstream, and the result is cumulative. That is why in Fig. 7 the watersheds were more impacted by the scale of soil map than the soil loss (Fig. 6).

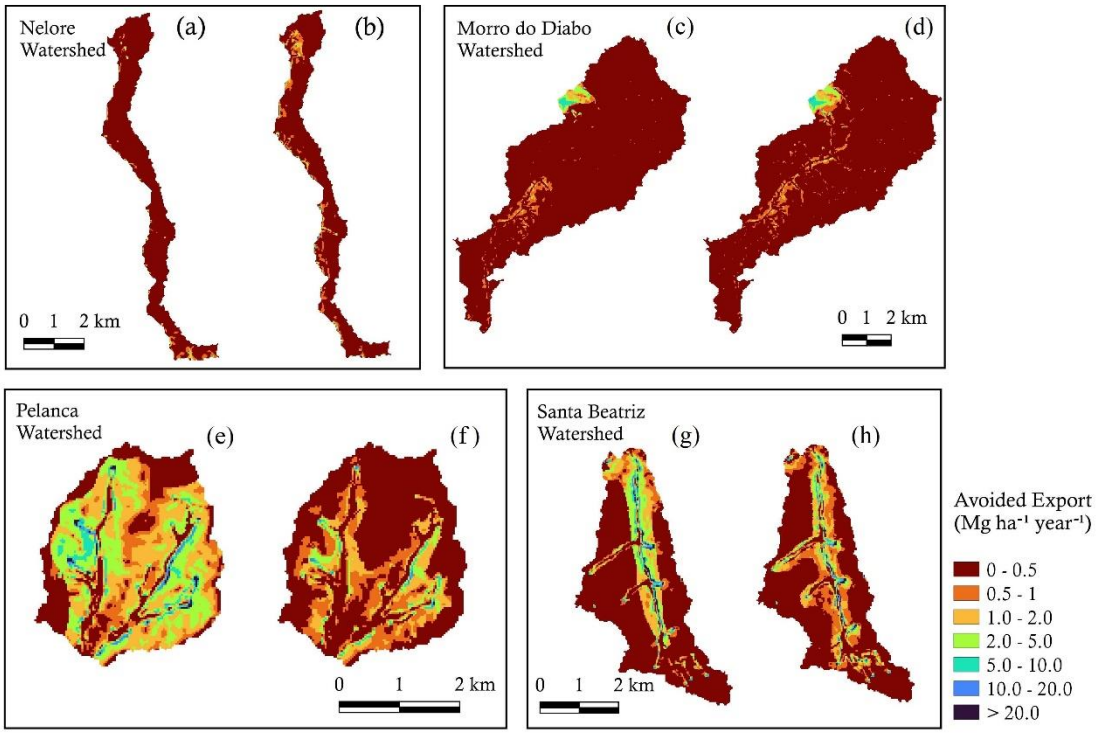

Fig. 7. Sediment potential retention in the watersheds Nelore, Morro do Diabo, Pelanca, and Santa Beatriz, in the Pontal do Paranapanema. Letter (a, c, e and g) represents the sediment retention based on the legacy soil map (Rossi, 2017), and letter (b, d, f, and h) represents the sediment retention based on the maps produced herein via the digital soil mapping technique.

Areas with higher potential soil losses, such as the Pelanca and Santa Beatriz watersheds (Fig. 6), exhibited correspondingly greater avoided sediment exports (Fig. 7). Conversely, a contrasting scenario can also be observed, as in the Nelore watershed, which presented the lowest potential soil loss, leading to the lowest avoided export. This insight is of great importance for making more assertive decisions on land management.

The detection of where sediment has been produced and delivered is of great importance for stakeholders who invest in watershed service programs (Martin-Ortega et al., 2013). Erosion is generally caused by inadequate soil use and management, particularly in production systems that lack soil conservation practices. To mitigate this, we must focus on retaining sediments (avoided export) in the same position as the watershed in which they were generated. Since the sediments reach watercourses, significant environmental damage will have already been done. In areas where soil

erosion is not significant, the impact of vegetation is less prominent. Consequently, in areas where soil is more vulnerable, such as the Pelanca and Santa Beatriz watersheds, the highest values of avoided sediment export are found in locations where vegetation cover helps to retain sediment more effectively. Figure 7 (e; f; g; h) illustrates that conservative management can have a more pronounced effect in certain areas, particularly in the PV and PA regions as shown in the detailed maps generated using fuzzy logic (Figure 7f; h). It's important to note that areas with native vegetation cover, such as those containing GX, are vital for conserving springs and water courses. Even though these areas do not export sediments, the presence of native vegetation cover leads to increased water infiltration and capturing of upstream sediment, which helps to prevent siltation in watercourses. With this information, we can delimit the areas to preserve/restore and identify the areas that need a more sustainable management.

3.3 Direct aquifer recharge and scale of information

Supported by environmental characterization, field campaign, and digital soil mapping information, scores were attributed to different soil-landscape units based on Menezes et al. (2009) and the literature review (Table 7). Martínez-Harms and Balvanera (2012) listed different approaches that can be used for ecosystem service assessment, and this method consists of an expert-based ranking of an environmental variable that influences ecosystem services supply. Soil types were firstly decoded based on their properties that benefit direct water recharge, and in this study case, the main contrasts are in charge of soil thickness, soil texture, type of soil structure at B horizon, and typical slope phases. Thus, soil and landscape were ranked according to their capability to promote direct aquifer recharge (Table 7).

The soil mapping task, including the field campaign is of great importance: the soils of a given watershed should first be fully raised to guide the range of scores of ecosystem supply. Unlike Menezes et al. (2009), the epipedon type was not applied as a criterion due to its low variability in the study sites. The relief phases that each soil type was typically found consist of slope ranges sliced based on Brazilian technical reports (IBGE, 2015; Santos et al., 2015) that suggest plain (0-3%), gently undulated (3-8%), undulated (8-20%), strong undulated (20-45%), and mountainous (45-75%), due to their meaningful concerning water infiltration and soil erosion. The lower the slope, the more likely water infiltration, increasing the aquifer recharge score and vice versa.

Table 7. Scores attributed to interpreting the potential for direct water recharge (Adapted from Menezes et al., 2009). A score of 0 means water discharge. From 1 to 4, the increase in scores means a potential increase in direct aquifer discharge.

Scores	Soil type	Relief phase
0	Gleissolo Háplico	Plain
1	Neossolo Litólico	Strong undulated, and mountainous
2	Organossolo Háplico	Undulated and strong undulated
3	Argissolo (Vermelho, Vermelho-Amarelo, Amarelo)	Undulated
4	Latossolo (Vermelho, Vermelho-Amarelo, Amarelo)	Gentle undulate

A direct aquifer recharge map from legacy data consists of decoded information directly from scores of Table 7 (Fig. 8a, c, e, and g). This is how a property map is generated from a traditional soil map (legacy data) under a discrete polygon-based model: a typical value is assigned and the whole polygon assumes only one value. This could be considered a limitation (Zhu et al., 2001) whose outcome is not even incompatible with new digital tools (digital terrain models or satellite images) nor hydrological dynamics that would be better represented by a continuous distribution.

Conversely, using a fuzzy logic approach, a property map can be generated with only one typical value of each typical soil-landscape unit (Qin et al., 2021) (Fig. 8b, d, f, and g). However, it still reveals a continuous distribution since a weighted average of fuzzy membership values and typical direct aquifer recharge scores were performed pixel by pixel (Menezes et al., 2018).

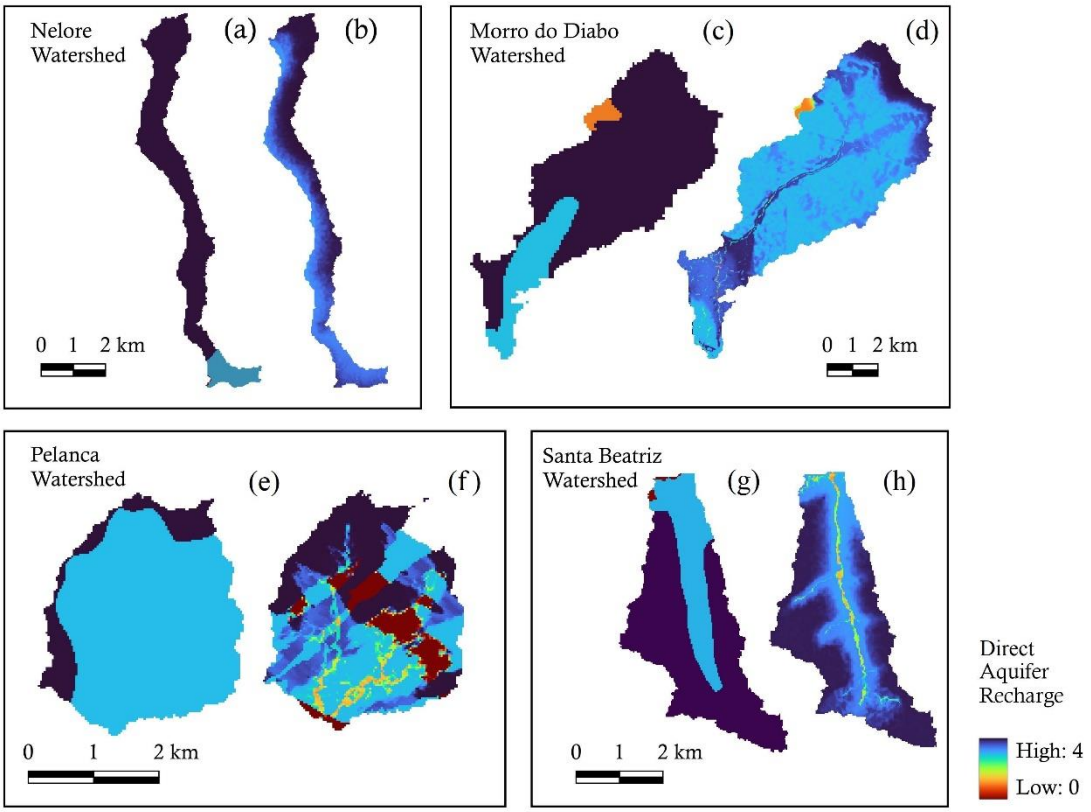

Fig. 8. Potential of direct aquifer recharge in the watersheds Nelore, Morro do Diabo, Pelanca, and Santa Beatriz, in the Pontal do Paranapanema. Letter (a, c, e, and g) represents the aquifer recharge decoded from legacy soil map (Rossi, 2017), and letter (b, d, f, and g) represents aquifer recharge on the maps produced herein via the digital soil mapping technique.

Concerning water, elements near the top of the slope are recharge runoff sites, while elements nearer the base of the slope may recharge or discharge sites, depending on local weather and subsurface geology (Khan and Fenton, 1994, Schaetzl and Anderson, 2005). Also, the main soil that was found near flat tops consists of Latossolos, favoring the recharge of the aquifers. Otherwise, when strong undulated, and mountainous relief occurs, the Neossolo Litólico predominate (Morro do Diabo watershed), and the runoff is expressive because these soils are shallow and underdeveloped in a constant process of rejuvenation, not favoring the water recharge due to the relief. Moura et al. (2024) highlight that soil, slope, land use, and soil management are significant factors that can lead to an adequate aquifer recharge or can reduce this potential. The latter occurs when the area presents steep slopes favoring runoff instead of the water infiltration, or when applied inappropriate soil uses, e.g., the Neossolos and Cambissolos are fragile soils that require sustainable management to avoid environment

degradation. This shows us the importance of more detailed soil maps for adequate management and improving the ecosystem services provision.

Comparing the maps in Fig. 8, we can observe that aquifer recharge was lower than one might suppose, considering the maps developed by traditional methods (Fig. 8a, c, e, and g) compared to those developed based on fuzzy logic (Fig. 8b, d, f, and g). Nevertheless, a relationship persists, with most watersheds having moderately high to high aquifer recharge rates (score: 3 to 4) and predominantly high recharge (score: 4) in three out of four watersheds (Nelore, Morro do Diabo, and Santa Beatriz), while in Pelanca, moderately high recharge (score: 3) predominates. When compared to maps produced by fuzzy logic, inversions of these trends occur in the first three watersheds, mainly due to the inversion of predominance of the soils present there. Previously, Latossolos were predominant compared to Argissolos, and in the maps elaborated by fuzzy logic (Fig. 8b, d, f, and g), it's the opposite. In Pelanca, significant areas of low aquifer recharge (score: 0) appear, mainly due to the inclusion of locations occupied by floodplain soils (GX), that is a discharge site (Khan and Fenton, 1994).

Now, considering aspects such as the lithology of the watersheds, we find that sandstone is generally a rock with great potential for aquifer recharge due to its porosity, especially coarser-textured sandstones (Feitosa et al., 2008; Schaetzl and Anderson; 2005). This coarse-grained sandstone is predominant in the Morro do Diabo and Nelore watersheds (Rio Paraná lithological unit). In the Pelanca watershed, containing two different lithological units (Rio Paraná and Santo Anastácio), areas to the south are predominantly coarse-grained sandstones, while the areas to the north are fine-grained. The Santa Beatriz watershed predominates the fine-grained sandstones (Rio do Peixe lithological unit). Thus, the Santa Beatriz watershed is the one whose water infiltration rate into the soil is hindered due to its fine-grained nature, which also occurs in the northern areas of the Pelanca watershed. However, the Morro do Diabo, Nelore, and southern Pelanca watersheds have gentle slopes in most areas combined with lithological aspects that favor aquifer recharge. In their study of the Rio das Velhas watershed in the Iron Quadrangle, Brazil, Moura et al. (2024) found low scores when evaluating the synergies among aquifer recharge, potential for agriculture, and soil resistance to erosion. This can be attributed to the significant occurrence of metamorphic rocks, such as orthogneiss, quartzite, and phyllites in their study area, combined with steep slopes.,. However, they highlight that where there is itabirite, a very porous rock, the aquifer

recharge is higher than in the other regions. This demonstrates how outstanding the area lithology is to this ecosystem service.

Regarding the management practices carried out in these watersheds (Fig. 2), in the case of Morro do Diabo, the management should aid in increasing aquifer recharge and reducing soil erosion is true since it is predominantly covered by forest, which reduces runoff effects, aiding in increased water infiltration. In areas occupied by annual crops and sugarcane, adopting no-till farming can help in water infiltration and maintenance of crops. Contrary to places where conservation management is not applied, these crops can contribute even more to runoff, accelerating erosive processes. An aspect particular to the Pontal do Paranapanema region is cassava growing (present in the land use mosaic), which occupies large areas and can also accelerate erosive processes because its harvesting requires soil disturbance. Therefore, it is advisable that its planting be carried out in flatter areas and, if possible, rotation the soil with crops that provide better soil cover.

The pasture area is predominantly degraded, leading to the necessity of sustainable management. This management should consider the area carrying capacity in terms of the number of cattle and its susceptibility to soil erosion and compaction. Additionally, agricultural practices such as liming and fertilization need to be implemented. Moreno-Llorca et al. (2020) found an association between the increase in areas planted with pine and a decrease in aquifer recharge, as this crop requires a large amount of water for its development. Conversely, they observed synergy between increased pasture and scrublands (native vegetation) areas and aquifer recharge in their study regarding the evolution of ecosystem services in a 50-year time series in Sierra Nevada, Spain. Demonstrating that although the pasture areas in our study are mainly degraded, they have the potential to increase aquifer recharge when well managed, promoting soil cover and protecting the soil from erosion.

Despite sandstone favoring water infiltration and aquifer recharge, it generally gives rise to fragile soils prone to erosion, mainly rill erosion, due to its low aggregation between particles and its texture ranging from medium to sandy. Thus, it is essential to protect these soils by implementing management practices that maintain vegetative cover and avoid soil disturbance, preventing soil erosion and loss of carbon and nutrients that could be utilized by crops and native vegetation, besides promoting water infiltration and aquifer recharge.

3.4 Discussions concerning the scale of ecosystem service spatial prediction

Overall, ecosystem services supplies were spatially modeled with more detail from methods with a digital soil map as a fundamental basis. InVest model and soil property maps generated from fuzzy logic explored spatially explicit environmental data and provided ecosystem service information following landscape connectivity (Hamel et al., 2015; Qin et al., 2021). This spatial configuration is proper for mapping watershed level configuration, where heterogeneity of ecosystem services has been found (Zhao et al., 2018).

Maes et al. (2012) attributed the use of direct interpretation of ecosystem services based on land use and land cover as a simple approach that may be appropriate for inferences at large scales for areas where the dominant service relates directly to land use. Technically, semi-detailed or larger-scale soil maps would be more appropriate for studies concerning integrated watersheds, local land use, and soil-water conservation planning (IBGE, 2015). The befitting scales must be equal to or greater than 1:50,000 and, in particular situations, may vary up to 1:100,000. However, in Brazil, there is still a shortage of soil information at a more detailed scale, with less than 5% of the national territory having soil maps at very detailed scales (1:100.000 or larger) (Pronasolos, 2016, available at https://ainfo.cnptia.embrapa.br/digital/bitstream/item/156792/1/Doc-183-Programa-Nacional-de-Solos-do-Brasil.pdf). The continental dimensions of the country worsen this scenario, along with the significant soil variability, and lack of pedologists for necessary fieldwork. Costa et al. (2009) have alerted about an incorrect technical practice that consists of plotting an area of exciting information from expanded maps from reconnaissance and exploratory surveys without additional soil campaigns that would minimize some soil limitations. This misuse can easily be implemented nowadays due to the popularization of geographical information system software. Thus, when detecting watershed-related ecosystem supplies, stakeholders must be aware of how improper the choice of an incorrect soil map scale could be for proper valuation. This inconsistency could be analogously related to the so-called science of scale pointed out by Grêt-Regamey et al. (2014) in mapping ecosystem services. If a model depends on soil information, errors or uncertainties would be directly incorporated into ecosystem services supply estimates.

The effect of increasing differences in ecosystem service estimates was inconsistent and varied across the four case studies. Notably, the greater detail in the soil

map resulted in more accurate soil loss prediction, given the essential role of the soil map in this process. Thus, after obtaining soil losses more precisely, the ecosystem services of soil retention also become more accurate. In a broad analysis, the Pelanca and Santa Beatriz watersheds experienced a reduction in soil retention ecosystem services (avoided export). However, these watersheds also saw reductions in soil loss, with decreases reaching an average of up to 3.1 times. Conversely, the Nellore watershed showed an increase in the average soil retention ecosystem service provided, but a proportional increase in soil loss accompanied this. A notable observation was made in the Morro do Diabo watershed, where the average ecosystem service provided nearly doubled despite similar average soil losses.

Aquifer discharge is the ecosystem supply that is more affected by the soil mapping scale. Also, trade-offs among ecosystem services were spatially detected since soil-landscape units that foster water infiltration, storage, and direct aquifer recharge are those that prevent soil loss with avoided erosion. In this case, the synergies arise when multiple services are enhanced simultaneously (Qiu and Turner, 2013).

4 Conclusions

By analyzing the increase of soil information from the digital soil mapping technique, contrasting soils that might influence ecosystem services differently were accurately revealed. Detailed soil mapping has enabled us to perceive the precise locations within each watershed where ecosystem services occur more intensely and their distribution across the landscape. The detailed soil maps had a greater impact on the direct aquifer recharge ecosystem service. The ecosystem service avoided export indicates that conservative management must be implemented in the PV and PA areas in the Pelanca and Santa Beatriz watersheds. Natural coverage must be maintained or restored, especially in the GX areas of all watershed.

ACKNOWLEGMENTS

Especially to the funding agencies Conselho Nacional de Desenvolvimento Científico e Tecnológico (CNPq) processes number 311743/2021-8; 307059/2022-7 and 307532/2022-4, along with the Coordenação de Aperfeiçoamento de Pessoal de Nível Superior (CAPES), code 001, the Fundação de Amparo à Pesquisa do Estado de Minas

Gerais (FAPEMIG), besides the Instituto de Pesquisas Ecológicas (IPÊ), and China Three Gorges Corporation (CTG), by the financial support that enabled the execution of this research, as for the analyses and materials.

REFERENCES

Akumu, C.E., Woods, M., Johnson, J.A., Pitt, D.G., Uhlig, P., McMurray S., 2016. GIS-fuzzy logic technique in modeling soil depth classes: using parts of the clay belt and hornepayne region in Ontario, Canada as a case study. Geoderma. 283, 78-87. Elsevier BV. http://dx.doi.org/10.1016/j.geoderma.2016.07.028.

Amadeu, R.A., Bernardes, T.L.S., Santos, R.S., Garcia, R.H.L., Velo, A.F., Cavallaro, F.A., Mesquita, C.H., Hamada, M.M., 2021. Characterization of the petrology of the tar sandstone rock of the Paraná basin. Brazilian Journal of Radiation Sciences. 1-17.

Amorim, J.V., Valladares, G.S., Pereira, M.G., Portela, M.G.T., Lima, A.M., 2023. Digital soil mapping for the Parnaíba River delta, Brazilian semiarid region. R. Bras. Cienc. Solo. 47, e0220160. http://dx.doi.org/10.36783/18069657rbcs20220160.

ANA - Agência Nacional de Águas (Brasil), 2012. Manual Operativo do Programa Produtor de Água / Agência Nacional de Águas, 2nd ed. Brasília.

Arana, A.R.A., Bezerra, J.P.P., Gonçalves, D.L., Leal, A.C., Osco, L.P., Ramos, A.P.M., 2018. Water management and environmental planning: permanent preservation areas at the high course of the Santo Anastácio river – SP. R. Bras. de Geografia Física. 11(2), 674-686.

Bertoni, J., Lombardi Neto, F., 1999. Conservação do solo, Livroceres, Piracicaba.

Beven, K.J., Kirkby, M. J., 1979. A physically based, variable contributing area model of basin hydrology. Hydrological Science Bulletin. 24 (1), 43–69. http://dx.doi.org/10.1080/02626667909491834.

Bracken, L.J., Turnbull, L., Wainwright, J., Bogaart, P., 2014. Sediment connectivity: a framework for understanding sediment transfer at multiple scales. Earth Surface Processes and Landforms, 40(2), 177-188. Wiley. http://dx.doi.org/10.1002/esp.3635.

Braido, L.M.H., Tommaselli, J.T.G., 2010. Caracterização climática e dos anos extremos (chuvoso e seco): seus efeitos na produção de cana-de-açúcar, milho e soja para a região do pontal do Paranapanema – SP. Revista Formação, 1(17), 13-34.

Braido, L.M.H., Tommaselli, J.T.G., 2012. Setorização de Fatores Ambientais – Clima, Solos e Relevo para o Planejamento Ambiental e Territorial na Região do Pontal do Paranapanema – SP – Brasil. Revista Geonorte, 3(4), 1268-1282. Edição Especial.

Brasil. Lei nº 12.651, de 25 de maio de 2012. Dispõe sobre a proteção da vegetação nativa; altera as Leis nºs 6.938, de 31 de agosto de 1981, 9.393, de 19 de dezembro de 1996, e 11.428, de 22 de dezembro de 2006; revoga as Leis nºs 4.771, de 15 de setembro de 1965, e 7.754, de 14 de abril de 1989, e a Medida Provisória nº 2.166-67, de 24 de agosto de 2001; e dá outras providências. DF: Diário Oficial da União, 2012.

Carpi Junior, S., Leal, A.C., Dibieso, E. P., 2012. Mapeamento de Riscos Ambientais e Planejamento Participativo de Bacias Hidrográficas: O Caso do Manancial Rio Santo Anastácio, SP-Brasil. R. Territorium: Riscos. 85-93.

Coelho, F.F., Giasson, E., Campos, A.R., Tiecher, T., Costa, J.J.F., Coblinski, J.A., 2021. Digital soil class mapping in Brazil: a systematic review. Scientia Agricola. 78(5), 20190227. FapUNIFESP (SciELO). http://dx.doi.org/10.1590/1678-992x-2019-0227.

Congalton, R.G., 1991. A review of assessing the accuracy of classifications of remotely sensed data. Remote Sens. Environ. 37, 35–46. http://dx.doi.org/10.1016/0034-4257(91)90048-B.

Conrad, O., 2002. *DIGEM* 2.0. Free Software for Scientic and Educational Proposes. Germany, Göttingen.

Conrad, O., Bechtel, B., Bock, M., Dietrich, H., Fischer, E., Gerlitz, L., Wehberg, J., Wichmann, V., Böhner, J., 2015. System for Automated Geoscientific Analyses (SAGA) v. 2.1.4. Geoscientific Model Development, 8(7), 1991-2007. Copernicus GmbH. http://dx.doi.org/10.5194/gmd-8-1991-2015.

Costa, A.M., Curi, N., Menezes, M.D., Araújo, E.F., Marques, J.J., 2009. Levantamento detalhado de solos da microbacia hidrográfica do horto florestal Terra Dura (RS) e considerações sobre escalas de mapeamento. Cienc. e Agrotecnologia. 33(5), 1272-1279. FapUNIFESP (SciELO). http://dx.doi.org/10.1590/s1413-70542009000500011.

Desmet, P.J.J., Govers, G., 1996. A GIS procedure for automatically calculating the USLE LS factor on topographically complex landscape units. J. of Soil and Water Conservation. 51(5), 427-433. Soil and Water Conservation Society.

Donagema, G.K., Campos, D.V.B., Calderano, S.B., Teixeira, W.G., Viana, J.H.M., 2011. Manual de Métodos de Análise de Solo, 2nd ed. Embrapa Solos, Rio de Janeiro.

Dransch, D., Rotzoll, H., Poser, K., 2010. The contribution of maps to the challenges of risk communication to the public. International Journal of Digital Earth. 3(3), 292-311. Informa UK Limited. http://dx.doi.org/10.1080/17538941003774668.

Feitosa, F.A.C., Manoel Filho, J., Feitosa, E.C., Demetrio, J.G.A. (org.), 2008. Hidrogeologia: conceitos e aplicações. 3rd ed. CPRM - Serviço Geológico do Brasil, Teresina.

Fernandes, L.A., 1998. Estratigrafia e evolução geológica da parte oriental da Bacia Bauru (Ks, Brasil). Thesis (Dissertation). – Universidade de São Paulo, São Paulo.

Fujihara, A.K., 2002. Predição de erosão e capacidade de uso do solo numa microbacia do oeste paulista com suporte de geoprocessamento. 118p. Thesis (Dissertation). Escola Superior de Agricultura “Luiz de Queiroz”. Univerdade de São Paulo.

Gallant, J.C., Dowling, T. I., 2003. A multiresolution index of valley bottom flatness for mapping depositional areas. Water Resources Research, 39(12), 1347. American Geophysical Union (AGU). http://dx.doi.org/10.1029/2002wr001426.

Gallant, J.C., Wilson, J.P., 2000. Primary topographic attributes, in: WILSON, J.P., Gallant, J. C. (Eds.), Terrain Analysis: Principles and applications. John Wiley & Sons, New York, pp. 51-85.

Gonçalves, M.G.M., Avalos, F.A.P., Reis, J.V., Costa, M.V., Silva, S.H.G., Poggere, G.C., Curi, N., Menezes, M.D., 2022. Pedology-based management class establishment: a study case in brazilian coffee crops. Precision Agriculture. 23(3), 1027-1050. Springer Science and Business Media LLC. http://dx.doi.org/10.1007/s11119-021-09873-0.

Grêt-Regamey, A., Weibel, B., Bagstad, K.J., Ferrari, M., Geneletti, D., Klug, H., Schirpke, U., Tappeiner, U., 2014. On the Effects of Scale for Ecosystem Services Mapping. Plos One. 9(12), 112601. Public Library of Science (PLoS). http://dx.doi.org/10.1371/journal.pone.0112601.

Hamel, P., Chaplin-Kramer, R., Sim, S., Mueller, C., 2015. A new approach to modeling the sediment retention service (InVEST 3.0): case study of the cape fear catchment, North Carolina, USA. Science of The Total Environment. 524-525, 166-177. Elsevier BV. http://dx.doi.org/10.1016/j.scitotenv.2015.04.027.

Haynes, K., Barclay, J., Pidgeon, N., 2007. Volcanic hazard communication using maps: an evaluation of their effectiveness. Bulletin of Volcanology. 70(2), 123-138. Springer Science and Business Media LLC. http://dx.doi.org/10.1007/s00445-007-0124-7.

IBGE, 2015. Manual técnico de pedologia, 3rd ed. IBGE, Rio de Janeiro.

IPBES - Intergovernmental Science-Policy Platform on Biodiversity and Ecosystem Services, 2024. Ecosystem Service: Definition. Disponível em: https://www.ipbes.net/glossary-tag/ecosystem-service. Acesso em: 20 jun. 2024.

Jenny, H., 1941. Factors of soil formation: A system of quantitative Pedology. McGraw-Hill Book Co., Inc., New York.

Jónsson, J.Ö.G., Davíðsdóttir, B., 2016. Classification and valuation of soil ecosystem services. Agricultural Systems. 145, 24-38. Elsevier BV. http://dx.doi.org/10.1016/j.agsy.2016.02.010.

Khan, F.A., Fenton, T.E., 1994. Saturated zones and soil morphology in a Mollisol catena of central Iowa. Soil Sci. Soc. of Am. J. 58, 1457–1464.

Köppen, W., 1948. Climatologia: com um estúdio de los climas de la tierra. México. Ed. Fondo de Cultura Econômica. Version de Pedro R. Hendrichs.

Kumar, P., 2010. The Economics of Ecosystems and Biodiversity: Ecological and Economic Foundations. Taylor & Francis.

Lacerda Filho, J.V., 2005. Mapa Geológico do Estado de São Paulo, escala 1:750.000. Programa Geológico do Brasil – PGB, CPRM, São Paulo.

Machado, D.F.T., Menezes, M.D., Silva, S.H.G., Curi, N., 2019. Transferability, accuracy, and uncertainty assessment of different knowledge-based approaches for soil types mapping. Catena. 182, 104134. Elsevier BV. http://dx.doi.org/10.1016/j.catena.2019.104134.

Maes, J., Egoh, B., Willemen, L., Liquete, C., Vihervaara, P., Schägner, J.P., Grizzetti, B., Drakou, E.G., Lanotte, A., Zulian, G., 2012. Mapping ecosystem services for policy support and decision making in the European Union. Ecosyst. Services. 1(1), 31-39. Elsevier BV. http://dx.doi.org/10.1016/j.ecoser.2012.06.004.

Magalhães, S.F.C., Barboza, C.A.M., Maia, M.B., Molisani, M.M., 2022. Influence of land cover, catchment morphometry and rainfall on water quality and material transport of headwaters and low-order streams of a tropical mountainous watershed. Catena. 213, 106137. Elsevier BV. http://dx.doi.org/10.1016/j.catena.2022.106137.

Mannigel, A.R., Passos, M., Moreti, D., Medeiros, L.R., 2002. Fator erodibilidade e tolerância de perda dos solos do Estado de São Paulo. Acta Scientiarum Agronomy. 24, 1335-1340.

Martínez-Harms, M.J., Balvanera, P., 2012. Methods for mapping ecosystem service supply: a review. International J. of Biodivers. Sci., Ecosyst. Services & Manag. 8(1-2), 17-25. Informa UK Limited. http://dx.doi.org/10.1080/21513732.2012.663792.

Martin-Ortega, J., Allott, T.E.H., Glenk, K., Schaafsma, M., 2014. Valuing water quality improvements from peatland restoration: Evidence and challenges. Ecosyst. Services. 9, 34–43. https://doi.org/10.1016/j.ecoser.2014.06.007

McBratney, A., Mendonça Santos, M., Minasny, B., 2003. On digital soil mapping. Geoderma, 117, 3–52. https://doi.org/10.1016/S0016-7061(03)00223-4.

Mello, C.R., Curi, N., 2012. Hydropedology. Cienc. e Agrotecnologia. 36(2), 137-146. FapUNIFESP (SciELO). http://dx.doi.org/10.1590/s1413-70542012000200001.

Mello, C.R., Ávila, L.F., Lin, H., Terra, M.C.N.S., Chappell, N.A., 2019. Water balance in a neotropical forest catchment of southeastern Brazil. Catena. 173, 9-21. Elsevier BV. http://dx.doi.org/10.1016/j.catena.2018.09.046.

Mello, F.A.O.; Demattê, J.A.M.; Rizzo, R.; Mello, D.C.; Poppiel, R.R.; Silvero, N.E.Q.; Safanelli, J.L.; Bellinaso, H.; Bonfatti, B.R.; Gomez, A.M.R., 2022. Complex hydrological knowledge to support digital soil mapping. Geoderma. 409, 115638. Elsevier BV. http://dx.doi.org/10.1016/j.geoderma.2021.115638.

Menezes, M.D., Silva, S.H.G., Mello, C.R., Owens, P.R., Curi, N., 2014. Solum depth spatial prediction comparing conventional with knowledge-based digital soil mapping approaches. Scientia Agricola. 71(4), 316-323. FapUNIFESP (SciELO). http://dx.doi.org/10.1590/0103-9016-2013-0416.

Menezes, M.D., Silva, S.H.G., Owens, P.R., Curi, N., 2013. Digital soil mapping approach based on fuzzy logic and field expert knowledge. Cienc. e Agrotecnologia, Lavras, 37(1), 287-298.

Menezes, M.D., Junqueira Junior, J.A., Mello, C.R., Silva, A.M., Curi, N., Marques, J.J., 2009. Dinâmica hidrológica de duas nascentes, associada ao uso do solo, características pedológicas e atributos físico-hídricos na sub-bacia hidrográfica do Ribeirão Lavrinha - Serra da Mantiqueira (MG). Scientia Forestalis (IPEF). 37, 175-184.

Menezes, M.D., Silva, S.H.G., Mello, C.R., Owens, P.R., Curi, N., 2018. Knowledge-based digital soil mapping for predicting soil properties in two representative watersheds. Scientia Agricola. 75(2), 144-153. FapUNIFESP (SciELO). http://dx.doi.org/10.1590/1678-992x-2016-0097.

Moniz, A.C., Carvalho, A., 1973. Sequência de evolução de solos derivados do arenito Bauru e de rochas básicas da região noroeste do estado de São Paulo. Bragantia. 32, 309-335. FapUNIFESP (SciELO). http://dx.doi.org/10.1590/s0006-87051973000100017.

Moonjun, R., Shrestha, D.P., Jetten, V.G., 2020. Fuzzy logic for fine-scale soil mapping: a case study in Thailand. Catena, 190, 104456. Elsevier BV. http://dx.doi.org/10.1016/j.catena.2020.104456.

Moreno-Llorca, R., Vaz, A.S., Herrero, J., Millares, A., Bonet-García, F.J., Alcaraz-Segura, D., 2020. Multi-scale evolution of ecosystem services' supply in Sierra Nevada (Spain): an assessment over the last half-century. Ecosyst. Services. 46, 101204. Elsevier BV. http://dx.doi.org/10.1016/j.ecoser.2020.101204.

Moura, M.S., Silva, V.C., Pacheco, F.A.L., Fernandes, L.F.S., Pissarra, T.C.T., Costa, A.M., 2024. Beyond land use planning and ecosystem services assessment with the conservation use potential framework: a study in the upper Rio das Velhas Basin, Brazil. Sci. of The Total Environ. 923, 171437. Elsevier BV. http://dx.doi.org/10.1016/j.scitotenv.2024.171437.

NASA, 2013. Shuttle Radar Topography Mission (SRTM) Global. Distributed by OpenTopography. https://doi.org/10.5069/G9445JDF.

Natural Capital Project, 2023. InVEST 3.14.0. Stanford University, University of Minnesota, Chinese Academy of Sciences, The Nature Conservancy, World Wildlife Fund, Stockholm Resilience Centre and the Royal Swedish Academy of Sciences. https://naturalcapitalproject.stanford.edu/software/invest.

Oliveira, V.A., Mello, C.R., Beskow, S., Viola, M.R., Srinivasan, R., 2019. Modeling the effects of climate change on hydrology and sediment load in a headwater basin in the Brazilian Cerrado biome. Ecol. Eng. 133, 20-31. Elsevier BV. http://dx.doi.org/10.1016/j.ecoleng.2019.04.021.

Pelegrino, M.H.P., Silva, S.H.G., Menezes, M.D., Silva, E., Owens, P.R., Curi, N., 2016. Mapping soils in two watersheds using legacy data and extrapolation for similar surrounding areas. Cienc. e Agrotecnologia. 40(5), 534-546. FapUNIFESP (SciELO). http://dx.doi.org/10.1590/1413-70542016405011416.

Perrotta, M.M., Salvador, E.D., Lopes, R.S., D'agostino, L.Z., Peruffo, N., Gomes, S.D., Sachs, L.L.B., Meira, V.T., Garcia, M.G.M., Petsch, D.K., Cionek, V.M., Thomaz, S.M., Santos, N.C.L., 2022. Ecosystem services provided by river-floodplain ecosystems. Hydrobiologia, 850(12-13), 2563-2584. Springer Science and Business Media LLC. http://dx.doi.org/10.1007/s10750-022-04916-7.

Qin, C., An, Y., Liang, P., Zhu, A., Yang, L., 2021. Soil property mapping by combining spatial distance information into the Soil Land Inference Model (SoLIM). Pedosphere. 31(4), 638-644. Elsevier BV. http://dx.doi.org/10.1016/s1002-0160(20)60016-9.

Qiu, J., Turner, M.G., 2013. Spatial interactions among ecosystem services in an urbanizing agricultural watershed. Proceedings of the National Academy of Sci. 110(29), 12149-12154. http://dx.doi.org/10.1073/pnas.1310539110.

Ramke, H.G., 2018. Collection of Surface Runoff and Drainage of Landfill Top Cover Systems. Solid Waste Landfilling. 373-416. Elsevier. http://dx.doi.org/10.1016/b978-0-12-407721-8.00019-x.

Renard, K.G., Foster, G.R., Weesies, G.A., McCool, D.K., Yoder, D.C. (Coordinators), 1997. Predicting Soil Erosion by Water: A Guide to Conservation Planning with the Revised Universal Soil Loss Equation (RUSLE), United States Government Printing, Washington DC.

Resende, M., Curi, N., Resende, S.B., Corrêa G.F., 2014. Pedologia: Base para distinção de ambientes, 6. ed. Editora UFLA, Lavras.

Rinklebe, J., Langer, U., 2008. Floodplain soils at the Elbe river, Germany, and their diverse microbial biomass. Archives of Agronomy and Soil Sci. 54(3), 259-273. Informa UK Limited. http://dx.doi.org/10.1080/03650340701661206.

Robinson, D.A., Hockley, N., Dominati, E., Lebron, I., Scow, K.M., Reynolds, B., Emmett, B.A., Keith, A.M., Jonge, L.W., Schjønning, P., Moldrup, P., Jones, S.B., Tuller, M., 2012. Natural capital, ecosystem services, and soil change: why soil science must embrace an ecosystems approach. Vadose Zone Journal, 11(1). http://dx.doi.org/10.2136/vzj2011.0051.

Rodrigues, A.F., Latawiec, A.E., Reid, B.J., Solórzano, A., Schuler, A.E., Lacerda, C., Fidalgo, E.C.C., Scarano, F.R., Tubenchlak, F., Pena, I., 2021. Systematic review of soil ecosystem services in tropical regions. R. Soc. Open Sci. 8(3), 201584. The Royal Society. http://dx.doi.org/10.1098/rsos.201584.

Rossi, M., 2017. Mapa pedológico do Estado de São Paulo: revisado e ampliado. Instituto Florestal, São Paulo.

Santos, H.G., Jacomine, P.K.T., Anjos, L.H.C., Oliveira, V.A., Lumbreras, J.F., Coelho, M. R., Almeida, J.A., Araújo Filho, J.C., Oliveira, J.B., Cunha, T.J.F., 2018. Sistema Brasileiro de Classificação de Solos, 5th ed. Embrapa Solos, Brasília.

Santos, R.D., Santos, H.G., Ker, J.C., Anjos, L.H.C., Shimizu, S.H., 2015. Manual de descrição e coleta de solos no campo, 7th ed. SBCS, Viçosa.

Schaetzl, R.J., Anderson, S., 2015. Soils: Genesis and Geomorphology, 2nd ed. Cambridge University Press, New York, USA.

Silva, S.H.G., Weindorf, D.C., Faria, W.M., Pinto, L.C., Menezes, M.D., Gulherme, L.R.G., Curi, N., 2021. Proximal sensor-enhanced soil mapping in complex soil-landscape areas of Brazil. Pedosphere. 31(4), 615–626.

Silva, A.M., Alvares, A.C., 2005. Levantamento de informações e estruturação de um banco de dados sobre erodibilidade de classes de solo no estado de São Paulo. R. Geociências. 24, 33-42.

Silva, B.P.C., Silva, M.L.N., Avalos, F.A.P., Menezes, M.D., Curi, N., 2019. Digital soil mapping including additional point sampling in Posses ecosystem services pilot watershed, southeastern Brazil. Scientific Reports, 9(1), 13763. Springer Science and Business Media LLC. http://dx.doi.org/10.1038/s41598-019-50376-w.

Silva, M.P., Santos, F.M., Leal, A.C., Leal, A.C., 2016b. Environmental planning of olga stream hydrographic basin, UGRHI Pontal do Paranapanema - São Paulo. Sociedade & Natureza. 28(3), 409-428. FapUNIFESP (SciELO). http://dx.doi.org/10.1590/1982-451320160307.

Silva, S.H.G., Menezes, M.D., Owens, P.R., Curi, N., 2016a. Retrieving pedologist's mental model from existing soil map and comparing data mining tools for refining a larger area map under similar environmental conditions in Southeastern Brazil. Geoderma. 267, 65-77. Elsevier BV. http://dx.doi.org/10.1016/j.geoderma.2015.12.025.

Somarathna, P.D.S.N., Minasny, B., Malone, B.P., 2017. More Data or a Better Model? Figuring Out What Matters Most for the Spatial Prediction of Soil Carbon. Soil Sci. Soc. of Am. J. 81(6), 1413-1426. Wiley. http://dx.doi.org/10.2136/sssaj2016.11.0376.

Vigiak, O., Borselli, L., Newham, L.T.H., McInnes, J., Roberts, A.M., 2012. Comparison of conceptual landscape metrics to define hillslope-scale sediment delivery ratio. Geomorphology. 138(1), 74–88. https://doi.org/10.1016/j.geomorph.2011.08.026

Vries, J.J., Simmers, I., 2002. Groundwater recharge: an overview of processes and challenges. Hydrogeology J. 10(1), 5-17. Springer Science and Business Media LLC. http://dx.doi.org/10.1007/s10040-001-0171-7.

Wadoux, A.M.J.C., Minasny, B., McBratney, A.B., 2020. Machine learning for digital soil mapping: applications, challenges and suggested solutions. Earth-Sci. Reviews. 210, 103359. Elsevier BV. http://dx.doi.org/10.1016/j.earscirev.2020.103359.

Zanatta, F.A.S., Leal, A.C., Piroli, E.L., 2012. Analysis of the use and cover of the land of permanent preservation areas along the main channel the lower course of Paranapanema's river. Cienc. e Geografia. Bauru, 62-70.

Zhao, M., Peng, J., Liu, Y., Li, T., Wang, Y., 2018. Mapping Watershed-Level Ecosystem Service Bundles in the Pearl River Delta, China. Ecological Economics, 152, 106-117. Elsevier BV. http://dx.doi.org/10.1016/j.ecolecon.2018.04.023.

Zhu, A. X., Hudson, B., Burt, J., Lubich, K., Simonson, D., 2001. Soil mapping using GIS, expert knowledge, and fuzzy logic. Sci. Soc. of Am. J. 65, 1463-1472.

Zhu, A.X.; Band, L.; Vertessy, R.; Dutton, B., 1997. Derivation of Soil Properties Using a Soil Land Inference Model (SoLIM). Soil Sci. Soc. of Am. J. 61(2), 523-533. Wiley. http://dx.doi.org/10.2136/sssaj1997.03615995006100020022x.

Zhu, A.X.; Band, L.E., 1994. A Knowledge-Based Approach to Data Integration for Soil Mapping. Canadian J. of Remote Sens. 20(4), 408-418. Informa UK Limited. http://dx.doi.org/10.1080/07038992.1994.10874583.

Zhu, A.X., Band, L.E., Dutton, B., Nimlos, T.J., 1996. Automated soil inference under fuzzy logic. Ecological Modelling. 90(2), 123-145. Elsevier BV. http://dx.doi.org/10.1016/0304-3800(95)00161-1.

Zhu, A.X., Qi, F., Moore, A., Burt, J.E., 2010. Prediction of soil properties using fuzzy membership values. Geoderma. 158(3-4), 199-206. Elsevier BV. http://dx.doi.org/10.1016/j.geoderma.2010.05.001.

Zhu, A.X., Qin, C.Z., Liang, P., Du, F., Du, F., 2018. Digital soil mapping for smart agriculture: the SoLIM method and software platforms. Rudn J. of Agronomy and Animal Industries, 13(4), 317-335. Peoples' Friendship University of Russia. http://dx.doi.org/10.22363/2312-797x-2018-13-4-317-335.

CHAPTER III:

Can environmental variables, high sampling density and machine learning deliver detailed maps of soil organic carbon and carbon stock in tropical regions?

*Article submitted at **Catena** in Abril 2024.

Fernanda Almeida Bócoli [a], Diego Ribeiro [a], Marcelo Mancini [a], Leonardo Augusto de Sousa [a], Samara Martins Barbosa [a], Milson Evaldo Serafim [b], Bruno Montoani Silva [a], Junior Cesar Avanzi [a], Nilton Curi [a], Sérgio Henrique Godinho Silva [a]*

[a] Federal University of Lavras/UFLA, Department of Soil Science/DCS, Lavras municipality, Minas Gerais State, Brazil, 37.200-900.

[b] Federal Institute of Education, Science and Technology/IFMT, Campus Cáceres, Cáceres municipality, Mato Grosso State, Brazil, 78201-380.

* Corresponding author: sergio.silva@ufla.br

Abstract

Studies on the spatial variability of soil organic carbon (SOC) and carbon stocks (CS) are mostly conducted in temperate regions. More research is needed to create SOC and CS maps with finer resolutions in tropical regions. This work aimed to (1) characterize the spatial distribution of SOC and CS under different land uses; (2) generate predictive models of SOC and CS using environmental variables and proximal and remote sensing, testing 22 combinations of covariate sets; and (3) apply the best models to map SOC and CS at detailed scale. In Lavras, Brazil, 90 locations were sampled in a regular grid (200 x 200 m) in two depths (0-20 and 80-100 cm). 28 locations were sampled for model validation. Samples underwent SOC and texture analyses, and were scanned by proximal sensors (portable X-ray fluorescence – pXRF and magnetic susceptibility – MS). Terrain attributes were calculated from a digital elevation model (12.5 m) and the normalized difference vegetation index (NDVI) and insolation indices were obtained from Sentinel2 and Landsat 8 imagery. The Random Forest (RF) algorithm was used for modeling. Higher SOC contents were found in soils derived from gabbro under native forest and pasture. High variation of SOC and CS was found even within the same land use, soil class and parent material. The prediction achieved an $R^2 = 0.47$ (SOC at 0-20 cm) using the variables related to remote sensing, parent material, soil class, texture, and land uses. Subsurface (80-100 cm) predictions were less accurate. Texture and remotely sensed data were the most important predictors. This study showed that high sample density along with environmental variables provided satisfactory accuracy. This motivates future work on obtaining more accurate and detailed SOC and CS mappings and the development of other strategies, such as the use of new variables or models.

Keywords: Climate change; sustainable agriculture; edaphoclimatic factors; SOC prediction; C stock prediction.

1 Introduction

Guaranteeing food security and more efficient agricultural production is an ongoing endeavor and relates directly to issues caused by climate change, which continues to preoccupy society and experts in the field (Lee et al., 2024; Liu et al., 2023; Shi et al., 2023; Paranavithana et al., 2023). Developing strategies to scale agricultural production while mitigating the negative effects caused by the food production chain (including food, fibers, and energy) is essential. Increasing the content of soil organic carbon (SOC) presents several benefits to productive systems by increasing productivity, besides mitigating the emission of gases such as CO_2 and methane (CH_4) into the atmosphere (Canellas et al., 2000; Paranavithana et al., 2023).

Studies have shown positive effects stemming from the interaction between SOC and physical, chemical, and biological soil attributes, including improvement of aggregation, total porosity, soil water retention, and infiltration capacity (Blanco-Canqui et al., 2013; Silva et al., 2022; Souza et al., 2023), especially in sandy soils and in the subsurface (Minasny; McBratney, 2017). Moreover, higher SOC levels increase the activity and diversity of microorganisms in the soil, contributing to the balance of organism populations, in turn reducing the occurrence of pests and diseases, increasing fertilizer efficiency, leading to the production of higher quality food while reducing the use of chemicals (Blanco-Canqui et al., 2013; Cotching, 2018; Fageria, 2012).

Carbon stock (CS) is defined as the amount of carbon stored in soils per area and depends on the SOC content, soil density, and the sampled layer thickness (Gomes et al., 2019). It is a tool used to quantify carbon and represent CO_2 equivalence per area used to calculate carbon units for greenhouse gas (GHG) emission reduction projects and carbon credit markets, in accordance with the Verified Carbon Standard (VCS, 2024). Generating

detailed maps of both SOC and CS entails high operational costs, as it requires a large amount of field-collected data, besides high laboratory analysis costs, which motivates the search for methods that facilitate obtaining such information. This issue has been investigated through predictive models created using algorithms such as the Random Forest, Support Vector Machine, and Artificial Neural Networks (Sothe et al., 2022; Taghizadeh-Mehrjardi et al., 2020; Tayebi et al., 2021). To reduce data acquisition costs, several studies have been conducted combining machine-learning algorithms with satellite and drone data (remote sensors) to infer SOC content (Li et al., 2018; Taghizadeh-Mehrjardi et al., 2020). Additionally, tools such as proximal sensors, which generate low-cost data quickly and without generating waste, have also been proven to provide valuable data complementary to remotely sensed data, contributing to more accurate modeling and mapping of SOC levels (Wang et al., 2015; Mukhopadhyay; Chakraborty, 2020; Cambule et al., 2012; Nawar; Mouazen, 2018; Faria et al., 2022) and CS (Li et al., 2018; Siewert, 2018).

Several studies around the world are evaluating the importance of different predictor variables to explain SOC variation, including variables from remotely and proximally sensed data (Taghizadeh-Mehrjardi et al., 2020; Gomes et al., 2019; Nuralykyzy et al., 2023). However, most of the studies conducted for the quantification and mapping of SOC are from temperate regions, where soil and climatic conditions act differently from those of the tropical regions (Nuralykyzy et al., 2023; Shi et al., 2023; Li et al., 2018; Taghizadeh-Mehrjardi et al., 2020; Poeplau et al., 2016). Studies of this nature in tropical soils at the property level (high detail) are particularly rare (Mantovani et al., 2024). Differences in soil forming factors (especially climate and age) lead to different predominating soil taxa, whereby highly weathered and old soil classes will predominate in tropical environments (e.g., Oxisols and Ultisols). Higher porosity and

aeration common in older soils combined with higher temperatures result in higher rates of decomposition and mineralization of organic matter in tropical regions, thereby hampering the increase of SOC (Fageria, 2012). Thus, factors influencing SOC dynamics may have a different degree of importance in tropical regions. Moreover, little is known about the spatial distribution patterns of C at a more detailed scale in Brazilian soils and the effects of variables such as soil class, parent material, and relief, among others, on the spatial distribution of SOC.

Several studies have mapped SOC and CS in large areas at coarser resolutions (Gomes et al., 2019; Vågen et al., 2016), but finer resolution maps are needed for reliable CS accounting, planning of conservationist practices, and precise soil fertility management at local scales, which motivates the search for variables, methods, and tools to facilitate accurate mapping. This study aims to (1) characterize the spatial distribution of SOC content and CS in an area within the Atlantic Forest biome, under different land uses, parent materials, and soil classes; (2) perform spatial predictions of SOC and CS levels through 22 combinations of environmental and remote and proximal sensing variables; and (3) map SOC and CS in detail using the Random Forest algorithm and a distance-based method (multilevel-b-spline), determining which variables best explain their spatial variability. Thus, the hypotheses of this study are: high sample density associated with high-resolution proximal and remote sensing data, as well as data on parent materials, soil classes, and land use, can provide accurate SOC and CS prediction, and that variables related to parent material, soil, and land use will be important for understanding the detailed spatial variability of SOC and CS.

2 Material and Methods

2.1 Study area and sampling

The study area is located in the campus of the Federal University of Lavras (UFLA) (Figure 1) in the municipality of Lavras, Minas Gerais state, Brazil, covering 315 ha. The slope varies from nearly level (<4%) to steep (20-60%). The parent materials of soils are gabbro and granite-gneiss (Curi et al., 2017). There is a high diversity of soil classes (7 orders) and land uses (7) in the study area (Figure 1). Vegetation is mostly Seasonal Semideciduous Forest (Atlantic Forest biome) and the local climate according to the Köppen classification is Cwa, defined as a humid subtropical climate with mild temperatures and rainy summers, with average annual temperature and precipitation of 19 ºC and 1530 mm, respectively (Alvares et al., 2013; Dantas et al., 2007).

Samples were collected at 90 locations at depths 0-20 and 80-100 cm following a regular grid (200 x 200 m), totaling 180 samples used to train the models. To validate models, 28 extra locations were sampled in the same two depths (56 samples). The sample density for the training set (n = 90) is of 1 sampled location every 3.5 ha, making this work one of the few studies with this level of detail for SOC and CS spatial modeling in the tropical literature.

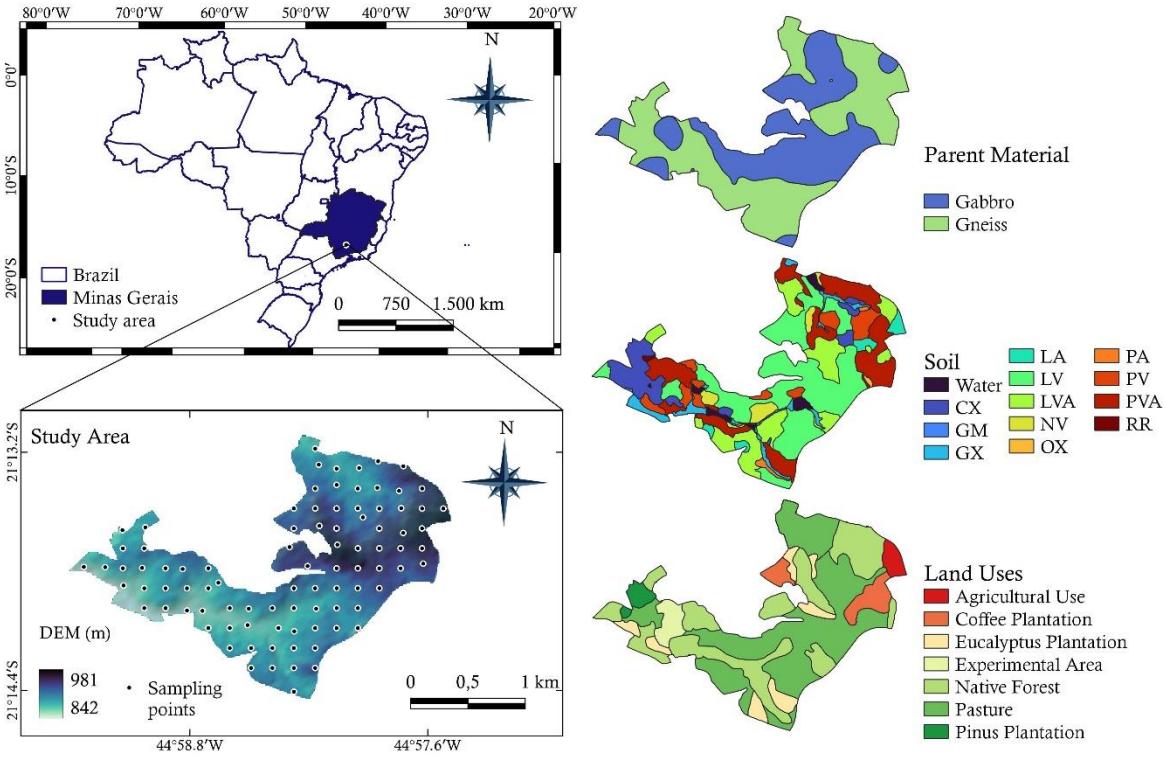

Figure 1. Location sampling points, parent material, soil classes, and land uses in the study area located in Lavras, Minas Gerais State, Brazil.

*CX: Cambissolos Háplicos; GM: Gleissolos Melânicos; GX: Gleissolos Háplicos; LA: Latossolos Amarelos; LVA: Latossolos Vermelho-Amarelos; LV: Latossolos Vermelhos; NV: Nitossolos Vermelhos; OX: Organossolos Háplicos; PA: Argissolos Amarelos; PVA: Argissolos Vermelho-Amarelos; PV: Argissolos Vermelhos; RR: Neossolos Regolíticos.

Soil classes found in the study area and the area each class occupies are presented in Table 1 along with the correspondences between the Brazilian Soil Classification System (Santos et al., 2018) and two other international classification systems, namely the World Reference Base for Soil Resources (FAO, 2022) and the US Soil Taxonomy (Soil Survey Staff, 2022).

Table 1. Soil orders and the area they occupy in the study area located in Lavras, Minas Gerais State, Brazil. Classifications are given according to the Brazilian Soil

Classification System (SBCS) with their respective equivalences with the World Reference Base for Soil Resources (WRB; FAO, 2022) and the US Soil Taxonomy (Soil Survey Staff, 2022).

SBCS	Acronyms (SBCS)	WRB	US Soil Taxonomy	Area (ha)
Cambissolos Háplicos	CX	Cambisols	Udepts	28.59
Gleissolos Melânicos / Gleissolos Háplicos	GM/ GX	Umbric Gleysols/ Reductigleyic Gleysols	Aqualf / Aquents	0.54 / 14.16
Latossolos Vermelhos / Latossolos Vermelhos-Amarelos / Latossolos Amarelos	LV/ LVA/ LA	Rhodic Ferralsols / Haplic Ferralsols / Xanthic Ferralsols	Udox	108.59 / 51.00 / 7.55
Nitossolos Vermelhos	NV	Rhodic Nitisols	Udalfs	9.17
Organossolos Háplicos	OX	Sapric Histosols	Folists	0.60
Argissolos Vermelhos / Argissolos Vermelhos-Amarelos / Argissolos Amarelos	PV/ PVA/ PA	Rhodic Lixisols / Haplic Lixisols / Xanthic Lixisols	Udults	20.33 / 54,52 / 2.23
Neossolos Regolíticos	RR	Regosols	Orthents	0.59

2.2 Laboratory analyses

2.2.1 Chemical and physical analyses

The 256 collected samples were air-dried and sieved (2 mm) to obtain the air-dried fine earth fraction (ADFE) prior to performing analyses of soil organic carbon (SOC) content and texture. The SOC content was measured using the Walkley and Black methodology (1934). Sand, silt, and clay fractions were separated and quantified according to Gee and Bauder (1986) (i.e. the pipette method). Undisturbed samples were collected in triplicate at the two studied depths (0-20 and 80-100 cm) in every condition of soil class, parent material, and land use for determination of soil bulk density (Ds).

Using the volumetric ring method (Viana et al., 2017), undisturbed samples were collected with an Uhland sampler in a cylinder of known volume. The samples were dried in an oven at 105 ºC for 48 hours and weighed to calculate their bulk density (Eq. 1). Subsequently, the triplicates' mean was obtained, allowing for the calculation of the CS performed as presented in Eq. 2 (Veldkamp, 1994).

$$\boldsymbol{Ds} = m/v \qquad \text{(Eq. 1)}$$

Where: Ds = density of the soil (kg dm^{-3}); m = mass of sample dried at 105 ºC (kg); v = volume of the cylinder (dm^3).

$$\boldsymbol{CS} = [COS \times Ds \times e]/10 \qquad \text{(Eq. 2)}$$

Where: CS = organic C stock at a given depth (Mg ha^{-1}); COS = total organic C content of the sampled layer (g kg^{-1}); Ds = soil density in the collected layer (kg dm^{-3}); e = collected layer thickness (cm).

2.2.2 Analysis with proximal sensors

Portable X-ray fluorescence spectrometer (pXRF) and the magnetic susceptibilimeter were chosen due to known relationships between data provided by the two proximal sensors and SOC content (Faria et al., 2022; Jakłík et al., 2016). PXRF was used to determine elemental contents of samples and the magnetic susceptibilimeter was used to measure the magnetic susceptibility (MS) of samples. 15 g of the ADFE fraction of samples were analyzed by a Bruker® S1 Titan 600 pXRF using the "Trace" mode. This pXRF model contains a Rh X-ray tube with 50 keV and 100 μA. Sample scanning was performed in triplicate for 60 s per sample (Weindorf; Chakraborty, 2016). To verify the accuracy of the equipment, results were compared to samples certified by the National Institute of Standards and Technology (NIST) and provided by the equipment

manufacturer. Comparisons were carried out by measuring the recovery rate of the elements detected by the equipment (Peinado et al., 2010). MS was measured using a Bartington MS2B susceptibility meter. 10 g of the ADFE fraction of each sample was scanned in triplicates in low frequency (LF) mode. The results were applied to Eq. 3 (Dearing, 1999).

$$MS\ (\chi) = \chi_{LF} / sample\ weight \qquad \text{(Eq. 3)}$$

Where: SM = magnetic susceptibility (10^{-7} m^3 kg^{-1}); χ_{LF} result = reading obtained on the equipment in low frequency; sample weight = mass (g).

2.3 Generation of terrain attributes, NDVI and indices related to insolation

A Digital Elevation Model (DEM) with a spatial resolution of 12.5 m (Alos Palsar) was used to create 15 terrain attributes (Table 2) for the study area via SAGA GIS 7.8.2 (Conrad et al., 2015). Gaps in the DEM were filled through the Fill Sinks tool (Wang; Liu, 2006). The generated terrain attributes highlight different aspects of the terrain, which were used for predicting SOC and CS in the study area.

Table 2. Description of the 15 terrain attributes generated to be used as SOC and CS predictor variables.

Terrain Attributes (TA)	Description
Analytical Hillshading (AH)	It facilitates terrain visualization, representing the angle between the surface and the incidence of light beams measured in radians.
Aspect (Ap)	It shows terrain characteristics through slope orientation, related to factors such as moisture and solar radiation on the terrain (Gallant; Wilson, 2000).
Channel Network Base Level (CNBL)	It interpolates the elevation of the base level of the channel network and then subtracts the obtained values from the original data, resulting in the approximate depth of the base flow of a watershed (Conrad, 2002).

Channel Network Distance (CND)	It shows how far a point is from the drainage network.
Convergence Index (CI)	Similar to Plan Curvature (PC), but returns smoother values, where the result is calculated as percentages from the aspects of neighboring cells, while PC calculates as a whole.
Flow Directions (FD)	Allows the analysis of water flow directions in a watershed.
Multiresolution Index of Valley Bottom Flatness (MRVBF)	It is an index calculated from the slope and percent elevation of the terrain, analyzing the DEM in a generalized manner combined with increasingly less steep slopes, highlighting the depressions in the area (Gallant; Dowling, 2003).
Multiresolution Index of the Ridge Top Flatness (MRRTF)	Although similar to MRVBF, it operates on the opposite principle, highlighting the peaks of the terrain (Gallant; Dowling, 2003).
Plan Curvature (PC)	It analyzes the ridges and valleys of the terrain, returning positive values for concave features and negative values for convex features (Gallant; Wilson, 2000).
Profile Curvature (PrC)	Curvature between the surface and the steepest slope.
Relative Slope Position (RSP)	It calculates the relative distance from a given point to the lowest area of the landscape.
Slope (S)	It represents the slope of the terrain at each point on the map in relation to a normal plane.
Topographic Wetness Index (TWI)	It is related to trends in soil moisture content according to local terrain (Beven; Kirkby, 1979).
Total Catchment Area (TCA)	The attribute processes the DEM to find the lowest areas of the landscape and is related to the water flow of a watershed.
Valley Depth (VD)	It represents the difference between the elevation of a point and the top of the landscape; the lower the index, the closer it is to the deepest areas of the landscape.

The current normalized difference vegetation index (NDVI) was calculated from bands 8 and 4 from Sentinel 2 (spatial resolution = 10 m), and bands 5 and 4 from Landsat 8 (spatial resolution = 15 m), using filtering to ensure a low amount of clouds and high image quality. Satellite imagery was obtained from the Sentinel Hub EO Browser (https://apps.sentinel-hub.com/eo-browser/). NDVI for both satellites was calculated using QGIS (QGIS Development Team, 2023) through the raster calculator through Eqs. 4a (Sentinel 2) and 4b (Landsat 8) (Tucker, 1979):

$$NDVI_{Sentinel\ 2} = Band\ 8 - Band\ 4 / Band\ 8 + Band\ 4 \quad \text{(Eq. 4a)}$$

$$NDVI_{Landsat\ 8} = Band\ 5 - Band\ 4 / Band\ 5 + Band\ 4 \quad \text{(Eq. 4b)}$$

Where band 4 corresponds to reflectance in the red region of the spectrum (0.64 to 0.67 μm), and bands 5 and 8 correspond to reflectance in the near-infrared (NIR) region (0.85 to 0.88 μm). NDVI relates visible red light absorbed by chlorophyll (band 4) and the NIR range reflected by the mesophyll (bands 5 or 8). The higher this difference (absorbed by chlorophyll vs. reflected by mesophyll), the lusher the vegetation. It varies from -1 to 1, with higher values representing lusher vegetation. The insolation indices (direct, diffuse, global, and reflected insolation, and insolation time) were also extracted from this platform herein since changes in solar radiation have a significant impact on the carbon balance of terrestrial ecosystems (Kanniah et al., 2012). NDVI and insolation indices were resampled with the same spatial resolution (12.5 m) of the other covariates utilized in this study for the modeling described below.

2.4 Statistical analysis and predictions of SOC and CS

Descriptive statistics were computed while grouping SOC content by soil class, parent material, and land use. Calculated statistics included maximum and minimum values, means, standard deviation (SD), and coefficient of variation (CV). Additionally, boxplots of CS were generated for while grouping CS per soil class, parent material, and land use. Statistical analyses and data visualization were performed using the R software (R Core Team, 2023) and the ggplot2 package (Wickham, 2016).

The modeling of both SOC and CS was performed using the RF algorithm (Ho, 1995). Variables representing four of the five major soil formation factors proposed by Jenny (1941) were used: climate (diffuse, direct, global, and diffuse radiation, and insolation time), organisms (NDVI and land use), relief (terrain attributes - TAs), and parent material (PM). In addition to these attributes, texture data and data from the

proximal sensors pXRF and MS were also used for modeling. The contents of the following elements detected by pXRF were spatialized by multilevel-spline: Al, Ca, Ce, Cl, Cr, Cu, Fe, K, Mn, Ni, P, Pb, Rb, Si, Ta, Ti, V, Zn, and Zr. A total of 22 combinations of explanatory variable datasets were tested, for example, only AT; AT + pXRF/MS; AT + PM; AT + pXRF/MS + PM + texture; etc. Both surface and subsurface predictions are considered analyses at both depths since subsurface soil properties may influence surface properties and vice versa.

For comparison purposes, the accuracy of SOC and CS maps were also assessed when using an interpolation algorithm based solely on distance, namely the multilevel-b-spline algorithm implemented in SAGA GIS (Conrad et al., 2015). SOC and CS contents were thus spatialized using the 90 regular grid samples and the accuracy was evaluated with the 28 validation points.

The accuracy of all generated models was tested by the coefficients of determination (R^2) (Eq. 5) and root mean square error (RMSE) (Eq. 6). R^2 is a metric indicating how much of the variability was explained by the model compared to the mean of observed values, with better models returning values closer to 1. Meanwhile, RMSE is related to the model's error, showing how far the predicted values are from the real ones; thus, lower values obtained by this metric indicate lower accumulated errors.

$$R^2 = \frac{\sum_{i=1}^{n}(P_i - \overline{Om})^2}{\sum_{i=1}^{n}(Om_i - \overline{Om})^2} \quad \text{(Eq. 5)}$$

$$RMSE = \left[\frac{1}{N}\sum_{i=1}^{N}(P_i - O_i)^2\right]^{\frac{1}{2}} \quad \text{(Eq. 6)}$$

Where: O_i = observed CS or COS content; Om = mean of observed CS or COS content, Pi = CS or COS content predicted by the models; n = number of points used in the predictions.

Plots presenting variables considered most important for models and the scatter plots of predicted data versus observed data were also created using the tidyverse (Wickham et al., 2019) and randomForest (Ho, 1995) packages.

2.5 SOC modeling

Point-data (e.g., elements from pXRF and MS) obtained for the sampling points (90 points on a regular grid) were spatialized using multilevel-b-splines (Lee et al., 1997) with spatial resolution of 12.5 m to match the resolution of the other used variables such as terrain attributes. Additionally, categorical variables (soil map, parent materials, and land use) were rasterized with the same spatial resolution. After spatializing point-data variables and rasterizing categorical variables, they were combined with remotely sensed data (NDVI and insolation indices) and used as inputs to the most accurate model to create the SOC map of the study area. Spatial data was handled using the raster (Hijmans, 2022), and RColorBrewer (Neuwirth, 2014) packages.

3 Results and Discussion

3.1 Characterization of SOC and CS contents

The highest surface SOC contents (0-20 cm) (Table 3) were observed in the pasture area, followed by native forest. Native forests presented the highest mean value, followed by pasture and eucalyptus forests. Soils under native forests accumulate plant

litter and tend to have lower organic matter decomposition rates due to the absence of anthropic influence, leading to an increase in SOC over time (Mantovani et al., 2024; Shi et al., 2023). High SOC content in soils under pasture may be related to root exudation and decomposition of dead roots, in addition to the input of animal manure. Furthermore, the protective function of vegetation cover prevents SOC losses through erosion and contributes to slower organic matter decomposition rates (Conrado Neto et al., 2015). At depth (80-100 cm), soils under pasture showed the highest SOC content, followed by native forest. This is mainly due to the presence of species with deeper root systems. Roots incorporate SOC in the subsurface and form a network of channels through which part of the SOC moves with water to greater depths in the soil profile (Souza et al., 2023). Additionally, roots favor SOC accumulation by releasing exudates in their surroundings, causing an increase in microbial activity and biomass production (Huang et al., 2022; Paranavithana et al., 2023).

Table 3. Descriptive statistical analysis of SOC levels in different uses, parent materials, and soil class, Lavras, Minas Gerais State, Brazil.

	Maximum	Minimum	Mean	SD	CV	Maximum	Minimum	Mean	SD	CV
Land Uses	**%**					**%**				
	Depth (0-20 cm)					**Depth (80-100 cm)**				
Pasture	8.18	1.22	3.42	1.54	44.97	16.36	0.12	1.37	2.44	177.56
Native Forest	6.32	2.38	4.23	1.17	27.69	2.67	0.29	1.11	0.70	63.32
Eucalyptus Plantation	5.34	1.97	3.42	1.18	34.53	1.80	0.46	0.96	0.54	56.27
Coffee Plantation	3.65	2.67	3.21	0.39	12.13	1.97	0.58	1.23	0.47	38.49
Pinus Plantation	3.89	2.49	3.17	0.70	21.98	1.51	0.58	0.93	0.51	54.49
Experimental Area	4.23	2.20	2.88	1.17	40.69	1.04	1.20	0.85	0.18	20.83
Agricultural Use	2.78	2.78	2.78	-	-	0.81	0.81	0.81	-	-
Parent Material										
Gabbro	8.18	1.22	4.14	1.53	37.1	16.36	0.46	1.72	2.49	145.21
Gneiss	5.80	1.22	3.20	1.01	31.72	1.97	0.12	0.83	0.42	50.8
Soil Class										
CX*	3.89	1.22	2.63	0.76	28.97	1.97	0.46	0.87	0.52	0.27
GM	2.67	2.67	2.67	-	-	0.64	0.64	0.64	-	-
GX	3.89	3.13	3.42	0.41	11.86	2.67	1.10	1.82	0.79	0.63
LA	3.48	1.97	2.64	0.65	24.70	1.16	0.64	0.83	0.23	0.05
LVA	6.32	1.97	3.41	1.40	41.04	1.51	0.29	0.95	0.42	0.17
LV	6.84	1.22	3.76	1.43	37.94	2.49	0.46	1.34	0.60	0.36
NV	4.23	2.67	3.60	0.82	22.87	1.22	0.52	0.77	0.39	0.15
OX	8.18	8.18	8.18	-	-	16.36	16.36	16.36	-	-
PA	3.89	3.65	3.73	0.13	3.59	0.52	0.29	0.43	0.12	0.01
PVA	6.50	1.97	3.82	1.29	33.86	1.97	0.29	0.87	0.45	0.21
PV	5.63	2.67	4.25	1.13	26.57	2.49	0.12	0.87	0.95	0.90
RR	4.12	4.12	4.12	-	-	0.58	0.58	0.58	-	-

*CX: Cambissolos Háplicos; GM: Gleissolos Melânicos; GX: Gleissolos Háplicos; LA: Latossolos Amarelos; LVA: Latossolos Vermelho-Amarelos; LV: Latossolos Vermelhos; NV: Nitossolos Vermelhos; OX: Organossolos Háplicos; PA: Argissolos Amarelos; PVA: Argissolos Vermelho-Amarelos; PV: Argissolos Vermelhos; RR: Neossolos Regolíticos.

Pasture soils presented both the maximum and minimum SOC contents and highest SD and CV among land uses, which can be explained by the presence of degraded pasture in some locations, leading to decreased SOC levels despite the generally positive

impact of pasture compared to other anthropic land uses. However, it should be noted that one of the sampled points under pasture use was in an Organossolo (Histosols) area, which may have significantly contributed to this result. The lowest average surface SOC contents were found in soils within agricultural and experimental areas due to constant soil disturbance, exposing SOC and accelerating its decomposition process. A similar trend was observed in the 80-100 cm layer, with soils of agricultural land presenting the lowest value, probably due to the area's history of intensive use, which could be improved with the adoption of conservation practices, favoring root growth, aggregate stabilization, and protection of organic particles (Souza et al., 2023). The highest SOC values at depth were found in pasture, coffee cultivation, and native forest. This underscores the importance of perennial crops for SOC conservation and maintenance, which incorporate carbon through the deposition of crop residues and deep roots, and slows the decomposition of organic matter by minimizing soil disturbance.

When grouping SOC by parent material, it is observed that soils derived from gabbro have higher values in all evaluated statistical parameters compared to soils derived from gneiss, both in the surface and subsurface. This happens because gabbro forms soils that are more clayey and well-structured, as it is composed of more easily weatherable minerals. According to Oliveira et al. (2015), soil mineralogy has a significant influence on SOC retention in tropical soils, as it controls texture, structure, porosity, and nutrient content, depending on the degree of soil weathering. Due to the higher clay and oxide content, the aggregation process is favored in tropical soils, along with the intra-aggregate C protection. In addition to the predominance of microporosity, soils with finer texture with higher clay or silt content are typically more prone to organic particle retention. Gioacchini et al. (2024) detected in their study higher SOC contents in microaggregates by occlusion and greater formation of macroaggregates compared to the control area.

Moreover, the higher the clay content, the greater the capacity for C storage in tropical soils. Higher clay content also increases the presence of positively charged Fe and Al oxides that collapse carboxyl radicals and thus increases the number of negatively charged sites (Sá et al., 2013). Additionally, most soils formed from gabbro are under native forest and pasture, which provide the necessary SOC input for the aggregation process through the formation of different aggregate classes. The opposite occurs, for example, in sandy soils where there is lower aggregation and smaller, less stable aggregates, therefore the surface layers of these soils tend to lose more SOC both by mineralization and translocation, accumulating SOC in deeper layers (podzolization) (Oliveira et al., 2015).

When grouping SOC by soil classes, the highest values for maximum, minimum, and mean were found in soils of the OX class (Histosols), followed by LV (Oxisols) in the surface. In the subsurface, highest SOC contents were found also for soils of the OX class, followed by GX (Aquents). The high contents in OX were due to their formation process (paludization), which causes the accumulation of organic material. The conditions for the formation of OX that lead to the accumulation and preservation of SOC (depositional anoxic environments) override the effect of parent material and land use.

Soils classified as LV had the second highest SOC levels, which may sound counterintuitive since they are known for their high degree of weathering, good drainage, and lack of nutrients, as they were formed by intense weathering and leaching under humid tropical climates (Ker, 1998). The explanation for the comparatively higher SOC in these soils may be their low levels of available phosphorus, which may inhibit microbial activity and hinder organic matter mineralization (Fageria, 2012). Another hypothesis is that the mineralogy may be contributing to preserve SOC in LVs. LVs in the studied area have clayey or very clayey texture and predominant kaolinitic mineralogy

with a significant presence of oxides. This clay mineralogy may favor direct C adsorption and soil aggregation, consequently protecting SOC from degradation by microorganisms and preserving it for longer periods of time (Huang et al., 2022; Mantovani et al., 2024). Additionally, Huang et al. (2022) highlighted that finer-textured soils may contain higher SOC levels also due to extrinsic factors such as the ability of this soil type to retain more water, favoring the growth of plants that input C into the soil. Rodríguez-Albarracín et al. (2023) observed that minerals like hematite and kaolinite, commonly found in Brazilian soils, have the highest potential to sequester SOC compared to minerals like goethite and gibbsite, which, despite having high affinity with organic particles, saturate more easily and stabilize SOC during a shorter period of time. Furthermore, it was reported by Zinn et al. (2007) that minerals with low crystallinity (e.g., amorphous Fe and Al oxides) also have great capacity for C adsorption, as they have a larger specific surface area than other clay minerals like kaolinite, analyzing Brazilian soils from the Cerrado biome.

LV was one of the soil classes that showed the highest standard deviation (SD) and coefficient of variation (CV) values on the surface, indicating high dispersion and variability of the data compared to the mean. This was likely due to the occurrence of this soil class in two parent materials under different land uses, resulting in differences in texture and chemical composition of deposited organic materials (litter from different species), leading to divergent amounts of accumulated SOC. In the subsurface SD and CV values were low, as SOC tends to decrease with depth (Gomes et al., 2019).

CS varied within the same soil class when grouped by land use and parent material (Figure 2). In the surface (0-20 cm), CS ranged from 26.3 to 148.5 Mg ha^{-1}, and in the subsurface (80-100 cm), from 2.6 to 105.9 Mg ha^{-1}. In the surface, CS was highest in LV under pasture and LVA (Oxisols) under native forest, both in areas where gabbro is the parent material. Higher clay contents in these soils assist in aggregate formation and

stability, aiding in the protection and retention of organic particles (Gholizadeh et al., 2018), which explains our results for areas with soils derived from gabbro. It is important to mention that the 0-20 cm depth layer of the OX presented sediments deposited due to erosion of the hills surrounding the OX area, which explains why OX did not present the highest CS values in the surface. Meanwhile, in the subsurface, the highest contents were observed in OX under native pasture and GX under native forest, derived from organic sediments and gabbro, respectively (organic sediments not shown in the parent material map due to its small extent in the study area). This agrees with Sá et al. (2013), who reported significant contribution of Organossolos (Histosols) and Latossolos (Oxisols) as important soil carbon reservoirs.

In the surface, the lowest CS levels were found in CX (Entisols) and LV under pasture, with soils from both classes being formed from gabbro and gneiss, respectively. In the subsurface, the lowest CS was found in PV derived from gneiss under pasture. As highlighted earlier, this may have occurred because some sections of the study area had degraded pastures. For instance, the studied soils classified as LV (Oxisols) and PV (Ultisols) occur in degraded pasture areas and are formed from gneiss, hence they likely have lower clay content than LV derived from gabbro, limiting the protection of SOC and accelerating its decomposition by microorganisms (Souza et al., 2023). Additionally, soils classified as CX have generally less developed structures and are highly susceptible to erosion, which is facilitated by its occurrence on steeper slopes in the study area, favoring SOC loss through erosion (Silva et al., 2005).

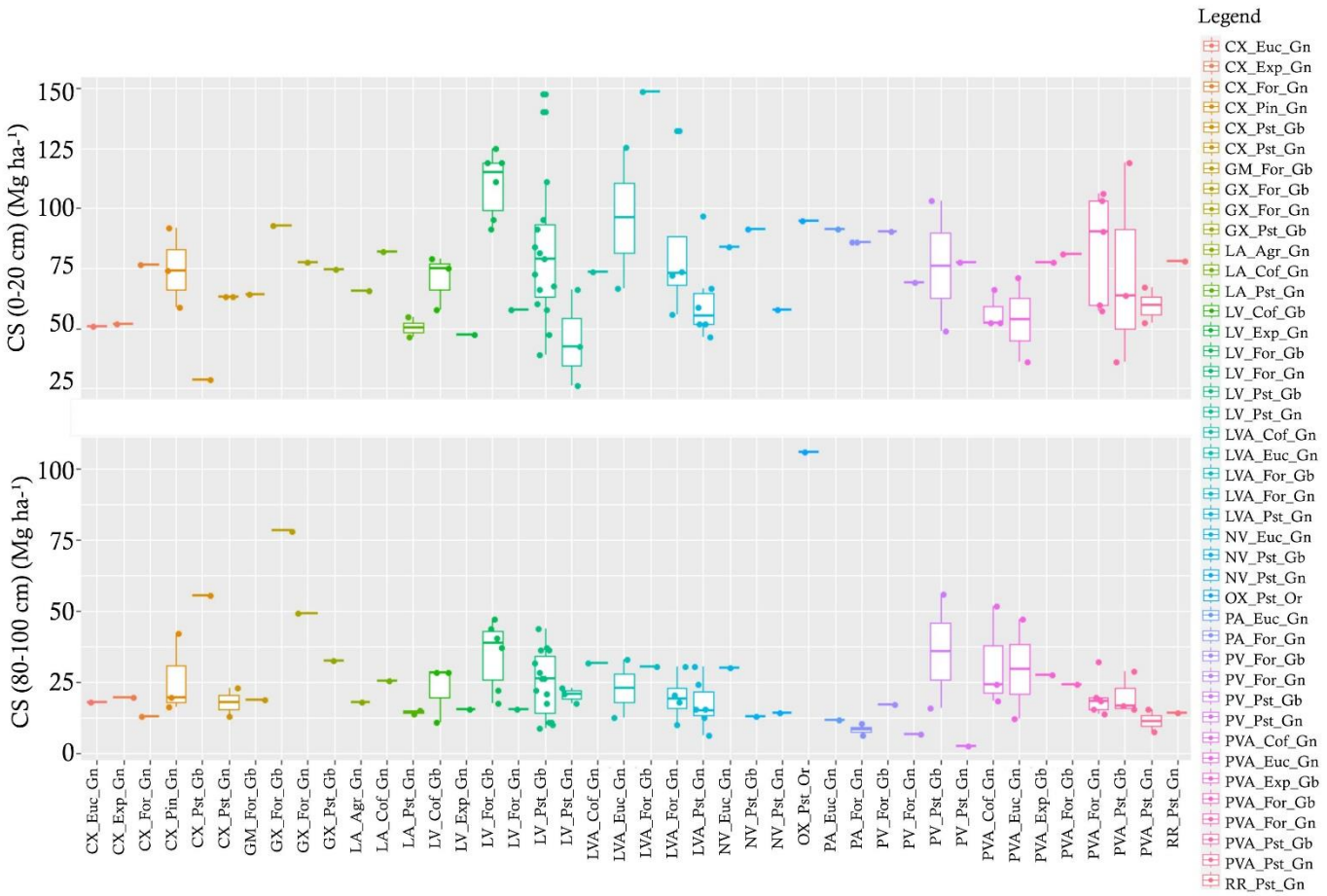

Figure 2. Carbon stock (CS) in different depths (0-20 and 80-100 cm) in combinations of soil class, land use and parent material found in the study area.

*Soil class: CX: Cambissolos Háplicos; GM: Gleissolos Melânicos; GX: Gleissolos Háplicos; LA: Latossolos Amarelos; LVA: Latossolos Vermelho-Amarelos; LV: Latossolos Vermelhos; NV: Nitossolos Vermelhos; OX: Organossolos Háplicos; PA: Argissolos Amarelos; PVA: Argissolos Vermelho-Amarelos; PV: Argissolos Vermelhos; RR: Neossolos Regolíticos. Land uses: Agr: Agricultural Use; Cof: Coffee Plantation; Euc: Eucalyptus Plantation; Exp: Experimental Area; For: Native Forest; Pin: Pinus Plantation; Pst: Pasture. Parent material: Gb: Gabbro; Gn: Gneiss; Or: Organic Sediments.

Greater data ranges were observed in the surface where CS levels were higher, especially for PVA (Ultisols) in two groupings, the first under native forest with gneiss as parent material (57.42 to 106.33 Mg ha^{-1}), while the second under pasture with gabbro

as parent material (36.15 to 119.09 Mg ha^{-1}). This variability persists even when grouping data by other criteria, as presented in Figure 2, highlighting some of the difficulties in mapping this attribute in the study area at a detailed scale.

3.2 SOC and CS predictions and model validation

Different combinations of independent variables used for the prediction of SOC and CS caused a wide variation in the R^2 values generated by the models (Table 4). The results show that a high sample density does not always result in high performance in soil attribute predictions (Loiseau et al., 2021). The prediction of CS showed lower performance, with lower R^2 values and higher RMSE values. This indicates that even considering the high variability of soils (12 suborders), land uses (7), and two-parent materials, terrain attributes and high sample density were not sufficient to explain the variability of SOC at a detailed scale. Especially for CS, as its calculation includes soil density, this increased the complexity of the data, as the same soil classes may have different soil density under the same land use given its high spatial variability (Mantovani et al., 2024).

Table 4. R^2 and RMSE values obtained from the different models tested for predicting soil organic carbon (SOC) and C stock (CS) in two depths (0-20 and 80-100 cm) using Random Forest with different datasets (a, b, c, d, and e) and the multilevel-b-spline interpolation algorithms.

Random Forest								
Dataset	SOC				CS			
	0-20	80-100	0-20	80-100	0-20	80-100	0-20	80-100
Predictor variables	R^2		RMSE		R^2		RMSE	
(a)	0.18	0.08	1.97	0.38	0.08	0.03	43.87	8.89
(a); (b)	0.15	-0.02	1.99	0.77	0.01	-0.01	43.70	11.26
(b)	0.13	0.01	2.03	0.95	0.01	0.06	44.60	11.89
(c)	-0.04	-0.03	1.96	0.65	-0.04	-0.04	45.65	10.39
(a); (c)	0.15	0.07	1.93	0.39	0.08	0.01	43.77	9.06
(b); (c)	0.12	0.01	2.01	0.86	0.01	0.05	44.13	11.82
(a); (b); (c)	0.16	-0.01	1.97	0.81	0.02	-0.01	43.63	11.01
(b); (d)	0.15	-0.01	1.99	0.77	0.00	0.06	43.76	11.54
(b); (c); (d)	0.13	-0.01	1.95	0.72	0.01	0.07	43.97	11.82
(a); (b); (c); (d)	0.16	-0.03	1.95	0.65	0.01	-0.02	43.43	10.83
(a); (c); (d)	0.39	0.14	1.72	0.37	0.16	-0.03	39.43	9.63
(c); (d)	-0.01	-0.02	1.82	0.46	-0.03	0.01	41.58	12.23
(e)	0.21	-0.04	2.14	0.5	0.00	0.00	45.71	11.35
(b); (e)	0.15	0.03	2.02	0.96	0.02	0.10	44.29	12.35
(a); (e)	0.28	0.01	2.02	0.4	0.11	-0.04	43.63	10.03
(c); (e)	0.10	0.01	2.04	0.52	-0.02	-0.03	45.39	10.95
(d); (e)	0.20	-0.01	1.84	0.44	0.03	0.03	40.33	11.13
(a); (b); (e)	0.17	0.00	1.99	0.85	0.02	0.01	43.9	11.31
(a); (b); (d); (e)	0.19	-0.04	1.95	0.67	0.02	0.01	43.72	11.13
(a); (b); (c); (d); (e)	0.16	-0.03	1.96	0.66	0.03	0.00	43.39	11.05
(a); (c); (d); (e)	**0.47**	0.08	1.76	0.39	0.17	-0.03	40.00	10.33
(c); (d); (e)	0.21	-0.01	1.84	0.45	0.03	0.02	41.21	11.55
Multilevel-b-spline								
Predicted variables	SOC				CS			
Depth (cm)	0-20	80-100	0-20	80-100	0-20	80-100	0-20	80-100
	R^2		RMSE		R^2		RMSE	
	0.25	0.03	2.30	0.85	0.05	-0.04	50.65	13.96

(a) Terrain Attributes; (b) pXRF, MS; (c) Land Use, Soil class, Parent material; (d) Texture; (e) NDVI (Sentinel 2 and Landsat 8), radiation (diffuse, direct, global and reflected) and insolation time.

The best prediction accuracy was obtained for surface SOC content (0-20 cm) (R^2 = 0.47 and RMSE = 1.76) (Figure 3a) when combining terrain attributes, land use, soil type, parent material, soil texture, NDVI, radiation (diffuse, direct, global, and reflected), and insolation time, representing four of the five soil formation factors. This is justified, as SOC depends on relationships between factors such as vegetation, drainage, climate, and management, as well as soil attributes such as texture, structure, and mineralogy (Scott et al., 1996; Schoenholtz et al., 2000; Telles et al., 2003; Oliveira et al., 2015). Huang et al. (2022) emphasized that obtaining accurate predictions of SOC at detailed scales was a challenge due to the availability of data, its representativeness, and the difficulty of selecting variables that can explain the spatial distribution of SOC in the area. They further highlighted that the best results usually come from models that incorporate the Scorpan model (McBratney et al., 2003) related to soil formation factors for digital soil mapping and its attributes. Figure 3b represents the model generated by the multilevel-b-spline, showing a large dispersion about the trend line, resulting in a low R^2 (0.25).

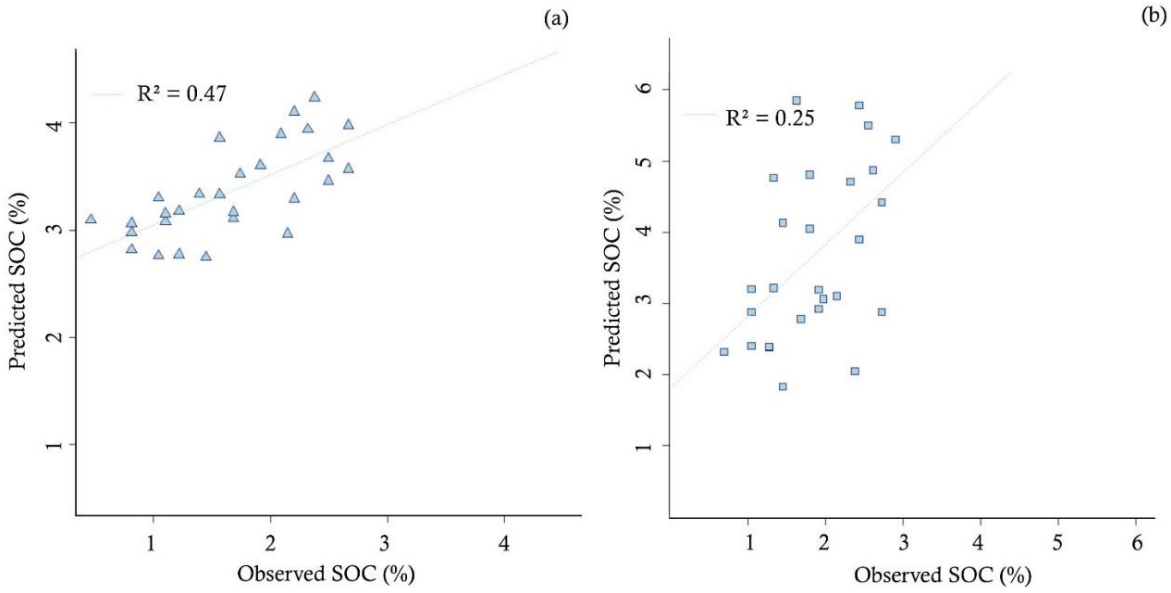

Figure 3. Predicted vs. Observed SOC values for the best model on surface (0-20 cm) based on Random Forest (a); and based on the multilevel-b-spline (b).

The top ten most important variables for generating the most accurate model included surface textural classes (0-20 cm), vegetation indices as NDVI (Sentinel 2), parent material, and some of the terrain attributes (CND, VD, DEM, RSP, and CNBL) (Figure 4). Texture is linked to organic particle retention and stabilization (adsorption and aggregation) (Huang et al., 2022; Mantovani et al., 2024). The textural control over SOC levels was observed by Zinn et al. (2005, 2007) in soils of the Brazilian Cerrado, where higher SOC levels correlated directly with the silt and clay fractions and inversely with sand, explained by the greater sorption of colloidal-soluble carbon in a larger specific surface area originating from the clay fraction, while silt indirectly contributes to soil plasm formation.

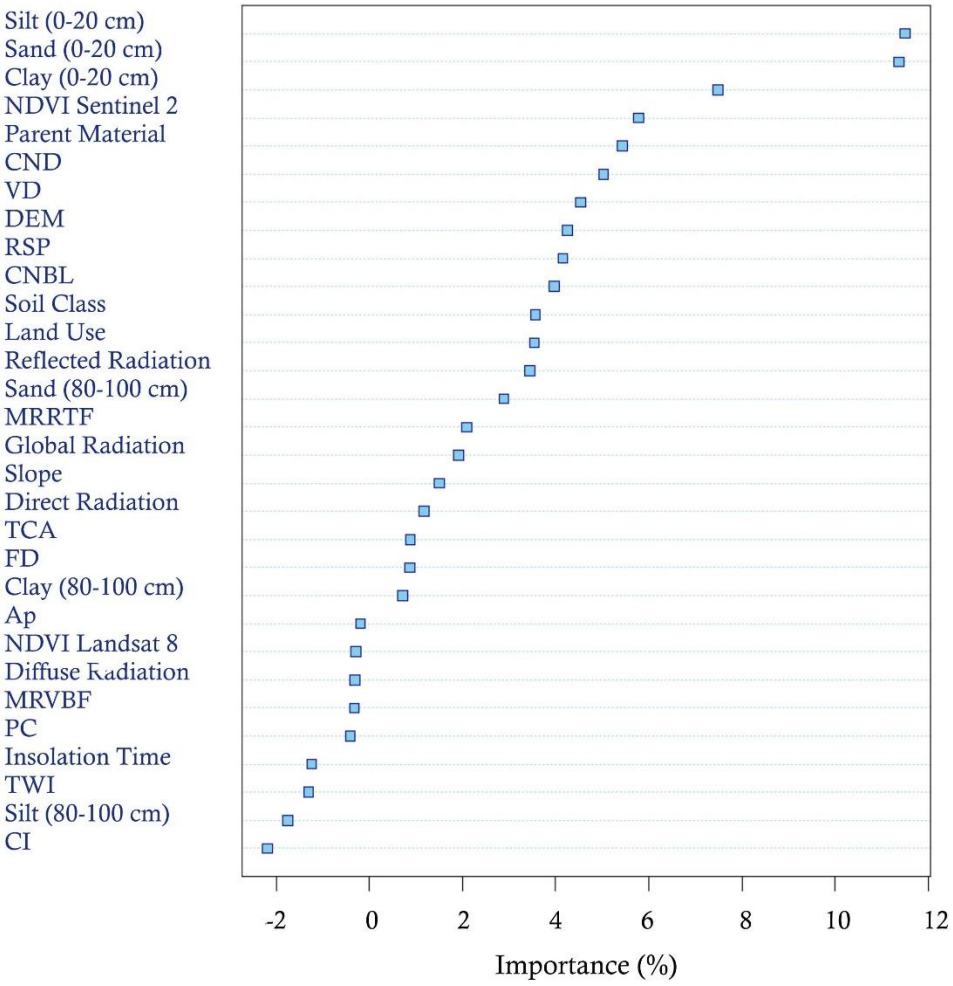

Figure 4. Variable importance for the best model of the SOC on horizon A (predictor variables: Terrain Attributes; Land Use, Soil class, Parent material; Texture; NDVI (Sentinel 2 and Landsat 8), radiation (diffuse, direct, global and reflected) and insolation time).

The importance of NDVI is related to land use, showing areas with greater input of organic material and consequently higher SOC levels. Other studies also used NDVI for SOC prediction, such as Siewert's (2018) study ($0.48 \leq R^2 \leq 0.74$), obtaining results similar to this study. Parent material is associated with various soil attributes, such as texture (as observed by comparing parent material and clay maps) and mineralogy, and

thus relates to the adsorption of organic compounds. For example, soils derived from gabbro have higher Fe content and, therefore, exhibit higher contents of Fe oxides, which favors the adsorption of organic compounds as shown by other studies (Rodríguez-Albarracín et al., 2023; Zinn et al., 2007).

The terrain attributes that were considered most important (Figure 4) by models help identify different depositional environments, i.e., areas where water may accumulate and create anoxic environments where microbial activity is lower. In these areas, the reduced oxygenation and lower temperatures decrease decomposition rates, favoring the accumulation of organic sediments. Li et al. (2018) also observed this trend when studying the effects of topography on SOC redistribution. Araújo et al. (2017) highlighted the effect of altitude over SOC, noting relatively high SOC and CS values in different soil classes regardless of texture and Fe and Al content for altitude conditions above 890 m, attributed to the relatively cold environment limiting organic matter decomposition.

The prediction of SOC based only on distance performed by multilevel-b-spline did not yield accurate results for both the surface and subsurface. Spline interpolations presented the highest RMSE for the surface (2.30) compared to all 22 datasets evaluated. This demonstrates that interpolations without considering the other variables that influence SOC content could not explain the variation in SOC across the area despite the high sample density.

The best predictive model was applied to the entire study area, generating the SOC map for a depth of 0-20 cm (Figure 5). It can be observed that SOC levels were lower in gneiss areas and higher in gabbro areas, corroborating what was observed in the descriptive statistics (Table 3).

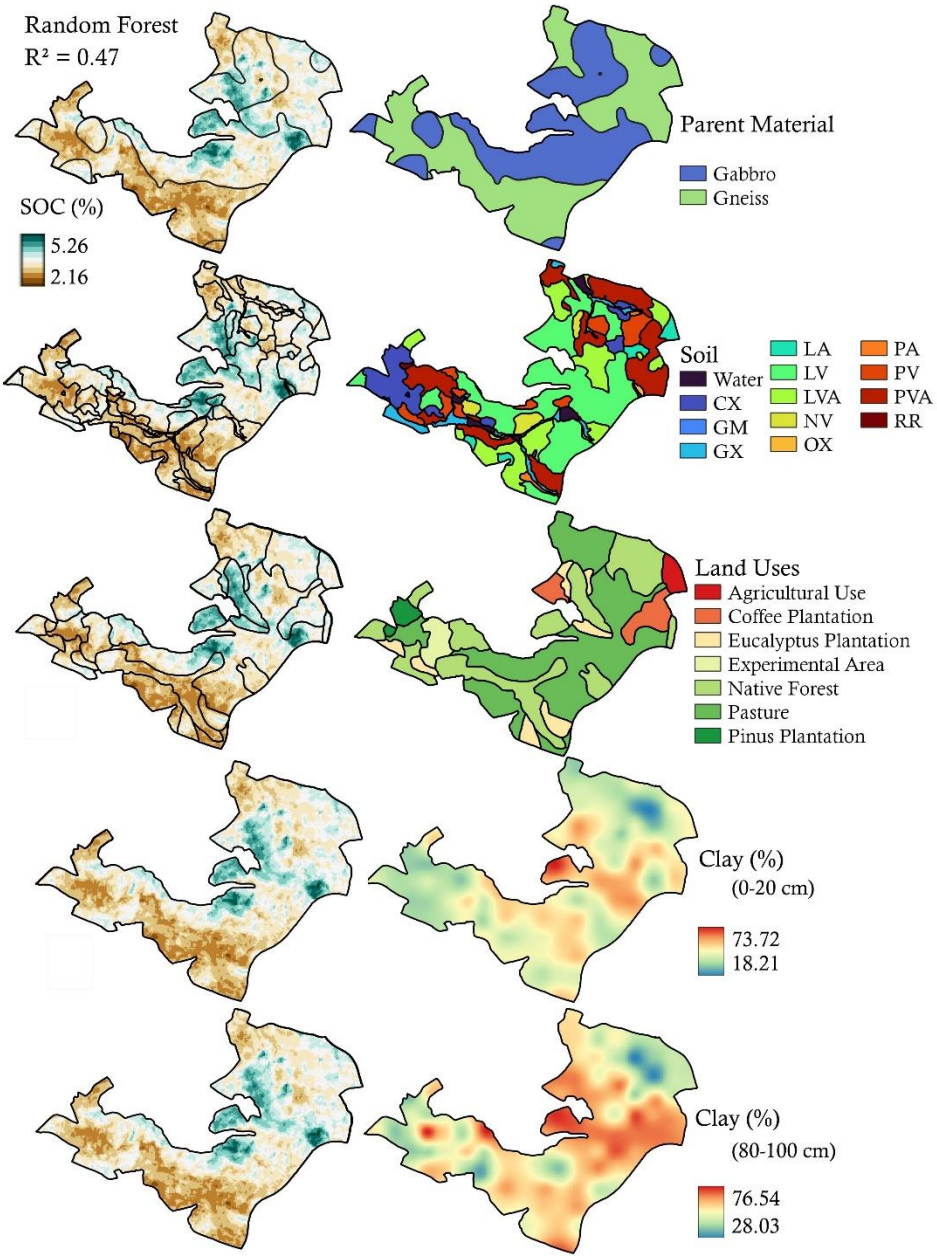

Figure 5: Maps of SOC contents (0-20 cm) created using the RF algorithm, compared to the maps of parent material, soil class, land use, and clay content in the study area in Lavras, Minas Gerais State, Brazil.

Soils classified as OX and LV derived from gabbro presented highest SOC contents, while younger soils such as CX and RR and soils derived from gneiss (LVA and LV) presented the lowest contents. Younger soils (RR and CX) generally have coarser texture or higher silt content and therefore have less stable aggregates, causing

them to have lower amounts of charges for the adsorption of organic compounds (Rodríguez-Albarracín et al., 2023) and being more susceptible to erosion, resulting in greater carbon losses due to erosion (Silva et al., 2005). As for land use, higher SOC was observed mainly in soils under native forest and pasture, especially when soils derived from gabbro. Huang et al. (2022) pointed out that one of the reasons why clayey soils have higher SOC levels is because their greater water retention capacity favors plant growth and consequently promotes the deposition of organic materials on the surface.

The results of this study were consistent with several other reports in the literature on the prediction of SOC and CS (Table 5). However, our results were superior to studies such as that of Lemercier et al. (2022), who reported unsatisfactory results for R^2 for SOC prediction at more detailed scales, as the predicted data differed from the actual values in 75% of cases due to the database lacking sufficient information to describe the variability of this attribute at local scales. This happened because carbon is a highly variable component, and it is difficult to determine all the variables that can influence SOC levels, making the prediction less accurate.

Table 5. Examples of results that can be found in the literature for modeling SOC and CS.

COS or CS	Depth (cm)	Predictor variables	Algorithm	Study area	R^2	Authors
CS	0–20 40–60 80–100	30 years of land use history, vegetation indexes, geology, soil properties, soil types, climate and TA	RF	Piracicaba, São Paulo State, Brazil (2229 points in 2577 km²)	$0.78 \leq R^2 \leq 0.92$	Tayebi et al. (2021)
CS	0-5 5-15 15-30 30-60	TA, Landsat 8 and Sentinel 2 bands, NDVI	Cubist, RF, XGBoost, ANN,	Arid and sub-humid regions of Iran (253 points in 3720 km²)	$0.17 \leq R^2 \leq 0.90$	Taghizadeh-Mehrjardi et al. (2020)

	60-100 100-200		AvNNet, and DNN			
SOC	0–20	Soil and climate data, land use and management	DNDC	Jiangsu Province in Eastern China (1319 points in ~97609.2 km²)	$R^2 = 0.24$	Zhang et al. (2018)
SOC	0-15	Soil color parameters (L*, a*, and b*) and MS values	SMLR, RF, and nonlinear regression	Behenjy and Antohobe, Vakinankaratra region, Madagascar (240 points in ~8.8 km²)	$0.47 \leq R^2 \leq 0.67$	Rakotonindrina et al. (2022)
SOC	5 cm intervals until 50 cm	NDVI, soil-adjusted vegetation index, NIR/SWIR bands (SPOT spectral Bands), TA, land use	MLR, ANN, SVM, and RF	Sub-Arctic mountain, Abisko region near Stordalen, northernmost Sweden (47 points in 65 km²)	$0.48 \leq R^2 \leq 0.74$	Siewert (2018)
CS	0-5 5-15 15-30 30-60 60-100	Climate and soil data; Lithology; TA	RF, Cubist, and GLMB, SVM	Brazil (8,227 points in 8.510.000 km²)	$0.12 \leq R^2 \leq 0.33$	Gomes et al. (2019)

ANN = Artificial Neural Network; AvNNet = Neural Network Ensemble Based on Model Averaging; DNDC = DeNitrification-DeComposition model; DNN = Deep Learning Neural Networks; GLMB = Generalized Linear Model Boosting; GWMR = Geographically Weighted Multiple Regression; MLR = Multiple Linear Regression; RF = Random Forest; SVM = Support Vector Machine; SMLM = Stepwise Multiple Linear Regression; XGBoost = extreme gradient boosting.

Regarding CS, greater efforts are needed to achieve models that provide accurate predictions, which is hindered by the lack of precise soil density measurements, increasing the uncertainty of models. This is because soil density can show high variability even under the same soil conditions, parent material, and land use (Reis et al., 2024; Mantovani et al., 2024). Therefore, more studies of this nature are encouraged to

achieve better predictions of SOC and, especially, CS, given the complexity of their data and the inherent difficulties in soil density sample collection.

4 Conclusions

Satisfactory SOC predictions ($R^2 = 0.47$) were possible when using as covariates remotely sensed data (NDVI and insolation indices), terrain attributes, parent materials, soil classes, texture, and land uses. Proximal sensor data (pXRF and MS) did not help explain the spatial variability of SOC. None of the generated models produced accurate results for SOC in the subsurface (80-100 cm) and CS. Therefore, the tested hypothesis was partially confirmed. The use of high sample density was aided by environmental variables representing four of the five main soil formation factors yielded accurate SOC predictions (0-20 cm). Results also demonstrated the high spatial variability of SOC and difficulties in spatially representing soil density to predict CS. Thus, there is a need for the development of other strategies, such as the use of new variables or models and more local testing to obtain accurate SOC and CS mappings for detailed scales and their applications.

Acknowledgments

The authors acknowledge Conselho Nacional de Desenvolvimento Científico e Tecnológico (CNPq), Coordenação de Aperfeiçoamento Pessoal de Nível Superior (CAPES), Fundação de Amparo à Pesquisa do Estado de Minas Gerais (FAPEMIG) that provided financial support and allowed the conduction of this research in the field and laboratory.

References

Alvares, C.A., Stape, J.L., Sentelhas, P.C., Gonçalves, J.L.M., Sparovek, G., 2013. Köppen's climate classification map for Brazil. Meteorologische Zeitschrift, 22, 711-728. Schweizerbart. http://dx.doi.org/10.1127/0941-2948/2013/0507.

Araújo, M.A., Zinn, Y.L., Lal, R., 2017. Soil parent material, texture and oxide contents have little effect on soil organic carbon retention in tropical highlands. Geoderma, 300, 1-10. Elsevier BV. http://dx.doi.org/10.1016/j.geoderma.2017.04.006.

Beven, K.J., Kirkby, M. J., 1979. A physically based, variable contributing area model of basin hydrology. Hydrological Sci. Bulletin, 24, 43–69. doi:10.1080/02626667909491834.

Blanco-Canqui, H., Shapiro, C.A., Wortmann, C.S., Drijber, R.A., Mamo, M., Shaver, T. M., Ferguson, R.B., 2013. Soil organic carbon: the value to soil properties. Journal of Soil and Water Conservation, 68, 129A-134A. Soil and Water Conservation Soc. http://dx.doi.org/10.2489/jswc.68.5.129a.

Cambule, A.H., Rossiter, D.G., Stoorvogel, J.J., Smaling, E.M.A., 2012. Building a near infrared spectral library for soil organic carbon estimation in the Limpopo National Park, Mozambique. Geoderma, 183-184, 41-48. Elsevier BV. http://dx.doi.org/10.1016/j.geoderma.2012.03.011.

Canellas, L.P., Berner, P.G., Silva, S.G., Barros e Silva, M., Santos, G.A., 2000. Frações da matéria orgânica em seis solos de uma toposseqüência no Estado do Rio de Janeiro. Pesq. Agropec. Bras., 35, 133-143. FapUNIFESP (SciELO). http://dx.doi.org/10.1590/s0100-204x2000000100016.

Conrad, O., Bechtel, B., Bock, M., Dietrich, H., Fischer, E., Gerlitz, L., Wehberg, J., Wichmann, V., Böhner, J., 2015. System for Automated Geoscientific Analyses

(SAGA) v. 2.1.4. Geoscientific Model Development, 8, 1991-2007. Copernicus GmbH. http://dx.doi.org/10.5194/gmd-8-1991-2015.

Conrad, O., 2002. *DIGEM* 2.0. Free Software for Scientific and Educational Proposes. Germany, Göttingen.

Conrado Neto, F.C., Sampaio, F.M.T., Veloso, M.E.C., Matias, S.S.R., Andrade, F.R., Lobato, M.G.R., 2015. Variabilidade espacial dos agregados e carbono orgânico total em Neossolo Litólico Eutrófico no município de Gilbués, PI. Revista de Ciências Agrárias, 8, 75-83.

Cotching, W.E., 2018. Organic matter in the agricultural soils of Tasmania, Australia – A review. Geoderma, 312, 170-182. Elsevier BV. http://dx.doi.org/10.1016/j.geoderma.2017.10.006.

Curi, N., Silva, S.H.G., Poggere, G.C., Menezes, M.D., 2017. Mapeamento de solos e magnetismo no campus da UFLA como traçadores ambientais. UFLA, Lavras, MG, Brazil.

Dantas, A.A.A., Carvalho, L.G., Ferreira, E., 2007. Classificação e tendências climáticas em Lavras, MG. Cienc. e Agrotecnologia, 31, 1862-1866. FapUNIFESP (SciELO). http://dx.doi.org/10.1590/s1413-70542007000600039.

Dearing, J., 1999. Environmental Magnetic Susceptibility. Using the Bartington MS2 system.

Fageria, N.K., 2012. Role of Soil Organic Matter in Maintaining Sustainability of Cropping Systems. Communications in Soil Sci. and Plant Analysis, 43, 2063-2113. Informa UK Limited. http://dx.doi.org/10.1080/00103624.2012.697234.

FAO, 2022. World reference base for soil resources/ International soil classification system for naming soils and creating legends for soil maps, 4th ed. FAO, Rome.

Faria, A.J.G., Silva, S.H.G., Andrade, R., Mancini, M., Melo, L.C.A., Weindorf, D.C., Guilherme, L.R.G., Curi, N., 2022. Prediction of soil organic matter content by combining data from Nix ProTM color sensor and portable X-ray fluorescence spectrometry in tropical soils. Geoderma Regional, 28, e00461. Elsevier BV. http://dx.doi.org/10.1016/j.geodrs.2021.e00461.

Gallant, J.C., Dowling, T.I., 2003. A multiresolution index of valley bottom flatness for mapping depositional areas. Water Resources Research, 39, 1347 (1-14). Am. Geophysical Union (AGU). http://dx.doi.org/10.1029/2002wr001426.

Gallant, J. C., Wilson, J.P., 2000. Primary topographic attributes, in: Wilson, J.P.; Gallant, J. C. (Eds.), Terrain Analysis: Principles and applications, New York: John Wiley & Sons, pp. 51-85.

Gee, G.W., Bauder, J.W., 1986. Particle-size analysis, in: Klute, A. (Ed.), Methods of Soil Analysis, Am. Soc. of Agronomy, Madison, pp. 383–412.

Gioacchini, P., Baldi, E., Montecchio, D., Mazzon, M., Quartieri, M., Toselli, M., Marzadori, C., 2024. Effect of long-term compost fertilization on the distribution of organic carbon and nitrogen in soil aggregates. Catena, 240, 107968. Elsevier BV. http://dx.doi.org/10.1016/j.catena.2024.107968.

Gholizadeh, A., Ŝižala, D., Saberioon, M., Borŏvka, L., 2018. Soil organic carbon and texture retrieving and mapping using proximal, airborne and Sentinel-2 spectral imaging. Remote Sensing of Environment, 218, 89-103. Elsevier BV. http://dx.doi.org/10.1016/j.rse.2018.09.015.

Gomes, L.C., Faria, R.M., Souza, E., Veloso, G.V., Schaefer, C.E.G.R., Fernandes Filho, E.I., 2019. Modelling and mapping soil organic carbon stocks in Brazil. Geoderma, 340, 337-350. Elsevier BV. http://dx.doi.org/10.1016/j.geoderma.2019.01.007.

Hijmans, R., 2022. raster: Geographic data analysis and modeling (R Package Version 3.5-21) [Computer software]. CRAN. https://rpkgs.datanovia.com/factoextra/index.html

Ho, T.K., 1995. Random Decision Forests, in: Proceedings of the 3rd International Conference on Document Analysis and Recognition, Montreal, QC. pp. 278–282.

Huang, H., Yang, L., Zhang, L., Pu, Y., Yang, C., Wu, Q., Cai, Y., Shen, F., Zhou, C., 2022. A review on digital mapping of soil carbon in cropland: progress, challenge, and prospect. Environmental Research Letters, 17, 123004. IOP Publishing. http://dx.doi.org/10.1088/1748-9326/aca41e.

Jenny, H., 1941. Factors of soil formation: A system of quantitative Pedology. McGraw-Hill, Book Co., Inc, New York.

Jakłík, O., Kodełová, R., Kapička, A., Klement, A., Fér, M., Nikodem, A., 2016. Using magnetic susceptibility mapping for assessing soil degradation due to water erosion. Soil and Water Research, 11, 105-113. Czech Academy of Agricultural Sci. http://dx.doi.org/10.17221/233/2015-swr.

Kanniah, K.D., Beringer, J., North, P., Hutley, L., 2012. Control of atmospheric particles on diffuse radiation and terrestrial plant productivity. Progress in Physical Geography: Earth and Environment, 36, 209-237. SAGE Publications. http://dx.doi.org/10.1177/0309133311434244.

Ker, J.C., 1998. Latossolos do Brasil: uma revisão. Geonomos, 5, 17-40.

Lee, C.C., Zeng, M., Luo, K., 2024. How does climate change affect food security? Evidence from China. Environmental Impact Assessment Review, 104, 107324. Elsevier BV. http://dx.doi.org/10.1016/j.eiar.2023.107324.

Lee, S., Wolberg, G., Shin, S.Y., 1997. Scattered data interpolation with multilevel B-splines. IEEE Transactions On Visualization and Computer Graphics, 3, 228-244.

Institute of Electrical and Electronics Engineers (IEEE). http://dx.doi.org/10.1109/2945.620490.

Lemercier, B., Lagacherie, P., Amelin, J., Sauter, J., Pichelin, P., Richer-De-Forges, A.C., Arrouays, D., 2022. Multiscale evaluations of global, national and regional digital soil mapping products in France. Geoderma, 425, 116052. Elsevier BV. http://dx.doi.org/10.1016/j.geoderma.2022.116052.

Li, X., Mccarty, G. W., Karlen, D. L., Cambardella, C. A., 2018. Topographic metric predictions of soil redistribution and organic carbon in Iowa cropland fields. Catena, 160, 222-232. Elsevier BV. http://dx.doi.org/10.1016/j.catena.2017.09.026.

Liu, J., Zhang, P., Gao, Y., 2023. Effects of vegetation rehabilitation on soil inorganic carbon in deserts: a meta-analysis. Catena, 231, 107290. Elsevier BV. http://dx.doi.org/10.1016/j.catena.2023.107290.

Loiseau, T., Arrouays, D., Richer-De-Forges, A.C., Lagacherie, P., Ducommun, C., Minasny, B., 2021. Density of soil observations in digital soil mapping: a study in the Mayenne region, France. Geoderma Regional, 24, e00358. Elsevier BV. http://dx.doi.org/10.1016/j.geodrs.2021.e00358.

Mantovani, V.A., Terra, M.C.N.S., Rodrigues, A.F., Silva, C.A., Guo, L., Mello, J.M.; Mello, C.R., 2024. Unprecedentedly high soil carbon stocks and their spatial variability in a seasonally dry Atlantic Forest in Brazil. Catena, 235, 107696. Elsevier BV. http://dx.doi.org/10.1016/j.catena.2023.107696.

McBratney, A., Mendonça Santos, M., Minasny, B., 2003. On digital soil mapping. Geoderma, 117, 3–52. https://doi.org/10.1016/S0016-7061(03)00223-4.

Minasny, B., McBratney, A. B., 2017. Limited effect of organic matter on soil available water capacity. European Journal of Soil Sci., 69, 39-47. Wiley. http://dx.doi.org/10.1111/ejss.12475.

Mukhopadhyay, S., Chakraborty, S., 2020. Use of diffuse reflectance spectroscopy and Nix pro color sensor in combination for rapid prediction of soil organic carbon. Computers and Electronics in Agriculture, 176, 105630. Elsevier BV. http://dx.doi.org/10.1016/j.compag.2020.105630.

Nawar, S., Mouazen, A. M., 2018. Optimal sample selection for measurement of soil organic carbon using on-line vis-NIR spectroscopy. Computers and Electronics in Agriculture, 151, 469-477. Elsevier BV. http://dx.doi.org/10.1016/j.compag.2018.06.042.

Neuwirth, E., 2014. RColorBrewer: ColorBrewer palettes (R Package) [Computer software]. https://rpkgs.datanovia.com/factoextra/index.html

Nuralykyzy, B., Nurzhan, A., Li, N., Huang, Q., Zhu, Z., An, S., 2023. Influence of land use types on soil carbon fractions in the Qaidam Basin of the Qinghai-Tibet Plateau. Catena, 231, 107273. Elsevier BV. http://dx.doi.org/10.1016/j.catena.2023.107273.

Oliveira, E.S., Reatto, A., Roig, H.L., 2015. Estoques de carbono do solo segundo os componentes da paisagem. Cadernos de Cienc. & Tecnologia, 32, 71-93.

Paranavithana, T.M., Anas, M.U.M., Karunaratne, S.B., Macdonald, B., Wimalathunge, N., Bishop, T.F.A., Ratnayake, R.R., 2023. Environmental factors and spatial dependence explain half of the inherent variation in carbon pools of tropical paddy soils. Catena, 231, 107278. Elsevier BV. http://dx.doi.org/10.1016/j.catena.2023.107278.

Peinado, F. M., Ruano, S. M., González, M. G. B., Molina, C. E., 2010. A rapid field procedure for screening trace elements in polluted soil using portable X-ray fluorescence (PXRF). Geoderma, 159, 76–82. http://dx.doi.org/10.1016/j.geoderma.2010. 06.019.

Poeplau, C., Bolinder, M. A., Kätterer, T., 2016. Towards an unbiased method for quantifying treatment effects on soil carbon in long-term experiments considering initial within-field variation. Geoderma, 267, 41-47. Elsevier BV. http://dx.doi.org/10.1016/j.geoderma.2015.12.026.

QGIS Development Team, 2023. QGIS Geographic Information System. Open Source Geospatial Foundation. https://qgis.org/en/site/

R Core Team, 2023. R: A language and environment for statistical computing. R Foundation for Statistical Computing, Vienna, Austria. Version 4.1.1. Available in: <https://www.rproject.org/>. Access in: August, 10, 2023.

Rakotonindrina, H., Moritsuka, N., Kawamura, K., Tsujimoto, Y., Nishigaki, T., Andrianary, H.B., Razafimbelo, T., Razakamanarivo, H., Andriamananjara, A., 2022. Prediction of the soil properties of Malagasy rice soils based on the soil color and magnetic susceptibility. Soil Sci. and Plant Nutrition, 69, 24-35. Informa UK Limited. http://dx.doi.org/10.1080/00380768.2022.2136929.

Reis, A.M.H., Teixeira, W.G., Fontana, A., Barros, A.H.C., Victoria, D. DE C., Vasques, G.M., Samuel-Rosa, A., Ottoni, M.V., Monteiro, J.E.B. DE A., 2024. Hierarchical pedotransfer functions for predicting bulk density in Brazilian soils. Sci. Agric. 81. https://doi.org/10.1590/1678-992X-2022-0255

Rodríguez-Albarracín, H.S., Demattê, J.A.M., Rosin, N.A., Contreras, A.E.D., Silvero, N.E.Q., Cerri, C.E.P., Mendes, W.S., Tayebi, M., 2023. Potential of soil minerals

to sequester soil organic carbon. Geoderma, 436, 116549. Elsevier BV. http://dx.doi.org/10.1016/j.geoderma.2023.116549.

Sá, J.C.M., Santos, J.B., Lal, R., Moraes, A., Tivet, F., Sá, M.F.M., Briedis, C., Ferreira, A.O., Eurich, G., Farias, A., 2013. Soil-Specific Inventories of Landscape Carbon and Nitrogen Stocks under No-till and Native Vegetation to Estimate Carbon Offset in a Subtropical Ecosystem. Soil Sci. Soc. of Am. Journal, 77, 2094-2110. Wiley. http://dx.doi.org/10.2136/sssaj2013.01.0007.

Santos, H.G., Jacomine, P.K.T., Anjos, L.H.C., Oliveira, V.A., Lumbreras, J.F., Coelho, M.R., Almeida, J.A., Araújo Filho, J.C., Oliveira, J.B., Cunha, T.J.F., 2018. Sistema Brasileiro de Classificação de Solos. 5. ed. Brasília: Embrapa Solos.

Schoenholtz, S. H., Van Miegroet, H., Burger, J. A., 2000. A review of chemical and physical properties as indicators of forest soil quality: challenges and opportunities. Forest Ecology and Management, 138, 335-356.

Scott, N.A., Cole, C.V., Elliott, E.T., Huffman, S.A., 1996. Soil textural control on decomposition and soil organic matter dynamics. Soil Sci. Soc. of Am. Journal, 60, 1102-1109.

Shi, J., Song, M., Yang, L., Zhao, F., Wu, J., Li, J., Yu, Z., Li, A., Shangguan, Z., Deng, L., 2023. Recalcitrant organic carbon plays a key role in soil carbon sequestration along a long-term vegetation succession on the Loess Plateau. Catena, 233, 107528. Elsevier BV. http://dx.doi.org/10.1016/j.catena.2023.107528.

Siewert, M.B., 2018. High-resolution digital mapping of soil organic carbon in permafrost terrain using machine learning: a case study in a sub-arctic peatland environment. Biogeosciences, 15, 1663-1682. Copernicus GmbH. http://dx.doi.org/10.5194/bg-15-1663-2018.

Silva, A.M., Silva, M.L.N., Curi, N., Lima, J.M., Avanzi, J.C., Ferreira, M.M., 2005. Perdas de solo, água, nutrientes e carbono orgânico em Cambissolo e Latossolo sob chuva natural. Pesquisa Agropecuária Brasileira, 40, 1223-1230. FapUNIFESP (SciELO). http://dx.doi.org/10.1590/s0100-204x2005001200010.

Silva, L.C.M., Peixoto, D.S., Gomes, J.B.V., Avanzi, J.C., Amorim, R.S.S., Borghi, E., Resende, Á.V., Silva, B.M., Mancini, M., Curi, N., 2022. Mineralogy and pore size distribution of clayey Oxisols with granular structure and the effect of management systems. Soil and Tillage Research, 223, 105479. Elsevier BV. http://dx.doi.org/10.1016/j.still.2022.105479.

Soil Survey Staff, 2022. Keys to Soil Taxonomy, 13th edition. USDA Natural Resources Conservation Service.

Souza, L.F.T., Hirmas, D.R., Sullivan, P.L., Reuman, D.C., Kirk, M.F., Li, L., Ajami, H., Wen, H., Sarto, M.V.M., Loecke, T.D., Rudick, A.K., Rice, C.W., Billings, S.A., 2023. Root distributions, precipitation, and soil structure converge to govern soil organic carbon depth distributions. Geoderma, 437, 116569. Elsevier BV. http://dx.doi.org/10.1016/j.geoderma.2023.116569.

Sothe, C., Gonsamo, A., Arabian, J., Kurz, W.A., Finkelstein, S.A., Snider, J., 2022. Large Soil Carbon Storage in Terrestrial Ecosystems of Canada. Global Biogeochemical Cycles, 36, e2021GB007213. American Geophysical Union (AGU). http://dx.doi.org/10.1029/2021gb007213.

Taghizadeh-Mehrjardi, R., Schmidt, K., Amirian-Chakan, A., Rentschler, T., Zeraatpisheh, M., Sarmadian, F., Valavi, R., Davatgar, N., Behrens, T., Scholten, T., 2020. Improving the Spatial Prediction of Soil Organic Carbon Content in Two Contrasting Climatic Regions by Stacking Machine Learning Models and

Rescanning Covariate Space. Remote Sensing, 12, 1095. MDPI AG. http://dx.doi.org/10.3390/rs12071095.

Tayebi, M., Rosas, J.T.F., Mendes, W.S., Poppiel, R.R., Ostovari, Y., Ruiz, L.F.C., Santos, N.V., Cerri, C.E.P., Silva, S.H.G., Curi, N., Silvero, N.E.Q., Demattê, J.A.M., 2021. Drivers of Organic Carbon Stocks in Different LULC History and along Soil Depth for a 30 Years Image Time Series. Remote Sensing, 13, 2223. MDPI AG. http://dx.doi.org/10.3390/rs13112223.

Telles, E.C.C., Camargo, P.B., Martinelli, L.A., Trumbore, S.E., Costa, E.S., Santos, J., Higuchi, N., Oliveira JR., R.C., 2003. Influence of soil texture on carbon dynamics and storage potential in tropical forest soils of Amazonia. Global Biogeochemical Cycles, 17, 1040.

Tucker, C.J., 1979. Red and photographic infrared linear combinations for monitoring vegetation. Remote Sensing of Environment, 8, 127-150. Elsevier BV. http://dx.doi.org/10.1016/0034-4257(79)90013-0.

Vågen, T.G., Winowiecki, L.A., Tondoh, J.E., Desta, L.T., Gumbricht, T., 2016. Mapping of soil properties and land degradation risk in Africa using MODIS reflectance. Geoderma, 263, 216-225. Elsevier BV. http://dx.doi.org/10.1016/j.geoderma.2015.06.023.

VCS - Verified Carbon Standard, 2024. Estimation of Carbon Stocks in the Soil Organic Carbon Pool. Disponível em: https://verra.org/methodologies-main/#vcs-methodologies. Acess in: 23 feb. 2024.

Veldkamp, E., 1994. Organic carbon turnover in three tropical soil sunder pasture after deforestation. Soil Sci. Soc. Am. J., 58, 175-80.

Viana, J.H.M.; Teixeira, W.G.; Donagemma, G.K., 2017. Densidade de partículas, in: Silva, A.E.; Fontana, A.; Melo, A.S.; Martins, A.L.S.; Inda, A.V.; Santi, A.; Madari, B.E.; Mattos, B.B.; Almeida, B.G.; Alves, B.J.R. et al., Manual de métodos de análise dos solos. 3. ed. Rio de Janeiro: Embrapa. pp. 76-81.

Walkley, A., Black., I.A., 1934. An examination of the Degtjareff method for determining soil organic matter and a proposed modification of the chromic acid titration method. Soil Sci. 37, 29–38. doi:10.1097/00010694-193401000-00003.

Wang, D., Chakraborty, S., Weindorf, D.C., Li, B., Sharma, A., Paul, S., Ali, M.N., 2015. Synthesized use of VisNIR DRS and PXRF for soil characterization: Total carbon and total nitrogen. Geoderma, 243-244, 157-167. Elsevier BV. http://dx.doi.org/10.1016/j.geoderma.2014.12.011.

Wang, L., Liu., H., 2006. An efficient method for identifying and filling surface depressions in digital elevation models for hydrologic analysis and modelling. International Journal of Geographical Information Sci., 20, 193-213.

Weindorf, D. C., Chakraborty, S., 2016. Portable X-ray Fluorescence Spectrometry Analysis of Soils. Methods of Soil Analysis, 1, 1–8.

Wickham, H., 2016. ggplot2: Elegant Graphics for Data Analysis. Springer-Verlag New York. ISBN 978-3-319-24277-4, https://ggplot2.tidyverse.org.

Wickham, H., Averick, M., Bryan, J., Chang, W., McGowan, L., François, R., Grolemund, G., Hayes, A., Henry, L., Hester, J., Kuhn, M., Pedersen, T., Miller, E., Bache, S., Müller, K., Ooms, J., Robinson, D., Seidel, D., Spinu, V., Takahashi, K., Vaughan, D., Wilke, C., Woo, K., Yutani, H., 2019. Welcome to the tidyverse. Journal of Open Source Software, 4, 1686. https://doi.org/10.21105/joss.01686

Zinn, Y.L., Lal, R., Resck, D.V.S., 2005. Texture and organic carbon relations described by a profile pedotransfer function for Brazilian Cerrado soils. Geoderma, 127, 168-173. Elsevier BV. http://dx.doi.org/10.1016/j.geoderma.2005.02.010.

Zinn, Y.L., Lal, R., Bigham, J.M., Resck, D.V.S., 2007. Edaphic Controls on Soil Organic Carbon Retention in the Brazilian Cerrado: texture and mineralogy. Soil Sci. Soc. of Am. Journal, 71, 1204-1214. Wiley. http://dx.doi.org/10.2136/sssaj2006.0014.

PART III: Final Considerations

3 Final considerations

The Paleosol studied herein in Chapter I, presented contrasting redoximorphic features, suggesting a change on the landscape to promote such variation. Moreover, the Ti/Zr ratio, delivered by pXRF, indicated different parent materials forming the reddish and gleyic unities of the Paleosol.

In this pilot study, the combined use of field morphology, physical, chemical, and mineralogical analyses, complemented by pXRF and MS data, provided details on the variation of soil properties formed under current pedalization and elutriation versus paleogleyzation, and delivered some insights on enhancing conservation practices and on assisting the characterization of climate change impacts.

The authors understand that there are Paleosols not yet studied in Brazil, for example the Latosols (Oxisols) located on the summits (*chapadas*) of the Brazilian Central Plateau, making part of the Cerrado biome (22% of the county). These *chapadas* were formed by pediplanation, under bioclimatic conditions much drier than nowadays. In other words, the relief is relict from dry climate and the Oxisols were formed under humid climate. Then, these Latosols are polygenetic: they are Paleosols. This approach may encourage future studies in this research line.

On Chapter II, aquifer discharge is the ecosystem supply which was more affected by the soil mapping scale. Also, trade-offs among ecosystem services were spatially detected since soil-landscape units that foster water infiltration, storage, and direct aquifer recharge are those that prevent soil loss with avoided erosion.

The incorporation of terrain attributes and legacy data was effective in generating predictive models for the spatial distribution of soil classes within the studied watersheds. The soil class maps generated through fuzzy logic showed high accuracy. For all studied watersheds, the overall accuracy surpassed 60%, and the Kappa index was higher in Pelanca and Morro do Diabo watersheds, with values exceeding 50%, indicating a high level of agreement in the predictions.

Detailed soil mapping has provided us to perceive the precise locations within each watershed where ecosystem services occur more intensely, as well as their distribution across the landscape.

In Chapter III, we emphasize the growing global importance of soil organic carbon (SOC) and carbon stocks (CS) due to climate issues. There is high variability in these attributes over short distances, and we encourage further research to identify variables for finer scale predictions. Our study revealed significant variability in soil density under similar conditions, highlighting the need for more research to improve predictions specially for CS.

Satisfactory SOC predictions ($R^2 = 0.47$) were possible when using as covariates remotely sensed data (NDVI and insolation indices), terrain attributes, parent materials, soil classes, texture, and land uses. Proximal sensor data (pXRF and MS) did not help explain the spatial variability of SOC. Predictions based solely on the distance between points did not yield satisfactory results, indicating that even with high sample density (1 sample per 3.5 ha), using predictor variables provides better results.

None of the generated models produced accurate results for SOC in the subsurface (80-100 cm) and CS. Therefore, the tested hypothesis was partially confirmed. The use of high sample density was aided by environmental variables representing four of the five main soil formation factors yielded accurate SOC predictions (0-20 cm). Results also demonstrated the high spatial variability of SOC and difficulties in spatially representing soil density to predict CS. Thus, there is a need for the development of other strategies, such as the use of new variables or models and more local testing to obtain accurate SOC and CS mappings for detailed scales and their applications.

Then, the present dissertation shows the importance of the study of soil to address issues about ecosystem services, climate change, and environment conservation, highlighting how fundamental a detailed analysis is to address these issues adequately from the profile to landscape scales. The combination of traditional and modern techniques leads us to advances in science, taking into consideration the tacit knowledge and recognizing the value of experienced professionals for robust and reliable studies. The results presented herein showed that although the proximal and remote sensors can help to increase the availability of data for more representative areas, they are not always the most accurate data for modeling and digital mapping of soil and its attributes, which underscores the importance of always addressing the reliability of the generated results to the users, for more accurate land and environmental management and policy planning.